

**POLITECNICO DI TORINO**

Collegio di Ingegneria Chimica e dei Materiali

**Corso di Laurea Magistrale in Ingegneria dei Materiali**

Tesi di Laurea Magistrale

**AUTOMATIC CHARACTERIZATION OF  
DISLOCATION STRUCTURES VIA  
SCANNING ELECTRON MICROSCOPY**

**and optimization of advanced clustering methods for the detection of defects in  
SEM images**



**Relatori**

Politecnico di Torino: prof. Pavese Matteo

INSA Lyon: prof. Langlois Cyril

**Candidato**

Bechis Andrea

Matricola 242629

Marzo 2019



## SUMMARY

---

A.	RIASSUNTO IN ITALIANO.....	1
I.	Introduzione.....	1
II.	Teoria ECCI.....	2
III.	Tecnica e-CHORD.....	3
IV.	Discriminazione dislocazioni grazie ai profili di contrasto.....	4
V.	Ottimizzazione delle condizioni sperimentali.....	4
VI.	Strategia delle mini-serie.....	5
VII.	Risultati di densità di dislocazioni.....	6
VIII.	Automatizzazione della ricerca dei criteri di invisibilità.....	6
IX.	Conclusioni e prospettive.....	7
B.	INTRODUCTION.....	9
I.	The issue.....	9
II.	The plan of the master's thesis.....	9
C.	STATE OF THE ART.....	11
I.	Crystallographic defects.....	11
Line defects: dislocations.....	11	
Stacking faults.....	13	
II.	Strengthening mechanisms in metals.....	14
Dislocation contribution to the yield stress: the strain hardening.....	14	
III.	Estimations of dislocation density.....	15
1. Transmission Electron Microscopy.....	15	
2. SEM-ECCI.....	17	
3. Global techniques.....	18	
Necessity of a new technique.....	20	
IV.	Overview on the instrument.....	22
V.	Ecci, theory behind the BSE channeling contrast.....	25
VI.	CHORD Method.....	31
Chord experimental set up.....	31	
Chord performances.....	34	
Orientation maps.....	35	
VII.	Similarities between dis-chord and chord.....	37
e-CHORD stacks acquisition protocol.....	37	
Image treatment on e-chord stacks.....	38	

VIII. dis-CHORD first results.....	42
D. EXPERIENCES.....	45
I. Objectives .....	45
II. Used microscope.....	45
III. Sample preparation.....	46
IV. Acquisition issues .....	47
E. RESULTS.....	51
I. First duplex experimental set of stacks: study of parameters and investigation on the possibility of determining the burgers vector.....	51
Acquired rotational series .....	52
Parameters considerations .....	57
Experimental parameters conclusion .....	66
Initial approach to the burgers vector determination via rotational stacks.....	67
Dislocation density via clustering.....	70
II. Second duplex experimental set of stacks: a strategy to improve stacks quality for clustering purposes .....	71
Rotational profiles of mini-stacks.....	73
F. DATA PROCESSING WITH CLUSTERING PROGRAMME .....	75
I. Clustering theory.....	75
II. How to use the program and how results are showed .....	77
A strategy for augmenting the quality of clustering.....	79
III. Other clustering possibilities .....	80
G. DEVELOPMENT OF A MATLAB AUTOMATIC METHOD WHICH USE CLUSTERING DATA FOR CHARACTERIZING DISLOCATIONS .....	85
I. Dislocation density obtained via clustering.....	85
Validation of the MATLAB PROCEDURE (on Copper images).....	87
Dislocation density uncertainty: dislocation width.....	88
Results of dislocation density via matlab .....	89
II. Detection of crystallographic defects visible for specific crossed tb conditions: toward the automatized detection of dislocations' nature.....	92
Further studies on best threshold to use.....	93
Results .....	95
H. CONCLUSIONS AND PERSPECTIVES .....	99
I. ANNEXES.....	103
Annex 1: example of total procedure for finding burger vector in the first set of stacks(on the 4 <sup>th</sup> grain stack6) .....	103

Annex 2: results of the research of burgers vector for the first set of stacks.....	107
Annex 3: GRAIN2 of the second set of stacks.....	112
REFERENCES.....	115



## A. RIASSUNTO IN ITALIANO

---

### I. INTRODUZIONE

---

Questo progetto di tesi ha avuto luogo presso l'Institut National de Sciences Appliquées (INSA) a Lyon, più precisamente nel laboratorio MATEIS specializzato nella scienza e nell'ingegneria dei materiali. Si tratta di un lavoro iniziato durante uno stage di due mesi nel sopraccitato laboratorio, che si è prolungato per altri quattro mesi grazie ad una borsa di studio per tesi su proposta.

L'obiettivo principe è stato lo sviluppo di una tecnica per caratterizzare strutture di dislocazioni in acciai austenitici utilizzando il microscopio elettronico a scansione (SEM). La tecnica prende il nome di *disCHORD*.

Le dislocazioni sono una delle tante tipologie di difetti cristallini particolarmente importante nei materiali metallici. Nello specifico si tratta di difetti lineari. Questi difetti creano un disordine nella microstruttura e possono essere di due diversi tipi: a spigolo o a vite, come mostrato in Figure 1, in natura, la maggior parte delle volte si presentano come un mix delle due tipologie.

La loro geometria nel cristallo è descritta dal vettore  $\mathbf{u}$  con la direzione della linea lungo la quale si propagano e del vettore di Burgers  $\mathbf{b}$  che descrive la direzione della deformazione elastica che provocano nel cristallo. Misure quantitative di questo difetto forniscono valori di *densità delle dislocazioni* ( $m/m^3$ ) ma tutt'oggi vi sono delle criticità nel determinare questo parametro ed i valori rimangono poco precisi.

L'importanza di caratterizzare le dislocazioni in materiali metallici è data dal fatto che queste sono intimamente correlate al meccanismo di deformazione plastica e quindi alla rigidità strutturale dei materiali. Infatti un metallo comincia a deformarsi plasticamente quando il carico di snervamento,  $\sigma_y$ , viene superato ed il movimento coordinato di un gran numero di dislocazioni diventa possibile. La soglia di snervamento è proporzionale alla densità di dislocazioni ed è per questo importante poter misurare questo parametro con precisione.

Esistono molte tecniche di caratterizzazione della densità di dislocazioni e quelle che ad oggi permettono una visualizzazione diretta ed una maggiore precisione sulla misura sono:

- *Microscopio elettronico a trasmissione* (TEM)
- *Electron Channeling Contrast Imaging* (ECCI) tramite l'utilizzo di un microscopio elettronico a scansione (SEM)

In entrambi i casi le dislocazioni sono visibili grazie al fatto che ad esse è localmente associato un campo di deformazione elastica e pertanto gli atomi vicini alla linea della dislocazione sono spostati dalle posizioni naturali che occuperebbero in un cristallo perfetto. Queste deformazioni fanno variare localmente gli angoli di diffrazione di Bragg (nel caso del microscopio elettronico a trasmissione) e di canalizzazione degli elettroni

(nel caso dell'Electron Channeling Contrast Imaging) e ciò comporta una variazione degli elettroni trasmessi (per il TEM) o retro-diffusi (per l'ECCI) rispetto alla matrice cristallina perfetta. Sotto queste specifiche condizioni di orientazione (diffrazione di Bragg o canalizzazione degli elettroni) ed in presenza di dislocazioni, un contrasto con la matrice è localmente prodotto. Esempi di visualizzazione diretta di questi difetti cristallini con le due tecniche sono mostrati in Figure 3 e 5.

Va puntualizzato che entrambi i metodi presentano dei problemi:

- Lunghe tempistiche per caratterizzare singoli grani cristallini e criticità nel raccogliere dati statistici su diversi grani.
- Necessità di una grande conoscenza in cristallografia per trovare le condizioni di orientazione specifiche nelle quali le dislocazioni risultano visibili.
- Rischio di una sottostima della densità di dislocazioni in quanto, anche sotto le orientazioni specifiche di Bragg o di canalizzazione, una frazione di questi difetti potrebbe essere invisibile se un *criterio di invisibilità* è presente.

Il lavoro di questa tesi di laurea magistrale è atto a superare queste difficoltà mettendo insieme la teoria ECCI con una tecnica di determinazione dell'orientazione cristallografica recentemente messa a punto dal laboratorio MATEIS di INSA Lyon, con il quale il candidato ha avuto la fortuna di lavorare. La tecnica prende il nome di *electron CHanneling ORientation Determination* (eCHORD).

## II. TEORIA ECCI

---

Conosciuta fin dagli anni '80, la tecnica di Electron Channeling Contrast Imaging comincia a riessere presa in considerazione in questi anni grazie ai miglioramenti nel campo della microscopia elettronica, che hanno permesso l'ottenimento di risultati molto interessanti. Grazie a questa tecnica è infatti possibile vedere le dislocazioni senza dover ricorrere all'utilizzo di un microscopio elettronico a trasmissione.

Per angoli ancora minori dei piccoli angoli di diffrazione di Bragg, associati al fascio di elettroni accelerato in un SEM, gli elettroni incidenti sono canalizzati in particolari *direzioni di canalizzazione* lungo le quali le interazioni con i nuclei cristallini del campione sono minimizzate. In queste condizioni il fascio primario è quasi parallelo ad un dato piano cristallino e l'onda di Bloch ad esso associata presenta i propri minimi sui nuclei atomici del reticolo cristallino, come mostrato in Figure 10. Di conseguenza gli elettroni penetrano a fondo nel campione prima di subire interazioni inelastiche con il reticolo ed essere retro-diffusi, solo pochissimi riescono ad uscire dalla superficie del campione contribuendo al segnale captato dal detector BackScattered Electrons (BSE), sotto le condizioni di canalizzazione il segnale BSE crolla.

Nell'intorno di una dislocazione, il campo di deformazione elastica associato ad essa sposta i nuclei atomici dalle loro posizioni "naturali", che intralciano quindi la direzione di canalizzazione degli elettroni. In questo caso l'interazione inelastica degli elettroni con i nuclei, avviene in maniera apprezzabile ed il detector BSE registra un segnale più alto rispetto ai punti in cui il cristallo è perfetto (ed in condizioni di canalizzazione).

Completata la scansione della regione di interesse, l'immagine mostra un contrasto tra matrice cristallina e dislocazioni.

In queste orientazioni precise e specifiche, esiste la possibilità che una frazione, anche significativa, di dislocazioni non produca un contrasto con la matrice, risultando invisibile. Ciò avviene quando la direzione della deformazione elastica provocata da una dislocazione ( $\mathbf{b}$ ) è parallela al piano cristallino interessato dalla canalizzazione. Si ha in questo caso un *criterio di invisibilità* ed il prodotto scalare  $\overline{\mathbf{g}}_{hkl} \circ \overline{\mathbf{b}}$  è nullo. In questa eventualità una sottostima della misura di densità di dislocazioni è prodotta. Va detto però che se queste condizioni sono individuate per due diversi piani cristallini (due diversi  $\overline{\mathbf{g}}_{hkl}$ ) è possibile determinare il vettore di Burgers che resta altrimenti ignoto.

### III. TECNICA E-CHORD

---

La tecnica eCHORD per la determinazione dell'orientazione cristallina tramite SEM, fa variare progressivamente l'angolo tra il fascio elettronico incidente ed il campione, in modo da esplorare un gran numero di orientazioni durante l'analisi. Per ogni diversa orientazione, le condizioni di retro-diffusione degli elettroni cambiano ed il detector rileva un'intensità di segnale differente per un dato punto del campione.

In pratica, il campione viene inclinato di circa 10° e fatto ruotare attorno alla sua normale, come mostrato in Figure 13a. Ciò avviene grazie ad un apposito 'sub-stage' (vedere Figure 15) installato nella camera del SEM, esso permette di allineare l'area scansionata dal fascio elettronico con l'asse di rotazione del campione in modo da non perdere la regione di interesse durante la rotazione. Grazie al sub-stage, la rotazione è automatizzata e molto precisa; ad ogni grado di rotazione viene acquisita un'immagine che verrà allineata alle altre per formare una serie di immagini.

Da ogni punto in queste serie di immagini, in cui il contrasto BSE varia con la rotazione, può essere estrapolato un profilo di variazione di intensità di grigio (vedere Figure 14b) che funge da impronta dell'orientazione del punto stesso. La variazione di contrasto BSE è infatti funzione dell'orientazione iniziale del cristallo preso in considerazione. Questi profili sperimentali vengono confrontati ad un database di profili simulati per moltissime orientazioni ed in questo modo si può risalire all'orientazione originale del grano analizzato.

In ogni rotazione, ci si imbatte in più di una orientazione di canalizzazione, in cui le dislocazioni sono visibili grazie alla teoria ECCI. Il vantaggio è che in questo modo non è necessaria una precedente analisi EBSD atta a conoscere l'orientazione del grano analizzato e a calcolare la specifica orientazione da applicare al campione per portarlo in condizioni di canalizzazione. L'analisi risulta quindi più accessibile all'utente medio e del tempo viene risparmiato. In più si analizzano diversi piani cristallini in condizioni di canalizzazione, azzerando gli errori dovuti a criteri di invisibilità e aprendo la possibilità ad un'analisi del vettore di Burgers.

#### IV. DISCRIMINAZIONE DISLOCAZIONI GRAZIE AI PROFILI DI CONTRASTO

---

Per un dato grano cristallino, i profili sperimentali provenienti dalla matrice o da difetti si sovrappongono durante tutta la rotazione tranne che negli angoli di canalizzazione, dove le dislocazioni sono in contrasto con la matrice ombrosa, producendo differenze in determinate porzioni angolari dei profili, come mostrato in Figure 20b. Queste differenze sono potenzialmente utilizzabili per discriminare i pixel delle dislocazioni con tecniche di clustering nello spazio vettoriale dei profili, che “clusterizzano” ossia raggruppano i pixel in diverse famiglie (matrice e dislocazioni) in base ai profili.

Il programma di clustering è stato codificato su misura per lo scopo e perciò è stato necessario capirne il funzionamento. Inserendo la serie d’immagini e selezionando un’area di interesse all’interno di un grano, il programma riconosce la più grande famiglia con profili simili come la matrice cristallina e discrimina gli altri clusters come dislocazioni, rumore o polvere (se il profilo è piatto). Molto tempo è stato dedicato a come meglio utilizzare i parametri. Ad oggi molti bug sono ancora presenti e, nonostante che buoni risultati possano già essere ottenuti, alcuni miglioramenti sono ancora necessari.

Il programma restituisce un file testo in cui, ad ogni pixel della serie di immagini, è associato un valore numerico che indica la tipologia a cui appartiene. Nel caso in cui il pixel faccia parte di una dislocazione, sono indicati anche gli angoli in cui c’è una differenza di contrasto con la matrice: gli angoli di canalizzazione in cui il difetto cristallino non è sotto un criterio di invisibilità.

Durante la tesi è stato implementato uno script Matlab che è in grado di utilizzare i file testo ottenuti tramite clustering e di visualizzare i risultati (vedere Figure 55). Se questi sono accettabili, è possibile calcolare un valore di densità di dislocazioni grazie ad una parte di codice aggiunta allo script.

#### V. OTTIMIZZAZIONE DELLE CONDIZIONI SPERIMENTALI

---

Le prime serie di immagini, mostrate in Figure 28, sono state fatte con un ingrandimento di 5000X variando diversi parametri per indagare sulle migliori condizioni sperimentali. Si è giunti alla conclusione che, ad un tale ingrandimento, i difetti cristallini sono poco visibili e una buona parte non risulta visibile per mancanza di risoluzione nei dettagli. Queste serie non possono essere utilizzate per caratterizzare la densità delle dislocazioni. Sono stati comunque cercati i criteri di invisibilità, sotto l’ipotesi che i difetti cristallini visibili condividessero lo stesso valore del vettore di Burgers. Per 2 degli 8 grani analizzati sono stati trovati due diversi criteri di invisibilità ed il vettore di burgers è stato determinato con successo. Bisogna far presente che l’orientazione iniziale del campione è determinante per il numero di condizioni di canalizzazione incrociate durante la rotazione e per le eventuali condizioni di invisibilità delle singole dislocazioni. Bisogna far presente che l’orientazione iniziale del campione è determinante per il numero di condizioni di canalizzazione incrociate durante la rotazione e per la presenza di eventuali condizioni di invisibilità.

Queste prime serie hanno condotto alle seguenti conclusioni per quanto riguarda i parametri sperimentali analizzati:

- *Inclinazione del campione (tilt iniziale)*: più è grande e più la probabilità di incrociare un gran numero di condizioni di canalizzazione durante la rotazione aumenta (vedere Figure 36). D'altro canto valori più piccoli di tilt comportano più ampi intervalli angolari nei quali le dislocazioni sono visibili. Un valore di tilt di  $10^\circ$  è un buon compromesso.
- *Energia del fascio incidente*: è necessario accelerare gli elettroni del fascio incidente con un potenziale minimo di 20 keV per ottenere un buon contrasto di canalizzazione e una buona visibilità delle dislocazioni. Non bisogna comunque sorpassare questo valore perché si favorisce la contaminazione del campione e l'accumulo superficiale di carica.
- *Diametro di apertura*: il valore massimo di 120  $\mu\text{m}$  è quello che massimizza il contrasto matrice-dislocazioni.
- *Velocità di scansione*: è correlata al valore di segnale/rumore, per tanto è necessario un valore minimo di 8 (12970 ns/pixel), in ogni caso superare un valore di 10 (61925 ns/pixel) non comporta miglioramenti nel contrasto tra matrice e dislocazione.
- *Ingrandimento*: per ottenere una buona risoluzione delle dislocazioni e per poterle risolverle singolarmente, un ingrandimento minimo di 15000/20000X è necessario, questo permette l'ottenimento di profili di contrasto accettabili per la caratterizzazione delle dislocazioni tramite clustering.

È necessario puntualizzare che l'alto ingrandimento e l'alto valore di velocità di scansione, necessari alla caratterizzazione delle dislocazioni, aumentano il flusso elettronico superficiale che investe il campione. Considerando che vengono prese molte immagini sulla stessa porzione del campione, queste condizioni diventano critiche in quanto un accumulo superficiale di carica è prodotto durante l'analisi. Ciò comporta problemi legati alla deflessione del fascio elettronico, che subisce l'influenza del campo elettrico degli elettroni in superficie. Di conseguenza durante l'analisi ci si imbatte in problemi di *defocusing*, *deriva della zona scansionata* e *deformazioni locali delle immagini*, che danneggiano la qualità delle serie acquisite, dell'allineamento e quindi dei profili di contrasto che anche in questo caso risultano non adatti ad una caratterizzazione delle dislocazioni via clustering.

## VI. STRATEGIA DELLE MINI-SERIE

---

Per ottenere serie ad ingrandimenti di 20000 X con valori di velocità di scansione accettabili, limitando al massimo i problemi dati dall'accumulo di carica, è stata studiata una strategia per diminuire i tempi di esposizione del campione al fascio incidente. Per un dato grano cristallino da analizzare, una serie preliminare a basso ingrandimento viene acquisita velocemente per individuare gli intervalli angolari di canalizzazione, in cui le dislocazioni sono visibili. Dopodiché vengono prese delle mini-serie su ogni intervallo angolare di interesse (di circa  $5-10^\circ$ ) con un passo angolare di  $0.5^\circ$ . I risultati sono buoni e i problemi di defocusing, deriva e deformazione delle immagini sono molto limitati.

La totalità delle mini-serie allineate viene unita insieme per dare una serie di immagini con una precisione sui profili tale da permettere il clustering. Il programma associa ad ogni pixel un valore numerico che lo caratterizza e per le dislocazioni riferisce gli angoli in cui vi sono differenze nei profili, dando così informazioni su eventuali criteri di invisibilità.

## VII. RISULTATI DI DENSITÀ DI DISLOCAZIONI

Il clustering a partire dai profili di contrasto di canalizzazione ha permesso di definire un valore di densità delle dislocazioni conoscendo i pixel della matrice e delle dislocazioni, i risultati per uno dei due grani analizzati sono mostrati in Figure 56. Due diverse formule, già esistenti nella bibliografia, sono state utilizzate per definire la densità di dislocazioni e i valori sono stati confrontati con il metodo delle intercette, eseguito sulle immagini ECCI dello stesso grano.

I valori derivanti dal clustering dipendono dal *noise size* utilizzato durante l'analisi dei profili, ossia dall'area in pixel sotto la quale una dislocazione è considerata rumore. Nel caso mostrato un valore di 1 pixel permette di avvicinarsi di più al valore delle intercette. Bisogna fare presente che il *noise size* ottimale dipende dal ingrandimento utilizzato, che influenza l'area media in pixel della dislocazione, ma anche dalla qualità di immagine (del rumore d'immagine potrebbe essere scambiato per dislocazioni dal programma).

Il valore trovato è dello stesso ordine di grandezza di quello trovato tramite il metodo delle intercette anche se leggermente inferiore. Questo può essere spiegato sostenendo che il metodo clustering sottostima la densità di dislocazioni ma bisogna anche riconsiderare l'affidabilità del metodo di riferimento. Infatti il metodo delle intercette fornisce un risultato diverso a seconda di come le linee vengono tracciate ed in più il valore è influenzato dalla scelta dell'operatore in quanto non è sempre chiaro se una dislocazione intersechi o meno una linea della griglia. Bisognerebbe anche calcolare l'incertezza di misura legata alla formula matematica che permette di definire un valore in lunghezza di dislocazioni a partire da quante volte queste intersechino una griglia di linee.

## VIII. AUTOMATIZZAZIONE DELLA RICERCA DEI CRITERI DI INVISIBILITÀ

Un'ulteriore parte nello script Matlab è stata implementata per l'analisi del vettore di Burgers delle singole dislocazioni individuate, il quale riconosce eventuali criteri di invisibilità per i diversi piani cristallini in condizioni di canalizzazione incontrati durante la rotazione. In questo caso il grano deve essere indicizzato via eCHORD in modo da definire quale piano cristallino è in gioco nei diversi intervalli angolari di canalizzazione.

Una difficoltà è data dal fatto che non sempre tutti i pixel di una dislocazione presentano esattamente gli stessi angoli in cui c'è una differenza di contrasto con la matrice e questo problema è dato dal non perfetto allineamento tra le immagini. Lo script Matlab è comunque in grado, per ogni piano cristallino interessato, di discriminare le dislocazioni visibili da quelle invisibili, come mostrato in Figure 62. Per alcune dislocazioni è possibile

trovare una doppia condizione di invisibilità e definire il relativo vettore di Burgers, in Figure 63 è possibile visualizzare un esempio.

## IX. CONCLUSIONI E PROSPETTIVE

---

I risultati ottenuti con questo primo approccio alla tecnica *disCHORD* sono molto promettenti, infatti è possibile affermare che gli obiettivi prefissati sono stati raggiunti con successo e che le difficoltà sperimentali incontrate durante il lavoro sono state superate. L'analisi permette di dare valori di densità di dislocazioni ad un qualsiasi grano cristallino coerenti con i metodi tradizionali, pur non conoscendone l'orientazione iniziale e senza doverlo ri-orientare, come succede per le tecniche ECCI e TEM. Inoltre, il fatto che si incontrino più condizioni di canalizzazione durante la rotazione permette di non tralasciare dislocazioni che si trovano sotto criteri di invisibilità e quindi evita eventuali sottostime del valore di densità delle dislocazioni.

La tecnica non è ancora perfetta ma i risultati di densità di dislocazione ottenuti sono ampiamente nell'ordine di grandezza di quelli ottenuti con il classico metodo delle intercette. Usare i profili rotazionali per caratterizzare le dislocazioni si è rivelata un'ottima strategia che semplifica il processo di analisi. Inoltre la determinazione del vettore di Burgers è potenzialmente possibile, anche se l'orientazione del cristallo non è sempre tale da ottenere risultati. A tal proposito, per ottenere la determinazione sistematica del vettore di Burgers bisognerebbe implementare la possibilità di un doppio tilt, in modo da poter ri-orientare i grani analizzati per esplorare altre condizioni di canalizzazione fino a trovare condizioni di invisibilità, similmente a come si fa con il TEM.

La rilevazione delle dislocazioni tramite clustering è coerente con le immagini ECCI, come mostrato in Figure 63, anche se non è ancora raggiunta la perfezione, effettivamente la geometria dei difetti a volte è leggermente diversa ed i più piccoli in alcuni casi non sono individuati. Questi difetti sono dovuti al non perfetto allineamento tra le immagini che fa muovere i difetti di qualche pixel nella serie di immagini e questo porta ad un danneggiamento dei profili di contrasto.

Si dovrebbe continuare ad implementare questa tecnica cercando di migliorare soprattutto l'allineamento delle immagini. Infatti, sono sempre stati utilizzati algoritmi che arrivano a considerare rototraslazioni e deformazioni di taglio globali nella serie d'immagini, ma sono presenti moltissimi altri algoritmi e sarebbe bene indagare verso la possibilità di correzioni locali tra le singole immagini.

Un'ulteriore fatto che rende questa tecnica molto promettente, è che si possono raggiungere dei risultati molto migliori con detector BSE di ultima generazione. Implementare il sub-stage su microscopi più performanti farebbe fare un salto enorme nella risoluzione delle dislocazioni come mostra la Figure 64. Di conseguenza migliorerebbe anche l'allineamento, infatti ci sarebbero più dettagli a cui l'algoritmo potrebbe riferirsi. Inoltre è ragionevole pensare che anche i problemi di accumulo carica

superficiale sarebbero meno marcati, anche se servono delle evidenze sperimentali per dimostrarlo.

## B. INTRODUCTION

---

### I. THE ISSUE

---

One of main objectives in material engineering is to shape materials proprieties thanks to an aware control of their chemical composition and microscopic structure during the processes by which they are made. Particularly, it is well know that real crystallographic materials, such as metals, are not perfect since they present micro-structural defects which influence their final properties. In order to understand their behavior, mathematical models that link these final properties with measurable values of micro-structural proprieties have been made during the years.

For that reason it is very important to make an effort in order to optimize both these models and the precision in measuring values which characterize the material composition and microstructure. Actually, a parameter of metals that is known to be very difficult to measure was chosen, its value being often measured with a poor precision. The concerned micro-structural property is the *dislocation density* (1).

Nowadays, the main techniques for measuring the dislocation density are the Transmission electron microscopy (TEM) and the Electron Channeling Contrast Imaging (ECCI) (2) (3), thanks to whom a direct visualization of dislocations can be obtained. However, these methods require a long time and a not negligible background in crystallography since these defects appear just in specific crystallographic orientations, so called Two Beam (TB) conditions. Moreover, a significant fraction of dislocations might be invisible under certain TB conditions, leading to an error in the measurement of their density. These precise orientations change with each analyzed grain, due to their different crystallographic orientation, therefore a statistic measurement, which consider more than a grain, is time consuming.

Other global techniques, which measures the dislocation density in an indirect way, exist. However, they entail large uncertainties linked both to the mathematical models of the indirect measurement and to assumptions that have to be made on the nature of dislocations.

### II. THE PLAN OF THE MASTER'S THESIS

---

This master's thesis aims at developing a new method for the characterization of dislocations in a meaningful number of grains and without any consideration about the grain orientations prior to the observations. This method is expected to characterize the nature of defects and to give quantitative information about their density (1) in briefer times than those reached with TEM or ECCI characterization.

It will be tried to reach this goal by melting together two existing techniques: ECCI and eCHORD, an analytical method developed by MATEIS microscopy researchers (from INSA Lyon) in the last few years. Electrons CHanneling ORientation Determination (eCHORD) uses a set of backscattered electrons (BSE) images, obtained with different angles between sample and electrons beam, to automatically map the crystallographic

orientation of grains in a polycrystal (without the use of EBSD detector) (4). In short, the contrast in these images changes with the angle and an intensity profile is obtained for each pixel belonging to a characteristic zone of the sample; this profile is effectively a signature of the orientation of the grain (4). The interesting point is that, while performing an eCHORD observation, each grain execute a  $360^\circ$  rotation, therefore, for each grain, different two beam (TB) conditions will be found. This will be used for visualizing dislocations without a previous study of the orientation and avoiding the problem of their invisibility under certain TB conditions.

Moreover, it will be tried to analyze these stack of images with a Clustering program in order to obtain exploitable data for studying both the nature and the density of dislocations. In short, thanks to the analysis of rotational profiles, the program allows the discrimination of zones with different behaviors such as different grains, different phases and crystallographic defects, letting therefore to distinguish matrix pixels from dislocations pixels. Hence, in optimal conditions it should be possible to obtain useful data and, thanks to a Matlab data processing, to determinate a value of dislocation density or to individuate TB conditions which concern a single dislocation.

A close examination of experimental parameters and a development of tools for data processing will be done. The resulting technique that is still in development takes the name of *disCHORD*.

## C. STATE OF THE ART

---

In this chapter the theoretical bases of the technique will be given, which have already been studied, in order to better understand the work done during this master's thesis.

### I. CRYSTALLOGRAPHIC DEFECTS

---

While thinking to a crystal, it is important to keep in mind that a perfect crystal is an idealization, in fact in nature atom arrangements do not follow perfect crystalline patterns. Due to the inescapable presence of impurities in materials and to the tendency of minimization of the total energy in bulk sample, there are always defects within a crystal, even if it can be considered with a very good approximation as a perfect crystal (5).

However, the fact that real materials are not perfect crystal is critical to materials engineering, in fact if they were perfect then their mechanical properties would be dictated by their composition and crystal structure alone, so it would be impossible for material engineers to shape material properties into the different combination that modern engineering device requires. For this reason it can be said that the defects within a crystal are fundamental, since they can be manipulated to control the mechanical behavior (5).

Different types of defects are present in crystals, the ones that will be of interest for this study are dislocations and stacking faults.

---

#### LINE DEFECTS: DISLOCATIONS

---

Dislocations create a lattice discontinuity and a local distortion, therefore around that kind of defect there are some zones in compression and others in tensions, i.e.: a strain field is related to this kind of defects.

A first way to describe dislocations could be to introduce *edge dislocations* that are supplementary semi-planes in the crystal. A dislocation is characterized by its unitary vector  $\vec{u}$  (that, for edge dislocations, gives the direction of the last atom line of the semi-planes: the *dislocation line*) and its Burgers vector  $\vec{b}$  (that gives the direction and the amplitude of the deformation caused by the supplementary plane) (6). In *edge dislocations*  $\vec{u}$  and  $\vec{b}$  are orthogonal, but *screw dislocations* also exist, with the two characterizing vectors that are parallel. Figure1 shows these two typologies of dislocations, but there are also combinations of edge and screw dislocations.

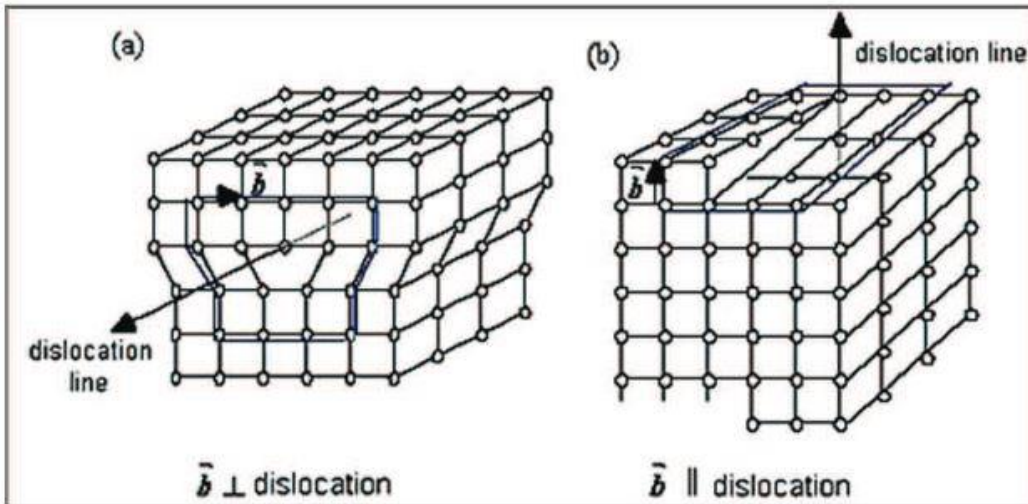


FIGURE 1: SCHEMATIC REPRESENTATION OF (A) EDGE AND (B) SCREW DISLOCATION.

In theory the Burgers vector could be any lattice vector but in nature this vector is almost always equal to the shortest lattice vector in the crystal and that is for minimizing the total energy stocked in the crystal (5).

Dislocations are responsible of the ductility in metal materials, in fact it's thanks to the movement of a great amount of these defects that the crystal lattice can get deformed under an external stress. Without the presence of dislocations, the mechanism of deformation would be the gliding among whole planes within a perfect crystal that requires a great amount of energy. A simple approach for calculating the shear strength  $\tau_0$  needed for that, in a material with shear modulus  $G$ , gives the following formula:

$$\tau_0 = \frac{G}{2\pi}$$

Since that  $G$  for metals is typically within the range of about 25 GPa to 200 GPa, the shear strength obtained from that formula is much bigger than the one observed experimentally for deforming such a type of material and that confirms the presence of another mechanism of deformation in metals.

Understanding the movement of a dislocation is a key to understanding how a metal really deform itself under a stress. In fact a chain of movements of a dislocation along a slip plane leads to the same result as a gliding of a whole plane on another, but the energy required is much lower. When a dislocation moves, the dislocation line slips on a close-packed plane progressively breaking boundaries with surrounding atoms and making new ones with the other neighbors, as showed in Figure2. In the case of the figure, the result is that a half plane of atoms is moved in response to shear stress by breaking and reforming a line of bonds (5). The energy required to break a single line of bonds is far less than that required to break all the bonds on an entire plane of atoms at once; this shows that plasticity is possible at much lower stresses than in a perfect crystal thanks to dislocation movement (7).

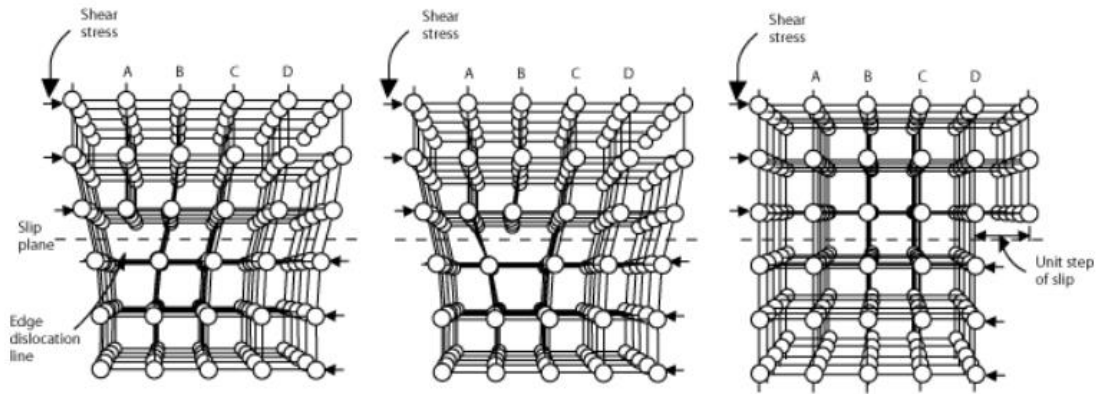


FIGURE 2: REPRESENTATION OF A DISLOCATION MOVEMENT.

Until the applied stress is in the range of the elastic domain dislocations don't move but, close to the yield stress, some dislocation in well oriented grains start to move and finally, when the yield stress is reached, all dislocations can move, and the material is effectively in the domain of plastic deformation.

The type, the vectors and the density characterize dislocations. The density is defined as the total length of dislocations in a volume ( $m/m^3$ ).

---

## STACKING FAULTS

---

Stacking faults are internal defects that disrupt the crystalline pattern over a surface within a crystal. For example, in a face centered cubic structure, the total structure is a repetition of three different types of planes A, B and C. Frequently, a deviation occurs and a plane slides and changes its types. The sequence presents a defect (for example, ...ABCABCABC... becomes ...ABCABABCAB...). Locally, the structure becomes hexagonal closed packed, which is a repetition of two types of plane A and B. Stacking fault are characterized by the energy (SFE for stacking fault energy) carried by the irregular planes (6).

## II. STRENGTHENING MECHANISMS IN METALS

---

As stated in the introduction, an effort in material engineering has been done in order to create mathematical models able to explain the mechanical behavior of materials. In this way, an accurate prediction of mechanical properties is possible starting from the knowledge of certain micro-structural parameters. This is the reason why it is important to have good techniques for characterizing them.

In a common metal, to predict the final yield stress, contributions of all present crystallographic defects have to be taken into account and summed to the intrinsic component in yield resistance, namely the Peierls stress ( $\sigma_0$ ). Two approaches can be used depending on the differences between defects type (7):

Considering that the plasticity of a metal is due to dislocations movements, when the needed strength for letting dislocations overcome different kind of crystallographic defects (which act as obstacles) is different, a simple sum is used.

$$\sigma_{tot} = \sigma_0 + \Delta\sigma_1 + \Delta\sigma_2 + \dots$$

When obstacles behave similar strength for being overcome, the addition will be quadratic:

$$\sigma_{tot} = \sigma_0 + \sqrt{\Delta\sigma_1^2 + \Delta\sigma_2^2}.$$

Clearly, the dislocation density is one of parameters that make a contribution in the final resistance of the material.

---

### DISLOCATION CONTRIBUTION TO THE YIELD STRESS: THE STRAIN HARDENING

---

It can seem paradoxical but, especially for high dislocation densities, the same defect that is responsible for the plasticity of metals can also act as an obstacle to it. Dislocations interact with one another and serve as obstacles which significantly impede their motion. This leads to an increase in the yield strength of the material and a subsequent decrease in ductility (7).

Since the dislocation density improves with the plastic deformation applied to the material, this hardening occurs with deformation. To value the hardening effect, the following formula can be used:

$$\Delta\sigma = M \alpha G b \sqrt{\rho} \quad (\text{Taylor equation})$$

Where  $M$  is the Taylor factor,  $\rho$  the dislocation density,  $\alpha$  is a dimensionless parameter which varies with the kind of material,  $G$  the shear modulus and  $b$  the Burgers' vector.

### III. ESTIMATIONS OF DISLOCATION DENSITY

---

This chapter aims at giving a global view on the existing methods to determine the value of dislocations density and at analyzing their advantages and issues.

#### 1. TRANSMISSION ELECTRON MICROSCOPY

---

Transmission Electrons Microscopy (TEM) is maybe the most traditional way to evaluate the dislocation density and to characterize them since it allows to visualize them under certain conditions. Anyway this method is really time consuming, not so easy to implement and it presents some issues (6).

First of all the preparation of the sample is very difficult, in fact it has to be thin enough to become electron transparent. There are many ways for preparing the sample and the chosen method will depend on the nature of the studied material. It is important to keep in mind that the preparation should not affect what it is observed and that is a real issue for the measurement of dislocation density, which vary when mechanical stress is applied and is affected by the presence of surfaces (7). Furthermore the local thickness of samples is often not constant and difficult to estimate.

Another disadvantage of TEM is that every grain has to be well oriented in the so-called two beams condition and that is time consuming; a really small number of grains can be characterized within a day (6). It is known that ductility in metals depends on the relative orientation of each grain with the deformation axis and, for this reason, measuring the dislocation density of a small number of grain could not be representative of the global behavior of the sample (6).

When the sample is oriented in a *two beams (TB)* condition there is only a kind of crystalline plane that is in diffraction condition and, when the visibility criterion  $\vec{g} \cdot \vec{b} \neq 0$  is respected, dislocations can be seen ( $g$  is the diffraction vector and  $b$  the Burgers vector). The reason of this behavior must be found in the local deformation of lattice associated with the dislocation, that lead to different diffraction conditions and so to a local non-transmission of the electron beam through the sample. As a consequence, the dislocation can be detected as a dark spot on the bright matrix (in a bright field imaging) as it can be seen in Figure3.

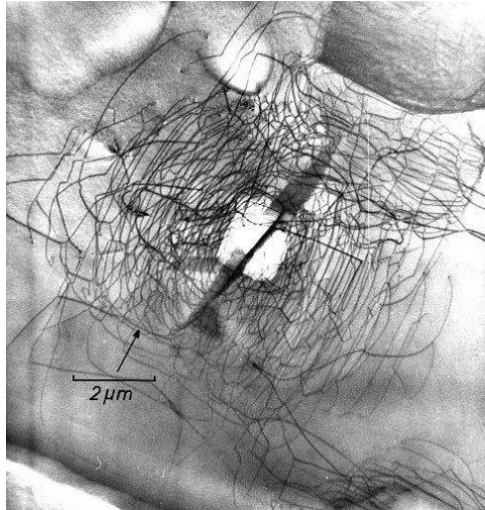


FIGURE 3: DISLOCATIONS IN A SILICIUM SAMPLE VIA TEM IMAGING.

For geometrical reasons, there are some conditions for which the dislocation cannot be seen even if the sample is in a two beam condition. When  $\vec{g} \cdot \vec{b} = 0$  an *invisibility criterion* is found. In that condition the diffraction vector and the Burgers vector are orthogonal as illustrated in the right part of Figure 4, and the dislocation loses its visibility.

Using two different extinction conditions, (two vectors  $\vec{g}$  perpendicular to  $\vec{b}$ ), the Burgers vector of the dislocation can be determined.

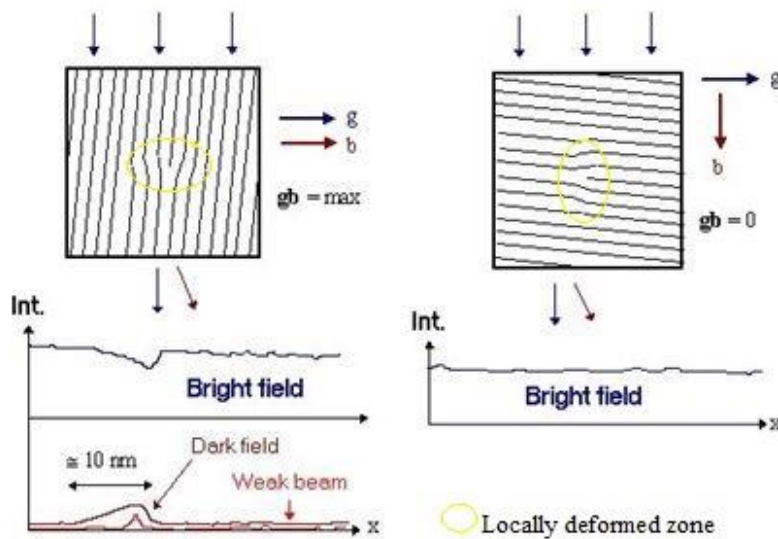


FIGURE 4: SCHEMATIC REPRESENTATION OF THE NON INVISIBILITY CRITERION (LEFT) AND THE INVISIBILITY CRITERION (RIGHT) IN WHICH DEFORMATION CARRIED BY A DISLOCATION DOESN'T AFFECT THE DIFFRACTION FOR ' $G_{HKL}$ ' PLANES.

Therefore, when observing one grain on a given two beam condition, if that grain contains different types of dislocations, some of them might be invisible, due to the invisibility criterion. If the dislocation density is determined from a simple counting of the apparent dislocations, an underestimation in dislocation density measurement will be made (6).

Moreover, the dislocation density measurement in TEM is dependent on the local thickness of the thin foil. This thin foil is usually not constant in thickness, and the

thickness determination is quite difficult. Therefore, combined with the extinction of some of the present dislocations, the measurement uncertainty is about one order of magnitude.

---

## 2. SEM-ECCI

---

Another way for visualizing dislocations is the Electron Channeling Contrast Imaging (ECCI) in Scanning Electron Microscopy via Back Scattered Electrons imaging (BSE) (2). The principle of the ECC is the dependency of the intensity of BSEs on the orientation between the crystal lattice and the primary electron beam (8).

Indeed, some angles between primary beam and the crystal provide a higher BSE intensity while other particular angles lead to a weak BSE intensity and so to darker images. These last cases are due to the fact that the electrons of the primary beam penetrate more deeply in the sample thanks to a channeling path within the lattice, therefore the fraction of back scattered electrons able to reach the BSE detector is lower. This channeling condition allows to see crystallographic defects; in fact, similarly to the case of TEM imaging, the presence of a defect locally affects the order of a crystal and so channeling conditions aren't respected in its surrounding of it (2). As a result a contrast between the dark matrix, in channeling conditions, and the defect is obtained, leading to a direct observation of dislocations or stacking faults.

Also for ECCI dislocation detection, the possibility of coming upon to invisibility criterion ( $\vec{g} \cdot \vec{b} = 0$ ) exists. That results really useful in characterizing the nature of a defect but also increases the incertitude of the calculation of the dislocation density; in fact, a fraction of the dislocations cannot be detected leading to an error in quantitative analysis.

This technique is known since the years '80 thanks to an overview published by Joy, Newbury and Davidson (9). Within the years great improvements have been performed both in the theory behind the technique and generally in the SEM analysis technique and nowadays ECC Imaging is really powerful. In the best experimental conditions amazing results are achieved, in fact the resolution of dislocations is comparable to that obtained by TEM analysis as illustrated in Figure5.

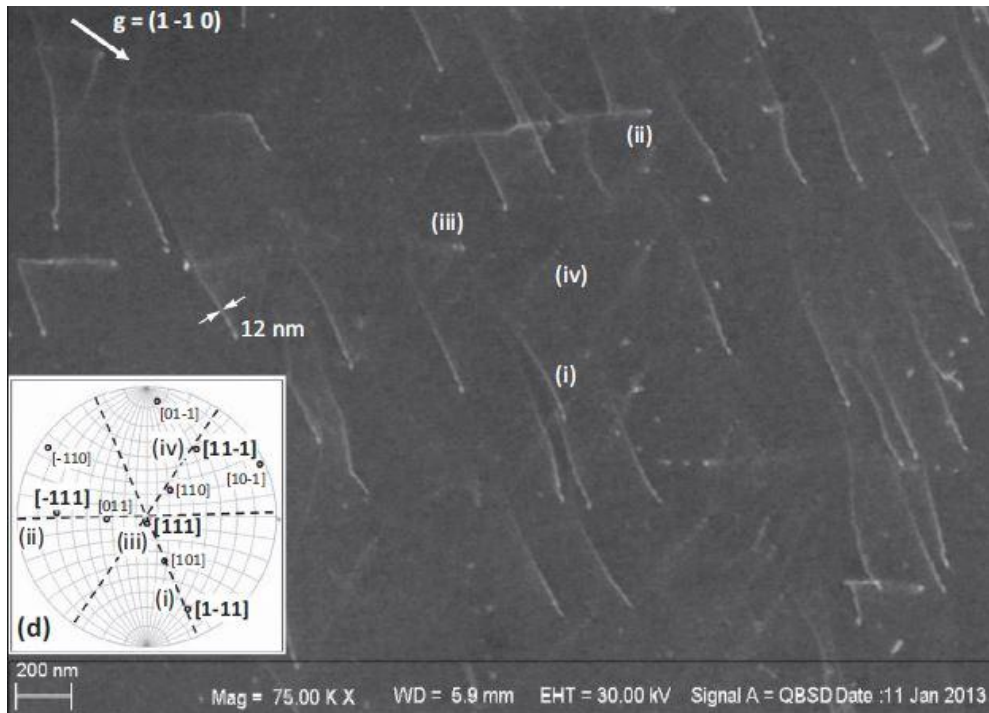


FIGURE 5: HIGHLY MAGNIFIED ECC IMAGE OF DISLOCATION IN BCC FE ALLOY. (FROM ZAEFFERER ET AL. (2) ).

It must be said that for obtaining this conditions a great work has to be done, in fact it is necessary to know the crystalline orientation of the analyzed grain for calculating the better tilt and rotation angles to apply to the sample. For this purpose the sample has to be submitted to an EBSD orientation analysis and, once the Euler's angles are known, computer simulations have to be performed for successfully tilting and rotating the sample. This is time-consuming and leads to issues that are similar to the TEM's ones, even if the preparation of the sample is much easier. Notably, analyzing a sufficient number of grains, in order to have statistically reliable results, becomes a hard job. Furthermore, the transition between the EBSD geometry (70 degrees tilted) and the BSE imaging one is delicate, and the scanned region cannot be lost.

Since the technique developed in this master's thesis is strictly correlated to ECCI, further information concerning the electron channeling contrast imaging will be given later.

### 3. GLOBAL TECHNIQUES

During the years, many techniques that allows to link a value of dislocation density to a global and easily measurable characteristic of a material have been developed. Some examples are shown here following:

- *Micro-hardness*: the increase of dislocation density brings to a hardening mechanism, that enlarge the elastic range of a material, consequently the plastic domain is reached for higher applied stress and so the hardness varies with the dislocation density. When a hardness measurement is taken, the smaller the indentation is, the higher is the hardness and so the higher is the dislocation density (6). This is called the indentation size effect (ISE) and can be used to find a value of dislocation density, using different models that have been developed. As

an example, in literature it is possible to find the Nix and Gao model (10) or the Ameri et al. one (11). It has to be taken into account that hardness doesn't depend just on dislocation density but other factors are involved.

- *X Ray Diffraction*: it is usually used to collect crystallographic information such as lattice parameters, crystalline structure and phase identification. Furthermore, a number of techniques based on analysis of X-ray diffraction peaks has been developed over the years in order to estimate the value of the dislocation density (6). Particularly, Malvika et al. have developed a method that studies the broadening of peaks and correlate it to a value of dislocation density, which actually finds a good fitting with the ones obtained with TEM analysis; in fact they are in the same order of magnitude (12). It is based on the analysis of tail portions of individual diffraction peaks and how they vary when the material is submitted to plastic deformation. Anyway is important to keep in mind that dislocation density isn't the only parameter influencing the shape of a peak, which is effectively dependent on many other factors such as the texture, the dispersion of grain size, the heterogeneity of chemical phases or possible distortions of the crystal lattice (6).
- *Differential scanning calorimetry (DSC)*: it is a thermoanalytical technique in which the difference in the amount of heat required to increase the temperature of a sample and a reference is measured. Hence, this instrument is able to directly measure energy stocked or accumulated by the analyzed material, in fact the energy required to keep both the reference and the sample at the same temperature is measured. It is known that heating to a sufficiently high temperature a material with dislocations leads to their rearrangement (recovery) or even to a recrystallization (in which dislocations are annihilated each others). These processes involve the releasing of energy associated with dislocations and this energy is measured. Thus, knowing the amount of self-energy of a dislocation, an estimation of the dislocation density can be achieved (13).
- *Electrical resistivity*: it is well known that crystallographic defects affect electrical proprieties in materials and the change of the electrical resistivity with the amount of dislocation is a great example. A dislocation is in fact a local breaking of the crystal potential periodicity and reduces the electron mean free path (14). As an example, Mohammad A. Omari et al. have documented that is effectively possible to link a value of dislocation density variation to electrical resistivity measurement (15). Anyway, to give a real value of dislocation density and not just a relative one, is necessary to know the value of dislocation density  $\rho_0$  before the plastic deformation. It must be said that resistivity depends on many other parameters such as the microstructure or the presence of impurities or other phases.

These indirect analyses are afflicted to an incertitude related to mathematical models describing the relationship between an experimentally measured parameter and the resulting dislocation density. Moreover, the experimental parameter is often dependent from many factors and it is a complex task to describe and separate accurately all the components. As a consequence assumptions have to be made and additional sources of error are added (6). Another problem is that for predicting the dislocation density, it is necessary to make hypothesis on the dislocations nature since that the value of the

Burgers vector  $\bar{b}$  is required in the mathematical formulas, leading to another systematic error.

## NECESSITY OF A NEW TECHNIQUE

An overview on mentioned techniques is shown in Table1.

*Table1: Recap of advantages and inconveniences of the different techniques*

	<b>Advantages</b>	<b>Inconveniences</b>
<b>TEM</b>	<ul style="list-style-type: none"> <li>&gt;Direct visualization</li> <li>&gt;Great spatial resolution</li> </ul>	<ul style="list-style-type: none"> <li>&gt;Possible invisibility of a fraction of dislocations</li> <li>&gt;Only local zone observed</li> <li>&gt;Tedious sample preparation</li> <li>&gt;Finding for optimal experimental conditions is time-consuming</li> </ul>
<b>Hardness measurements</b>	<ul style="list-style-type: none"> <li>&gt;Fast sample preparation and simple procedure</li> </ul>	<ul style="list-style-type: none"> <li>&gt;Low accuracy of hardness measurements at submicrometric scales</li> <li>&gt;Indirect method</li> </ul>
<b>XRD</b>	<ul style="list-style-type: none"> <li>&gt;Measurement on the whole sample</li> </ul>	<ul style="list-style-type: none"> <li>&gt;Several microstructural factors contribute to peak broadening and limitations in separating them out</li> <li>&gt;Indirect method</li> </ul>
<b>DSC</b>	<ul style="list-style-type: none"> <li>&gt;Measurement on the whole sample</li> </ul>	<ul style="list-style-type: none"> <li>&gt;Several factors contributes to the internal energy modification</li> <li>&gt;Indirect method</li> </ul>
<b>SEM-ECCI</b>	<ul style="list-style-type: none"> <li>&gt;Direct visualization</li> <li>&gt;Great spatial resolution</li> </ul>	<ul style="list-style-type: none"> <li>&gt;Possible invisibility of a fraction of dislocations</li> <li>&gt;Only local zone observed</li> <li>&gt;Finding for optimal experimental conditions is time-consuming</li> </ul>
<b>ELECTRICAL RESISTIVITY</b>	<ul style="list-style-type: none"> <li>&gt;Measurement on the whole sample</li> <li>&gt;Fast sample preparation and simple procedure</li> </ul>	<ul style="list-style-type: none"> <li>&gt;Several factors contributes to the variation of resistivity</li> <li>&gt;Indirect method</li> <li>&gt;Just a variation of dislocation density can be detected</li> </ul>

In conclusion it's clear that many ways for detecting dislocation density exist but each of them is related to issues that carry a significant incertitude and so this micro-structural parameter remains not well measured.

As said, all indirect analysis for detecting the dislocation density are affected by major incertitude concerns. To overcome this problem, direct analysis can be used even if also in these cases issues remains. Using TEM analysis, which actually is the most common technique, entails lots of time both for preparing the sample and for realizing a statistic analysis on a sufficient number of grains. Furthermore the value obtained could be inaccurate if some dislocations are under the invisibility criterion. Using the ECCI analysis

could be a good solution, in fact the sample preparation is much easier and even finding two beam conditions for detecting dislocations could be a little faster. Anyway the possibility of having certain dislocations under the invisibility criterion still remains and the analysis on a representative number of grains is far from being a fast process.

For all of these reasons, it is worth to investigate further in order to find a technique that allows a direct visualization of dislocations without any orientation information of the ROI and for a significant number of grains. Moreover, this technique should be able to overcome the problem of the invisibility criterion and not be time-consuming. As said in the introduction, the point of this study is to find a technique that meets all of these criteria by coupling ECCI to *CHORD*.

## IV. OVERVIEW ON THE INSTRUMENT

---

Since that both ECCI and eCHORD methods are performed on a SEM, it is worth to explain the main parameters that are involved while using such an instrument. A SEM electron beam can be firstly characterized as follow:

- **BEAM ENERGY:** it is the energy of electrons that hit the sample surface. It is usually measured in keV and a typical range of a SEM could be 1 to 30 keV, knowing that 1eV is the energy associated to electrons accelerated with a tension of 1V. The choice of the energy used affects the dimension of the volume of interaction between the primary beam and the matter, as showed in Figure6. Keeping constant the material, lower energy will generate a smaller volume of interaction and so detected electrons (both SE and BSE) will come from a smaller area, therefore the analysis will be more superficial and the resolution will be a little higher, on the other hand, the signal/noise ratio will decrease cause less SE or BSE would be generated.

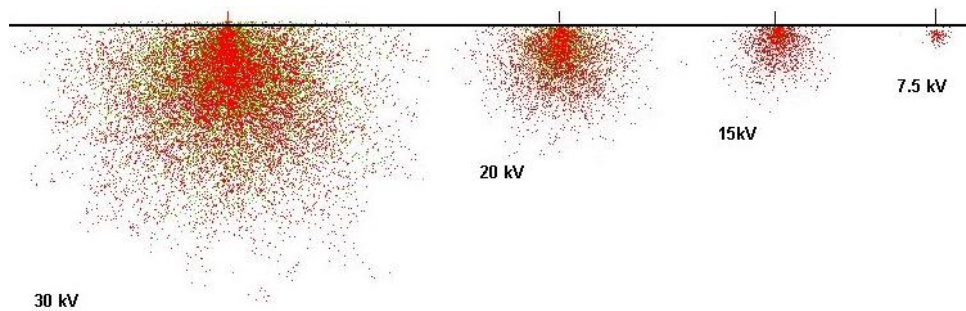


FIGURE 6: MONTECARLO SIMULATION OF THE VOLUME OF INTERACTION WHILE CHANGING THE TENSION APPLIED ON THE ELECTRON BEAM.

- **BEAM DIAMETER  $d_p$ :** it refers to the diameter of the beam as it impacts on the sample surface and It usually fall within the broad range of 1nm to 1 $\mu$ m. This parameter is related to the resolution of images.
- **BEAM CURRENT AND CURRENT DENSITY:** beam current ( $I_p$ ) simply characterizes the number of electrons per second that impact the specimen and is measured in fraction of Ampere, a typical SEM beam current could be of above 1 nA. Consequently, the current density ( $J_p$ ) is defined as the beam current per unit area, this parameter depends on and varies with the beam diameter that actually characterizes the area hit by electrons during the scansion. Since that this area varies when focus is changed, the current density will vary too.
- **APERTURE DIAMETER ( $d_{apt}$ ):** it is represented by the diameter of the final objective lens from which the beam goes out in the vacuum chamber, converging

toward the sample. This dimension varies depending on SEM model and the regulation chosen by the operator but it doesn't exceed the fraction of a millimeter.

- WORKING DISTANCE ( $W$ ): it consists in the distance between the final aperture of the objective lens and the point where the beam converges that, if the focus is achieved, is also the point where the beam lands on the sample ( $S$ ), as shown in Figure 7b.
- BEAM CONVERGENCE ANGLE ( $\alpha$ ): considering that the shape of the primary electron beam isn't cylindrical but rather cone shaped, the beam narrows from the final aperture of the objective lens to the specimen surface where it converge in a very small spot of diameter  $d_p$  (if well focused). The beam convergence angle describes how quickly the beam narrows to its focus and is well defined by a geometrical correspondence between  $d_{apt}$  and  $W$ , as shown in Figure 7a. Note that the representation has just schematic purposes and that in reality the cone is much sharper and narrower.

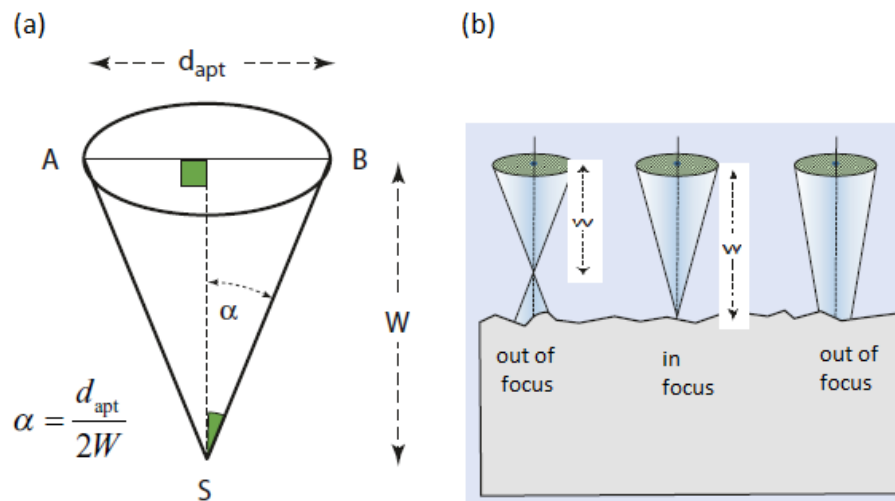


FIGURE 7: SCHEMATIC REPRESENTATION OF THE CONE SHAPED ELECTRON BEAM, WITH ITS TYPICAL DIMENSIONS (A) AND DIFFERENT SITUATION OF FOCUS(B).

- ELECTRON OPTICAL BRIGHTNESS  $\beta$  : it represents the intensity of the flux of electrons belonging to the beam, and considering that the beam has a 3D geometry, this parameter is measured as a current density per unit solid angle ( $A/m^2 sr$ ). In other words, two beams with same current, same beam diameter and therefore same current density, don't necessarily have the same brightness, in fact this parameter is maximized for the one with the smaller convergence angle, in which electrons are more "concentrated". On the other hand, if a beam is brighter than one other geometrically identically to the first, that means that it "carries" more electrons. An important characteristic of this parameter is that, keeping the beam energy constant, the brightness remains constant along the beam even if the lens setting is changed (16). Note that the main reason of the improvement in performances when a FEG SEM is used is that the optical brightness gets larger with this kind of electrons source.

Since the same kind of microscope has been used by Zaefferer et al. (2) while studying best parameters for seeing dislocation in ECC Imaging, the same parameters have been taken as reference within this work, even if some changes have also been performed in order to study performances.

Zaefferer et al. affirm that in order to achieve the best contrast and signal-to-noise ratio, while detecting dislocations via ECCI, the smallest possible beam convergence and beam diameter are needed, coupled with the highest beam current. In this way sharp two beam diffraction conditions are obtained and a good resolution is achieved too. An angle of convergence small enough can only be achieved with the presence of a field emission gun (FEG) as the source of electrons using a relatively small aperture diameter and a large working distance, anyway it has to be considered that this approach conflicts with the desired high beam current for a good signal/noise ratio. Indeed a compromise should be reached and so a working distance of 7mm with an aperture of 120 $\mu$ m have been chosen by Zaefferer et al., operating with the high current mode. Therefore, the following parameters were used: energy beam 15 keV, probe current above 9 nA, spot size above 3 nm, beam convergence 0.6°.

## V. ECCI, THEORY BEHIND THE BSE CHANNELING CONTRAST

As mentioned before, ECC imaging works thanks to the dependency of the detected BSEs intensity on the angle between the crystal lattice and the primary electron beam (8). With certain angles the backscattering yield is maximized leading to a bright image. With others, electrons of primary beam penetrate more deeply in the sample following channeling paths within the lattice and the backscattering yield fall, in that case less BSE are detected and darker images are obtained. It's in these conditions that it is possible to visualize dislocations and stacking faults.

Hence, it is normal to see a contrast between different crystalline grains in a BSE image, as it can be seen in Figure8(a), due to the different orientations of each grain with respect to the incident primary electron beam resulting in different backscattering contrasts. Always for the same reason is possible to see Electrons Channeling Patterns (ECP) when small working distance and lower magnification are used in SEM imaging of a monocrystal. In fact, in these conditions the scanning procedure has a significant impact on the angle between sample and primary beam and that will lead to a channeling contrast also within different scanned points of a single crystalline grain (see figure8(b) ) (8). These patterns are similar to Kikuchi lines from the EBSD analysis (see Figure8(c) ) and it is thought that dark lines on the side of a band, namely Kikuchi lines, correspond to a lower backscatter signal and that is interpreted in terms of channeling of the primary beam along particular crystal directions (2).

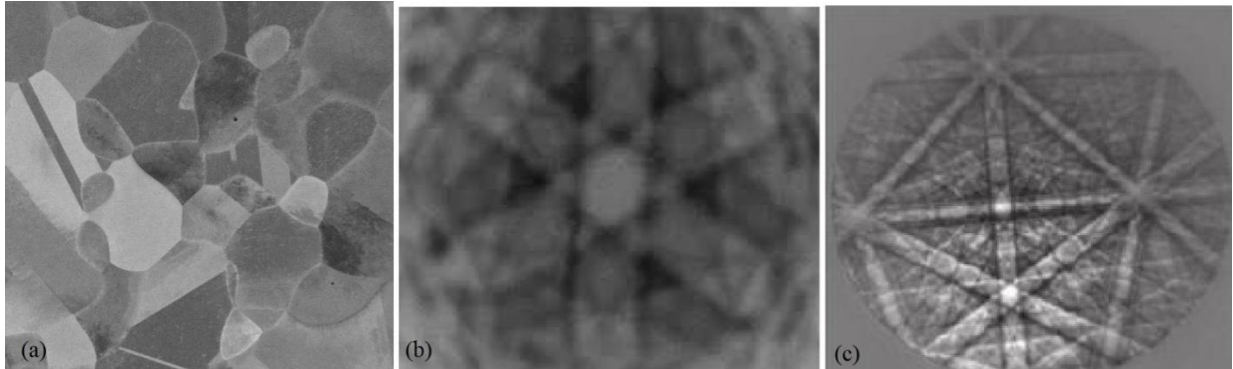


FIGURE 8: EXAMPLES OF CHANNELING EVENTS. BSE ORIENTATION CONTRAST (A), ELECTRON CHANNELING PATTERN WITHIN A CRYSTAL (B), IN WHICH THE ROCKING OF ELECTRON BEAM LEADS TO A VARIATION OF THE ANGLE WITH THE SAMPLE, AND KIKUCHI FIGURES (C), NAMELY INELASTIC SCATTERING PATTERNS COMING OUT FROM A SCANNED POINT AND THEN DETECTED.

In order to explain these contrasts, a closer examination of the interaction between high energy electrons and solid matter needs to be done. As Zaefferer and al. discussed, electrons of the primary beam are subject to different scattering mechanisms that could be resumed as following (2):

- *Bragg scattering*: elastic and coherent. It leads to a lattice-periodic density distribution of electrons and, consequently, to a conventional Bragg diffraction  $\theta = \theta_B$ .
- *Phonon scattering*: quasi-elastic but incoherent. Consequence of the interaction between electrons and the vibrations of lattice planes.

- *Core-loss scattering*: Inelastic and incoherent. It is due to a group of different inelastic and incoherent processes that occur close to the atomic nuclei and it correspond to the formation of electromagnetic radiations, plasmons and secondary electrons.

Inelastic and phonon scattering events combine each other to form a chain of scattering events so called *multiple scattering*.

Two different kind of channeling events have to be distinguished:

- *Channeling IN*: is the one responsible of the different amount of BSE detected according to the angle between sample and the electron beam. When the primary beam hit the sample with a specific angle, is coherently and elastically diffracted to form a single and coherent Bloch wave. That wave loses intensity while going deeper in the sample and this is due to the multiple scattering (inelastic) that occurs in every direction. As a consequence, a fraction of the electrons of the primary beam is retro-diffused (backscattered) toward the sample surface and can actually reach the BSE detector giving a signal. The intensity of that signal is obviously related to the intensity of multiple scattering events that vary with the angle between the crystal lattice and the Bloch wave (and so the primary beam), as explained later, leading to channeling contrast.
- *Channeling OUT*: This phenomenon is the one taken in charge by the theory behind Kikuchi figures. Basically, as said before, the primary beam undergoes to incoherent scattering and, since that it happens toward every direction, many Bragg conditions are achieved with different types of lattice planes. That leads to the propagation of many coherent Bloch waves along specific directions through the sample and, when is possible to detect them, a Kikuchi figure is then collected. So these figures are the result of the diffraction of the backscattered electrons within a crystalline lattice.

The main difference between ECPs and Kikuchi images is the setting of the experiment; two different geometries are indeed involved.

In ECP imaging (figure9 left) the channeling 'IN' is involved. The sample is not tilted and, as usual, a variation of the angle between the crystalline lattice and the primary beam is needed to produce a contrast within the scan of a single crystal. Historically, the first observation of an ECP was made by simply running the instrument at its lowest magnification and at small working distance, that effectively leads to a variation of the angle during the scan (9). Therefore, contrast in the resulting image is influenced by channeling (2). BSEs, originated by the scattering of primary electron beam, come out with intensity proportional to the scattering rate and so linked with the scan angle of the electron beam. Anyway, to obtain a good ECP image, a large scanned area is needed in order to enable the scanning beam to cover a sufficient angular range and so to obtain a contrast. Nowadays, in some microscopes (Tescan microscopes) a system that allows to vary the angle between the sample and the beam without changing the scanned point is implemented (precession system). That leads to the possibility of obtaining ECP images even for smaller ROI.

For having a Kikuchi figure the sample is highly tilted (around 70 degrees) and so the interaction volume is cut by the surface of the sample, as seen in the right part of Figure 9. In this way diffracted Bloch waves of BSE, which compose a Kikuchi figure (see channeling OUT explained above), cross a smaller volume of the sample before reaching the surface. As a consequence, incoherent and inelastic core-loss scattering interactions between BSE and crystalline lattice are reduced and the crystalline information is kept. In these conditions is effectively possible to detect these diffraction patterns, known as Kikuchi figures, for every scanned point in the sample with the help of a phosphor screen or a diode detector. These patterns are mainly used in EBSD analysis for detecting orientations of crystalline grains, in fact every scanned point will be related to a Kikuchi image and so to an orientation.

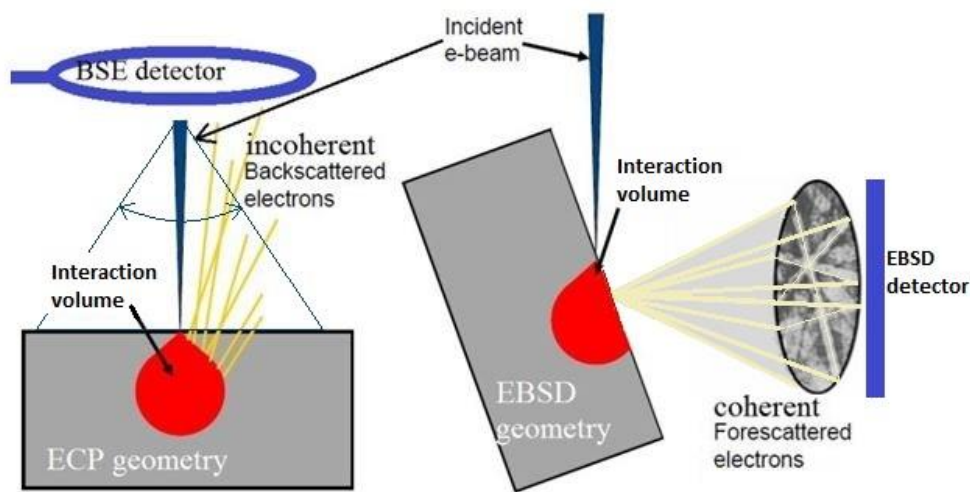


FIGURE 9: DIFFERENCES BETWEEN EXPERIMENTAL SETS UP IN SEM FOR OBTAINING ECP FIGURES (LEFT), THE SET UP IS EXACTLY THE SAME AS TRADITIONAL BSE IMAGING, AND EBSD ANALYSIS (RIGHT) IN WHICH KIKUCHI FIGURES ARE INVOLVED.

ECCI technique uses EBSD analysis just for have the orientation of a given crystal in order to know how to move the sample for having best orientation conditions, namely two beam conditions, and therefore seeing crystallographic defects such as dislocations. Note that the detection of defects is done with the BSE imaging analysis and not with EBSD.

As said, the contrast formation in BSEs imaging is due to the channeling "IN" phenomenon. The primary electron beam is coherently Bragg-scattered to form a single Bloch wave field that propagates through the sample. A key point for understanding the phenomenon is that backscattering is a result of the interaction of this wave field with the potential of the crystal lattice, since this wave field changes its shape depending on the angle between the primary beam and the crystal surface (see Figure 10b) different inelastic backscattering yields will be produced with different angles, as described by Zaefferer and al. (2). In particular backscattering is maximized when the wave peak superposes with atomic nuclei. Effectively, while propagating through the sample, the Bloch wave field loses its intensity after a chain of multiple scattering events caused by the above mentioned interactio. It is because of such scattering events that some electrons of the primary beam are incoherently backscattered out of the sample, giving a detected signal and so impacting on the contrast of the scanned point. Since the BSE intensity is proportional to the total electron density found at the atomic nuclei (multiplied by the scattering cross

section of the respective atoms) (2), and since the electron density found at atomic nuclei is linked to the angle between the primary beam and the crystal lattice, the crystal orientation in the microscope reference system is well related to the channeling contrast.

Around the Bragg diffraction condition, in which  $\lambda_e = 2d_{hkl}\sin(\theta_B)$ , backscattering intensity vary significantly (see Figure11) with the deviation parameter  $w$  (2). This parameter represent the angular deviation of the primary electron beam wave vector  $k_0$  from its exact Bragg position for a given set of planes, characterized by a reciprocal lattice vector  $g_{hkl}$  (see Figure10(a) ) (2). Knowing that  $\alpha$  is the angle included between  $k_0$  and the excited set of lattice planes, three main conditions are possible:

- “ $w = 0$ ” indicates that the primary beam is exactly in Bragg condition.  $\alpha = \theta_B$ .
- “ $w < 0$ ” indicates that the primary beam is closer (more parallel) to the lattice planes with respect to the Bragg condition.  $\alpha < \theta_B$ .
- “ $w > 0$ ” indicates that the primary beam is further away from the lattice planes.  $\alpha > \theta_B$ .

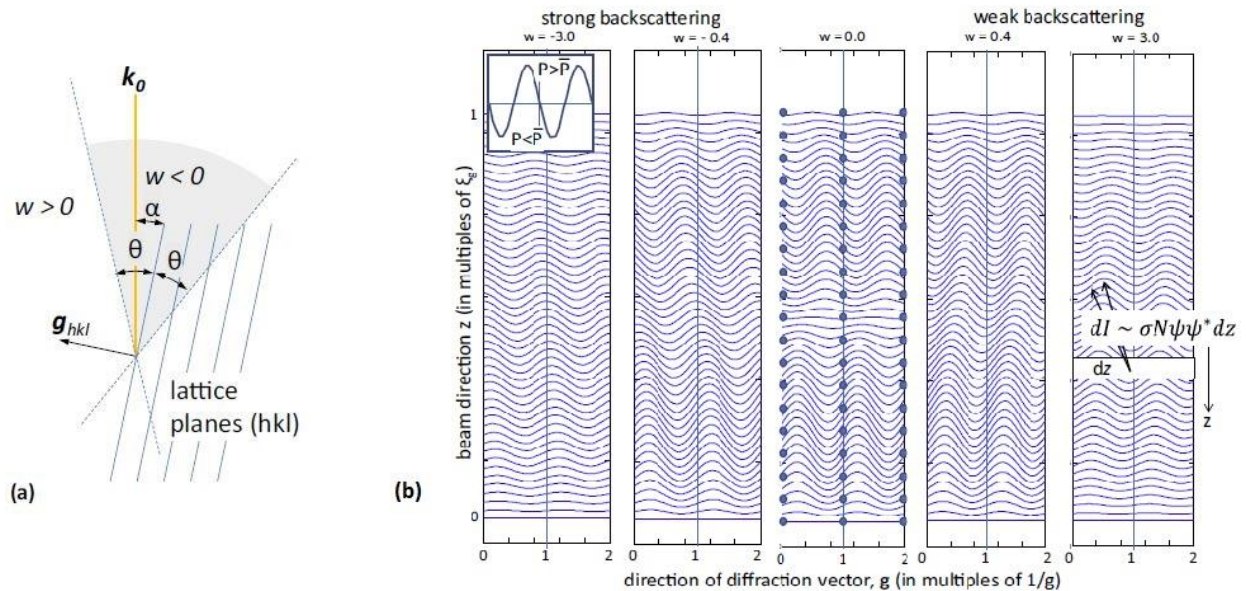


FIGURE 10: (A) SCHEMATIC DRAWING INDICATING THE MEANING OF THE DEVIATION PARAMETER ‘ $w$ ’. (B) SPATIAL DISTRIBUTION OF THE TOTAL ELECTRON DENSITY CALCULATED FROM A TWO BEAM BLOCH WAVE MODEL FOR DIFFERENT DEVIATION PARAMETERS, IT IS SHOWN THAT MAXIMUM DENSITY ON THE ATOM NUCLEI IS OBTAINED FOR WEAK NEGATIVE VALUES OF  $w$  ( $<0.5$ ) AND MINIMUM INTENSITY FOR WEAK POSITIVE VALUES OF  $w$ . (FROM ZAEFFERER ET AL. (2))

As said, the intensity of BSEs emitted from the sample surface is proportional to the density of electrons at the atomic nuclei, and this value depends on  $w$  if diffraction conditions are close to the Bragg condition, as predicted by Zaefferer et al. For this reason is possible associate to specific values of  $w$  a situation of strong backscattering or a situation of weak backscattering, *i.e.* a channeling situation. In particular for  $w < 0$  intensive backscattering occurs and, when the deviation parameter grows toward positive values, the intensity decreases rapidly from a maximum to a minimum value where channeling conditions are achieved (2). If an ECPs is taken this will lead to the formation of a Kikuchi band (see Figure11), representing the diffracting plane for a given

Bragg condition and, if the Bragg condition refers to a single set of planes, the darker Kikuchi line will refer to a two beam condition.

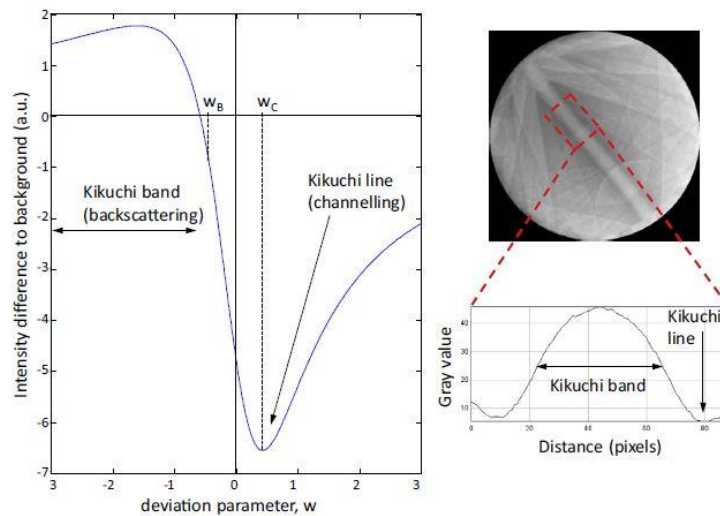


FIGURE 11: BACKSCATTERING INTENSITY DEPENDENT ON  $w$  FOR TWO BEAM CONDITIONS.  $w_c$  INDICATES A CHANNELING CONDITION AND  $w_B = -w_c$  A BACKSCATTERING CONDITION. THE PLOTTED CURVE REPRESENTS ONE HALF OF A TYPICAL TWO BEAM PROFILE OF A KIKUCHI BAND.

Knowing that the contrast in BSE imaging is strictly related to the crystalline order and disposition within the space, the fact of seeing the effect of an interruption in crystalline order, namely a crystalline defect, is not astonishing. As said, if the crystal is illuminated in channeling conditions ( $w = w_c$ ), the electron density is highest between the atoms nuclei, but in the surrounding of a crystal defect the situation changes. As showed in Figure12, in these zones atomic columns aren't perfectly aligned and that involves that the electron density below a dislocation or a stacking fault will be highest along the atom columns, if the assumption that the atoms are shifted by exactly half an atomic plane distance is taken (2).

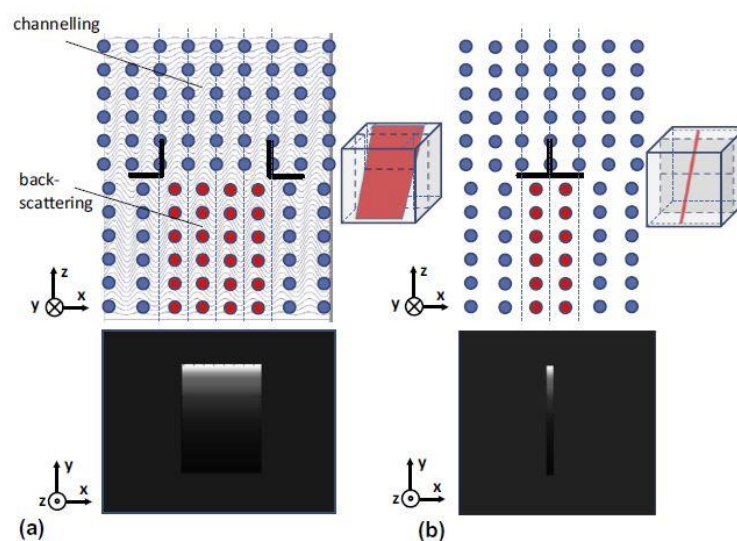


FIGURE 12: REPRESENTATION OF BLOCH WAVE THEORY FOR THE FORMATION OF DEFECT CONTRAST FOR (A) A STACKING FAULT AND (B) AN EDGE DISLOCATION. THE BLOCH WAVE FIELD ENTERS THE PERFECT CRYSTAL IN CHANNELING CONDITIONS AND PASSES UNDER STRONG BACKSCATTERING CONDITIONS BELOW DEFECTS. (FROM ZAEFFERER ET AL. (2))

So using ECCI in SEM, it is possible to observe crystalline defects with a great spatial resolution and they are visible through the sample for a thickness that is about five times a parameter called extinction parameter (that depends on sample composition and accelerating voltage used). Therefore, the visibility of defects under the surface may vary between 50 and 100 nm, for usual SEM conditions (2). The contrast of an edge dislocation is similar to that of a stacking fault, but confined to a much narrower width, in fact the atomic arrangement for these two kinds of defects is very similar. It is found that also for a screw dislocation the contrast is similar to other cases, in fact the lattice planes are also shifted by half a lattice vector above and below the dislocation line (2).

As a consequence strong backscattering condition around a defect ( $w = w_b$ ) are achieved even if the matrix is effectively in channeling conditions. For this reason a contrast is achieved between matrix (in dark) and a defect (bright), which can consequently be detected as shown in Figure 5. More specifically, even if more difficult to detect, another scenario exists, in which the dislocation is in channeling condition and appears dark whereas the matrix is bright under high backscattering condition.

As mentioned, also in ECCI detection of defects the invisibility criterion can be achieved, in which shifted lattice planes doesn't show any deformation along the direction of their normal vector (parallel to  $g_{hkl}$ ) and so  $\vec{b}$  will not have any components along that direction and consequently  $\vec{g} \cdot \vec{b} = 0$ .

It has to be said that a long time for orientating the sample is needed and that is a real issue for having statistic results thanks to detection on many grains. Briefly two options for finding dislocations contrast conditions can be used. If the used microscope allows the rocking of the primary beam to obtain an ECP (precession technique on Tescan), then the sample can be tilted and the rotated in order to fit a dark Kikuchi line through the center of the pattern for having channeling conditions, after that the microscope is switched into imaging mode and defects should be visible (2). The second method is longer but more common, is used in microscopes that don't allow the rocking of the beam or in which the spatial resolution of the rocking beam isn't enough (2). It consists in making an EBSD orientation maps and using this information for simulating the ECP of the analyzed grain with a computer program called "TOCA", subsequently it is also used to determinate tilt and rotation for an optimal experimental condition (2). Performing this last method, care has to be taken in order not to lose the zone while changing the experimental geometry from the EBSD to the ECCI. Furthermore, this variation leads to errors since both stage tilting/rotating accuracy and alignment of the stage with respect to the EBSD detector carries an uncertainty (2). For this reason the perfect condition to achieve channeling condition is time-consuming and could be difficult to find. These issues lead to the development of ECCI under controlled diffraction conditions, namely c-ECCI.

## VI. CHORD METHOD

---

In 2011, C. Langlois (17) from MATEIS laboratory (INSA Lyon), started to work on an idea based on a previous work of Yahiro et al. according to which the orientation of a grain could be retrieved from the variation of intensity observed during a tilt series of the sample. The idea was to illuminate the sample with an ion beam and collect a stack of images during the sample rotation. The evolution of the Secondary Electron Channeling over the rotation angle could then be used as a signature for each grain orientation. The method was named iCHORD for ion CHanneling ORientation Determination. Few years later, the method was adapted for electron channeling in a conventional SEM equipped with a BSE detector and named eCHORD for electron CHanneling ORientation Determination (Lafond et al 2018).

The great advantage of a similar method would be to have the possibility of obtaining orientation information without an EBSD detector (17) and so keeping simpler the acquisition geometry. That involves advantages such as a larger scale of movements of the sample and the eventuality of having a 3D indexation of the sample, with the use of an ion beam (18).

---

### CHORD EXPERIMENTAL SET UP

---

The key of the CHORD technique is to obtain a channeling 'IN' contrast profile of the analyzed ROI that describes how this contrast varies with the variation of the angle between the primary electron beam and the crystal lattice. Indeed, it is necessary to have an experimental set up that allows this angle to vary in order to collect a set of images for different angles and, as a consequence, with different channeling contrasts. It is from such stacks of ECC images that, after an efficient image processing, it's possible to extrapolate the contrast profile of a given point in the sample, related to the crystalline orientation (18).

To progressively vary the angle during the acquisition of a stack of images, the sample is firstly tilted at  $10^\circ$  and then rotated from 0 to 360 degrees, as seen in Figure 13a. An image is then taken at each step of rotation (0.5, 1 or 2 degrees according to the purpose) (18).

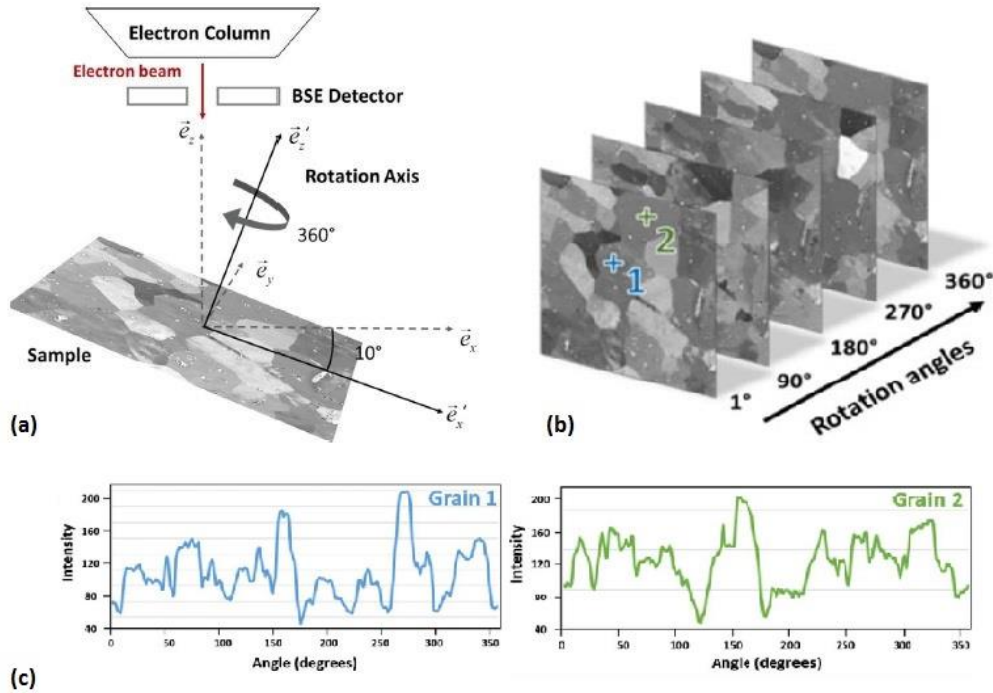


FIGURE 13: (A) SAMPLE SET UP, THAT LEAD TO A VARIATION OF THE CHANNELING CONTRAST DURING THE ACQUISITION OF A CHARACTERISTIC STACK OF ECC IMAGES (B) USED IN THE DETECTION OF GRAINS' ORIENTATION, TO EVERY PIXEL IS ASSOCIATED A CHANNELING CONTRAST PROFILE (C). (FROM LAFOND ET AL. (18))

Depending on the resolution needed, and so on the parameters used during the scan, a complete rotation can take anywhere from few minutes to few hours, with the best compromise that must be found in each analysis, according to the purpose. To make a stack, all images are stacked together in ImageJ software, then denoised and aligned (18) in order to link every pixel of the stack to a single real point of the sample. In this way the extrapolated contrast profile of a pixel of the stack can effectively be considered representative for a given point of the sample.

Examples of experimental profiles related to a pixel are given in Figure13c, and from such profiles the orientation can be recovered as explained below. Briefly an experimental profile is compared to many others that have been simulated for a reasonable number of crystalline orientations, this number must be big enough to represent the whole spectrum of orientations of the crystal, obviously, the bigger is and the longer will be the simulation. All the orientations taken into account are statistically sampled using symmetry operations of the crystal within specific algorithms. As an example, good results are obtained for FCC structures when one million of orientations are simulated (mean disorientation between neighbors of  $0.5^\circ$ ), but a different crystalline structure leads to a different result, in fact others symmetries are involved (18). Once obtained a set of simulated profiles, the most similar to the experimental one is taken as a reference for giving the orientation of the analyzed pixel (see Figure14b).

In order to obtain simulated profiles starting from whatever orientation is necessary to pass through the simulated ECP belonging to such orientation. In fact, in an ECP the diffraction intensity is plotted as a function of the orientation of the primary beam relative to the crystal normal, with stereographic projection representation (17). The center of the

ECP (point P in Figure14a) corresponds to a situation in which the normal is parallel to the beam ( $\vec{e}_z // \vec{e}_z'$ , see Figure13a) and to vary the physical tilt angle corresponds to a translation shift in the ECP stereographic representation (P to P' in Figure14a). Finally, the simulated intensity profile, as a function of the rotation angle, corresponds to the grey intensity collected along the perimeter of a circle with a radius corresponding to the applied tilt and centered in the center of the ECP (18), as showed in Figure14a. ECPs are calculated using EMsoft simulation suite from De Graef et al. (19). For speeding up the process, nowadays simulated ECPs are not completely computed, but only the part concerning to the perimeter of the tilt-circle, and so linked to the profile, is simulated.

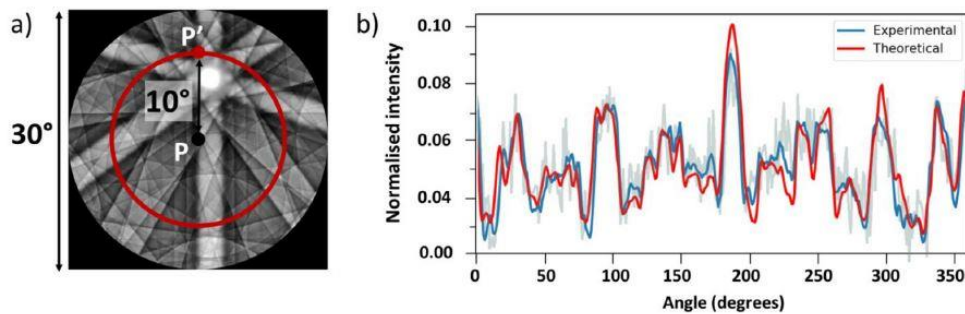


FIGURE 14: (A) SIMULATED ECP FOR GIVEN EXPERIMENTAL PARAMETERS (15 KV, FCC SIMMETRY) AND ORIENTATION (EULER'S ANGLES: 300.7°, 40.6°, 6.7°). THE RED CIRCLE CORRESPOND TO THE BEAM PATH WHEN THE SAMPLE IS TILTED AT 10° AND THEN ROTATED FROM 0° TO 360°. THE INTENSITY VARIATION ALONG THIS CIRCLE ALLOWS OBTAINING THE SIMULATED PROFILE (B), WHICH HAS TO BE COMPARED TO THE EXPERIMENTAL ONE. (FROM LAFOND ET AL. (18))

Note that the angular variation along the rotation (0° to 360°) is collected along the tilt circle starting to the point P' of Figure16a and anticlockwise.

In summary, to every simulated orientation is correlated an ECP and so a contrast profile, which is compared to the experimental one. When a simulated profile fits to the experimental one, the orientation is found. Moreover, a gaussian filter is applied to the ECP in order to take into account the fact that the electron beam is not perfectly parallel but is cone shaped. This lead to an intrinsic incertitude of the angle between electron beam and sample, basically, the real crystalline information achieved, comes not just from a single point on the circle drawn on ECP, but there is an influence of the surrounding points representing the little angular variation that the shape of the electron beam carries (18).

A real issue while performing this technique is to keep the ROI well centered with the real scanned area during the rotation. It is found that, even for low magnifications, the zone to be analyzed has a significant tendency to leave the "view field" of the SEM and that is correlated to a misalignment between the ROI and the rotation axis of the SEM stage (17). In order to overcome this problem many solutions could be taken; the ROI can be re-centered for every rotation step, but that's the longer and less efficient solution. Another way could be the centering of the ROI with the rotation axis of the microscope stage, but that carries some issues. Effectively, to fit this axis, the sample has to be in the center of the rotating stage and the ROI cannot be changed without opening the microscope chamber and physically moving the sample, therefore the view field that can be effectively used during the analysis is significantly reduced. Using the compucentric mode, that

allows to automatically re-center the ROI following a rotation or a tilt variation, is another solution but this system isn't implemented in all microscopes and it could not be well performing with the high magnification used for dislocations detection. MATEIS laboratory researchers started their work using the compucentric mode till they found a better solution: they implemented a custom-made sub-stage (shown in figure15) that allows centering the rotation axis with almost whatever zone of the sample, without the need of opening the vacuum chamber of the microscope (17). This result has been achieved by simply putting the X-Y translation system above the rotational one, the opposite of traditional SEM stages.

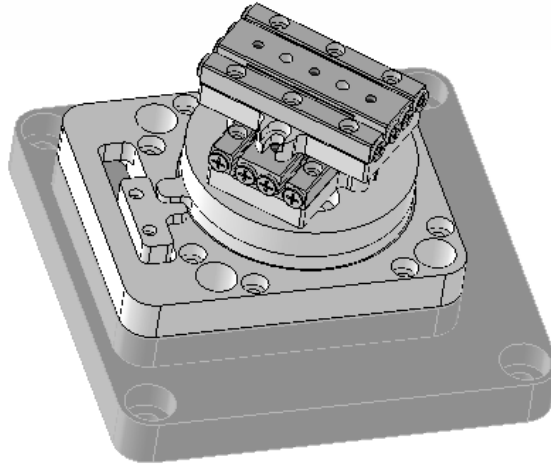


FIGURE 15: IMPLEMENTED SUB-STAGE MADE BY SMARACT.

Another improvement carried by the sub-stage has been the better translation and rotation precision achieved using a piezoelectric moving system instead of one based on gears. Furthermore, the acquisition time during a rotation is highly reduced.

---

## CHORD PERFORMANCES

---

To verify the efficiency of the technique, EBSD results in indexation have been taken as a reference, this technique is effectively the primary one for what concerns this kind of analysis. Anyway it has to be said that, similarly to c-ECCI, differences between EBSD and CHORD experimental geometry (the tilt angle) also impact on differences between EBSD and eCHORD results, which depend on stage tilting accuracy. Anyway, almost all grains are correctly indexed with a main error inferior to 1 degree. CHORD method is then able to reach a good accuracy in indexation crystalline orientation and it has shown excellent performances also in phase discrimination of multiphase materials (17).

Moreover, eCHORD could have a better spatial resolution than EBSD, in fact in the last months promising results are being obtained for what concern indexation with low beam voltage, typically 5 kV or even less (channeling contrast has been detected at 1.5 kV, with perfect experimental conditions). This is not possible in EBSD orientation mapping, that requires voltage of 7 kV or more in order to obtain Kikuchi figures. The voltage value affects the size of the volume of interaction between electron beam and sample, and low voltage leads to smaller volumes and so to higher resolutions. Furthermore, EBSD geometry entails a bigger intersection between interaction volume and sample surface

(see Figure 9) and that means that the collected signal comes from a larger portion of the sample; for this reason spatial resolution is better in eCHORD even using the same voltage.

For what concerns the time needed for the analysis, it can vary a lot according to the desired quality that clearly depends on the purpose of the analysis. For example nowadays, to collect a stack of 360 images, one minute could be enough for a bad quality orientation maps but the main time of a typical acquisition is something like 10-15 minutes. If a high image quality is needed, and that is the case of stacks for the crystalline defects characterization, the experimental collection of data can take more than one hour. It has to be said that the quality of the used microscope affects significantly the performance. Also the data treatment needs time in fact, even if the indexation is really fast ( $\sim 500$  experimental profiles indexed per second) (18), the ECP database generation is much longer and depends on the crystalline geometry. C. Lafond et al. (18) showed that to make one million database in a FCC crystal takes 45 min on 8 cores Intel®Core i7-CPU @ 2.60 GHz workstation. As already said, modifications have been done and nowadays generating such a kind of database take just a few minutes. Moreover, a database can be stored and reused if others analysis with same material and experimental conditions are done. However, complicating the crystal geometry could significantly affect the computing time.

---

## ORIENTATION MAPS

---

Results for both CHORD and EBSD analysis can be shown thanks to an orientation map. The orientation with respect to a fixed reference system is described by Euler angles: three angles that are associated to as many elemental rotations. If the three axis of the reference system are denoted as  $x,y,z$  and the three axis of the moving system as  $X,Y,Z$ , as shown in Figure18, Euler angles are described as follow:

- $\varphi_1$  (from  $0^\circ$  to  $360^\circ$ ): is the angle between the  $x$  axis and the projection of the  $X$  axis on the plane  $xy$ , namely  $x'$ . It represents a rotation around the  $z$  axis. The reference system after this rotation is called  $x',y',z'$ .
- $\Phi$  (from  $0^\circ$  to  $90^\circ$ ): is the angle between the  $z$  ( $= z'$ ) axis and  $Z$  axis. It represent a rotation around the  $x'$  axis. The reference system after this rotation is called  $x'',y'',z''$ .
- $\varphi_2$  (from  $0^\circ$  to  $90^\circ$ ): is the angle between the  $x'$  axis and the  $X$  axis. It represent a rotation around the  $z''$  axis. After this last rotation the moving system  $X,Y,Z$  is achieved.

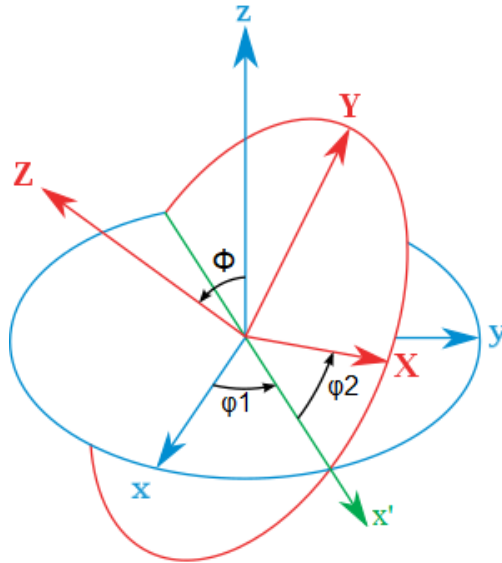


FIGURE 16: GEOMETRICAL DEFINITION OF EULER ANGLES. THE FIXED SYSTEM IS SHOWN IN BLUE AND THE ROTATED SYSTEM IS SHOWN IN RED.

In an orientation map, to every crystallographic grain is associated a color thanks to which it is possible to find Euler's angles. In fact, every grain has a color represented in the RGB color system, an additive model in which the three primary colors (Red, Green and Blue) are added together in various proportions to reproduce a broad array of colors (up to 16 millions). Hence, for the color associated to every grain, it is effectively possible to make a relationship between three Euler's angles and each value associated to every one of the three primary colors, that goes from 0 to 255 (8bit):

$$\varphi_1 = R * \frac{360}{255} \quad \Phi = G * \frac{90}{255} \quad \varphi_2 = B * \frac{90}{255}$$

where R, G and B represent the intensity value of each one of the primary colors used to define the color of the grain and therefore its orientation.

## VII. SIMILARITIES BETWEEN DIS-CHORD AND CHORD

---

It must be said that this master's thesis puts its own foundations on CHORD researchers' experiences, in fact, the technique used for the stack acquisition is exactly the same of the one used in eCHORD analysis. It is thanks to the sub-stage that has been possible to achieve experimental stacks and the experience of the CHORD team has been really useful for understanding how to reach an image quality good enough to see crystallographic defects such as dislocations and stacking faults. However, critical experimental conditions that the purpose of this work requires, such as the great magnification, have made necessary to develop certain aspects of the experimental technique and to study the best parameter to use for reaching satisfying results.

Moreover, the knowledge of CHORD researchers in images alignment and denoising led to the possibility of obtaining good quality channeling profiles, thanks to which the clustering program has been able to discriminate dislocations by matrix and a quantitative evaluation of their density have been possible. Finally, eCHORD indexation can also allow identifying the vector  $g_{hkl}$  which characterize the diffracting plane family in TB conditions, and that might be really useful to investigate on Burgers vector associated to dislocations.

---

### E-CHORD STACKS ACQUISITION PROTOCOL

---

As mentioned, R-ECCI stacks are acquired exactly in the same way of eCHORD stacks, indeed the detector used is the BSE one and channeling conditions are searched. Thus, it is worth to better explain how these rotational stacks are achieved.

1. SEM is switched on.
2. Sample is positioned on the rotating sub-stage
3. Sub-stage is installed in the SEM sample chamber and linked to the dedicate controller through a cable.
4. The sample chamber is closed and the void is made in it; some minutes are needed.
5. Stage parameters (working distance and tilt angle) are set up.
6. The primary beam is turned on, choosing the beam energy and the aperture diameter.
7. BSE detector is switched on, focused on the sample and a suitable area is chosen.
8. The ROI is centered with the rotation axis of the microscope sub-stage, using the dedicated controller. A virtual grid, identical to the one showed in Figure17, is added to the scanned image and a recognizable reference point is moved toward the center of this grid thanks to a translation of the sub-stage, using the controller. At this point a rotation of the sub-stage is performed in order to find the rotation axis around which the chosen reference point is moving. Once approximately identified this rotation axis, it is centered in the center of the grid, this time thanks to a translation of the *total* stage of the microscope. This process is done many times going further with the magnification, and so choosing smaller reference points each time, in order to reach the better precision as possible. A good result is achieved when, performing a rotation of the sub-stage, no translation of the chosen reference point is observed, i.e. it remains in the center of the grid just rotating on itself. This result must be reached at least at the

magnification used in the eCHORD analysis, that depends on the purpose of the analysis.

9. The best focus and astigmatism regulations are found, in order to obtain the best possible image quality. If crystallographic defects are searched in the analysis, adjustments have to be done referring to one of them.
10. The automatic acquisition of the stack is launched, once chosen the acquisition time, the resolution and the rotational interval angle (e.g.  $1^\circ$  or  $2^\circ$ ).

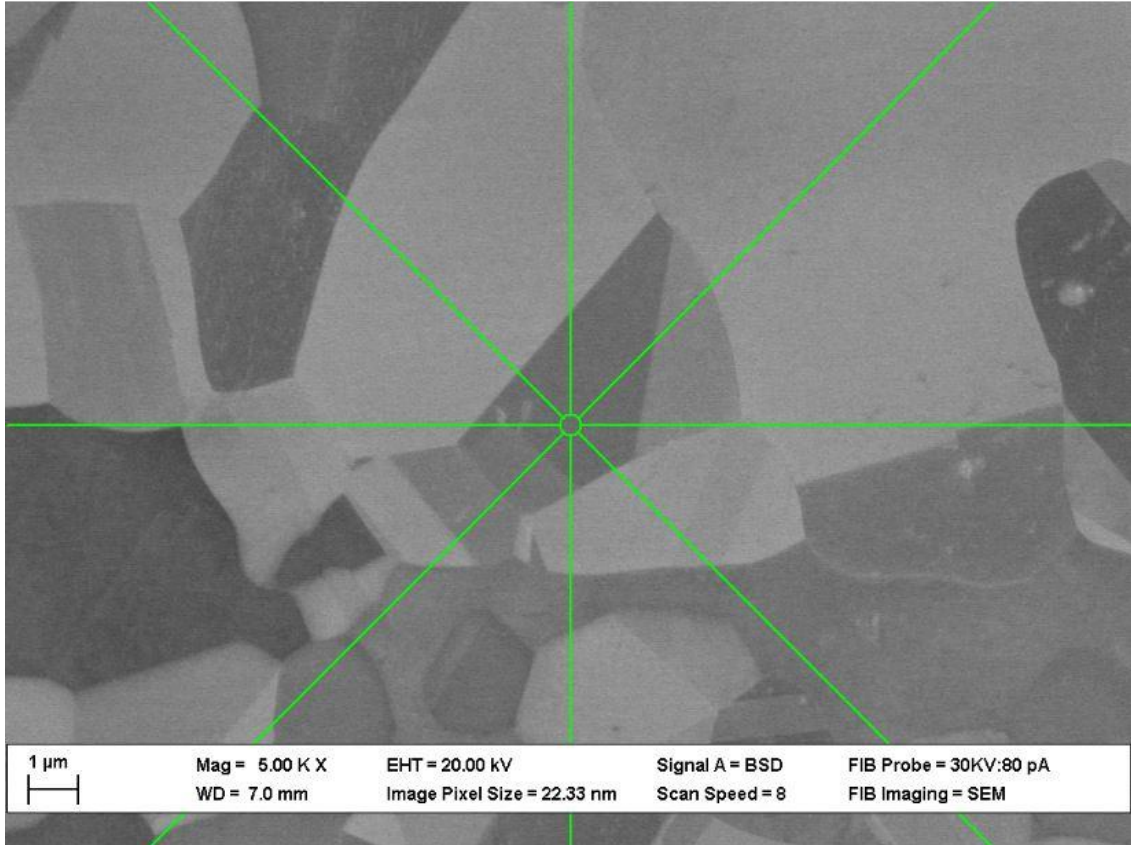


FIGURE 17: SEM IMAGE OF A DUPLEX ALLOY WITH THE GRID USED FOR THE CENTERING OF THE ROTATION AXIS. THE USED REFERENCE POINT HAS TO BE PUT IN THE CENTER OF THE GRID IN ORDER TO OBSERVE HOW IT MOVES WHILE PERFORMING A FAST ROTATION. IN THAT WAY IT IS POSSIBLE TO OBSERVE THE ROTATION AXIS AROUND WHICH THE REFERENCE POINT IS MOVING.

## IMAGE TREATMENT ON E-CHORD STACKS

Even if an “in situ” scan rotation correction is applied during the analysis, a CHORD raw stack needs a post image treatment in order to obtain good profiles from each pixel of the stack. That can be accomplished with many programs and algorithms, in this thesis a Java-based image processing program called *ImageJ* has been used, but many other ways could be explored.

It should be recalled that a stack is a superposition of many images of the same ROI, taken in different channeling conditions given by an angular variation between the sample and the primary beam. To obtain useful CHORD profiles it is crucial to minimize the noise and to assure that every image is perfectly aligned with the rest of the stack. Only if these two conditions are met, it will be possible to use the stack for detecting crystallographic defects with the clustering program. The used magnification and image size define the

physical dimension of the virtual pixel of the stack, for example for an image taken with a image size of 1K and a magnification of 20kX, the size of a virtual pixel of the stack measures 5.6 nm.

## DENOISING

---

As already mentioned, the signal/noise ratio is proportional to the acquisition time, which has to be as long as possible in order to get a low noise. However, the choice of this parameter has to be evaluated considering that the acquisition of a stack should not take an excessive amount of time. Moreover, the problems related with the surface charging effect definitely impose a limit threshold on the scanning time and so on the signal/noise ratio. Effectively, the need of having a stack without excessive drift or deformation is a much bigger issue. Anyway, it is possible to improve the above-mentioned signal/noise ratio thanks to a post-analysis digital *denoising*. There are many different algorithms available but since in this work it is important to preserve the shape and the crystallographic information of features (in order to not modify channeling profiles), a “*Gaussian blur*” cannot be used. Instead, the algorithm of “*anisotropic diffusion 2D*”, present in the XLIB library for ImageJ, has been chosen (developed by Tschumperlé et Deriche (20)). Another good algorithm that exists on the image treatment program is the “*non local means denoising*” that can be downloaded as a plugin. Finally, a great potential has been found in the “*BM3D*” algorithm (developed by Dabov, Foi, Katkovnik, Egiazarian (21)) that is unluckily not available as an ImageJ plugin and so further studies should be tried using others platforms that allow it to be used, such as Matlab. It has to be said that this subject presents a rich bibliography and many others possibilities are present. Parameters in denoising algorithms have to be set in order to reduce the noise without blurring the image and to keep well defined grains and features boundaries; this process must not modify the shape and the size of a defect.

## ALIGNMENT

---

As previously said, in a raw CHORD stack all images are never perfectly aligned the one with the other. This happens for many phenomena that take place during the stack acquisition, such as the not perfect centering of the rotation axis or other issues that will be mentioned after. For this reason, it is impossible to extrapolate useful CHORD channeling contrast profiles without a finer alignment. In fact, without a perfect alignment, for each pixel it would be associated the signal from different points of the real ROI, which is actually moving through the raw stack, therefore the profile wouldn't be representative of a single point of the ROI. Only after a finer alignment the *correspondence between a pixel*, characterized by specific coordinates, *and a specific point of the sample, can be kept along all images of the stack. Therefore, the associated channeling profile can really characterize the chosen portion of the sample.*

Alignment algorithms work by identifying identical zones between the images for computing the transformation matrix to apply during the alignment. The main issue in using these kinds of algorithms in eCHORD stacks is that, thanks to the channeling theory, the contrast intensity varies a lot while changing images. Therefore, if there aren't details that keep the contrast constant during the rotation, such as porosities and dust, the algorithm isn't able to recognize identical zones and so it fails. A way for overcoming that problem is to apply the algorithms not on the raw stack, but on a modified one; more

precisely an “*edge detection*” is performed. In this way the transformation matrix is built up from a stack in which almost only grain boundaries are visible, and so contrast effect in the matrix is deleted, as shown in Figure 20. Since the crystallographic information is lost in that stack, a *Gaussian blur* is also performed in order to improve the resolution of boundaries and to lower the noise. Once a satisfying alignment is achieved on the modified stack, the same transformation matrix, that has been saved, is then applied to the initial raw stack, obtaining the alignment. However, the contrast changing might make some grain boundaries to disappear, that happens if the grains are under angular conditions such that their channeling contrast is the same. As a consequence, the alignment is never perfect.

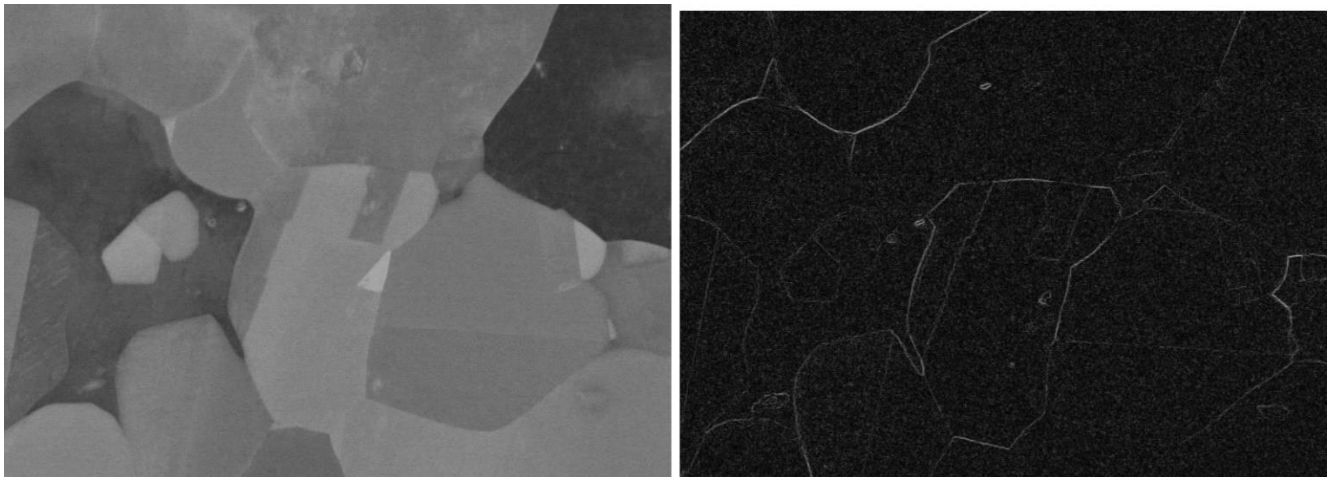


FIGURE 18: THE SAME REGION OF A DUPLEX STEEL NOT TREATED (LEFT) AND TREATED WITH AN “EDGE DETECTION” ALGORITHM (RIGHT), IT IS ALSO VISIBLE THE EFFECT OF THE NOISE IN THE MATRIX, THAT COULD HAVE BEEN CLEANER WITH A BETTER DENOISING.

Algorithms are found in specific ImageJ plugins, precisely the plugin “*beat*” has been used for the edge detection, using the algorithm called “*Canny Edge*”. For the alignment, the plugin “*Registration*” has to be installed, then the specific algorithm “*MultiStackReg*” will be available, it takes the first image as a reference for the alignment and it calculates the transformation matrix for every other image of the stack. The inconvenience of this method is that the difference between the first image and one in the middle of the stack could be too high to achieve a good correlation, therefore an algorithm able to use the last aligned image as a reference could improve results (6). The “*MultiStackReg*” plugin lets the operator to choose the way to align the stack (see Figure19), it can be used:

- *Translation transformation.*
- *Euclidean transformation (rigid body).* Translation and rotation are allowed
- *Affine transformation:* let to change angles within the transformed volume but maintaining parallel all the lines that were parallel in the original volume.

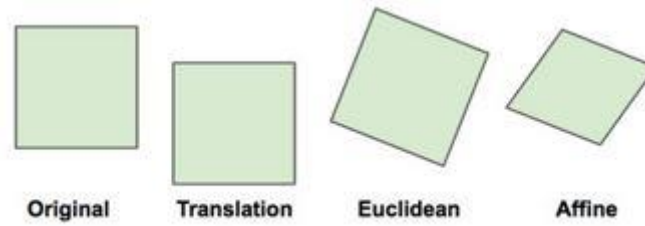


FIGURE 19: DIFFERENT TYPES OF TRANFORMATIONS PRESENT IN THE PLUGIN “MULTISTACKREG” FOR IMAGEJ.

To obtain the best result it could be necessary to first pass through a translation and then re-try to align the modified stack with an affine transformation. Sometimes just the translation is enough for a good result but it depends on the used stack. A denoising further helps to achieve better results.

In order to align details one with respect to each other, images are translated, rotated and deformed and that will result in a shrinkage of the useful ROI, in which all images of the stack must overlap. For example, if a translation is needed it means that the scanned area of an image is not exactly the same of another image and so a part of boundaries of the image of reference will not be covered by other images. Since that dimensions of the reference image characterize the stack, parts not covered by others images will be fitted by dark frames in the edge of images. It is therefore necessary to crop the stack in order to obtain a smaller ROI in which, along the entire stack, to all pixels correspond a signal owned by a specific part of the sample. To crop the stack it is firstly necessary to extract the “*Min Intensity*”, an image in which every pixel has the lowest grey level achieved along all the stack. In this way the dark frame is well defined and it is possible to draw a square selection contained in it, this selection can be restored in the stack, that is then cropped for deleting all dark boundaries out from that selection.

To evaluate the quality of the alignment it is possible to extract the “*average intensity*” of the stack, the resulting image must not be blurred and edges have to be well defined.

## VIII. DIS-CHORD FIRST RESULTS

The conclusion of the chapter focused on the theory of ECC is that it is possible to achieve a significant contrast difference between matrix and crystalline defects at certain angles.

This phenomenon obviously takes place also during eCHORD scans since the sample is submitted to a rotation of  $360^\circ$  and many angles between sample and electron beam are achieved. Therefore, in each grain many TB conditions will be found for sets of angles that depend on experimental parameters and on the specific orientation of the grain taken into account (1), in fact the ECP crossed during the scansion is orientation dependent.

One of first works for investigating such a kind of issue have been made by L. Casiez (6), where a rotational stack along 80 degrees have been made without the use of the sub-stage, that wasn't available yet. This work pointed out that, in the aligned stack of images, pixels belonging to a crystalline defects show the same channeling contrast in the most part of images, but when a dark Kikuchi line is crossed through the ECP a two beam condition is achieved and the lighting of crystalline defects is produced, as indicated by red arrows in Figure20a. Stacking faults are also visible and they are indicated by a yellow arrow. As a consequence, in specifics sets of angles, there is a difference in channeling contrast between pixels belonging to the perfect crystal and pixels belonging to defects. This leads to differences in intensity profiles in these angles and the example relative to the Grain3 is given in Figure20b, in which two profiles coming from the stack are represented. The red one belongs to a matrix pixel and the blue one to a stacking fault pixel (6).

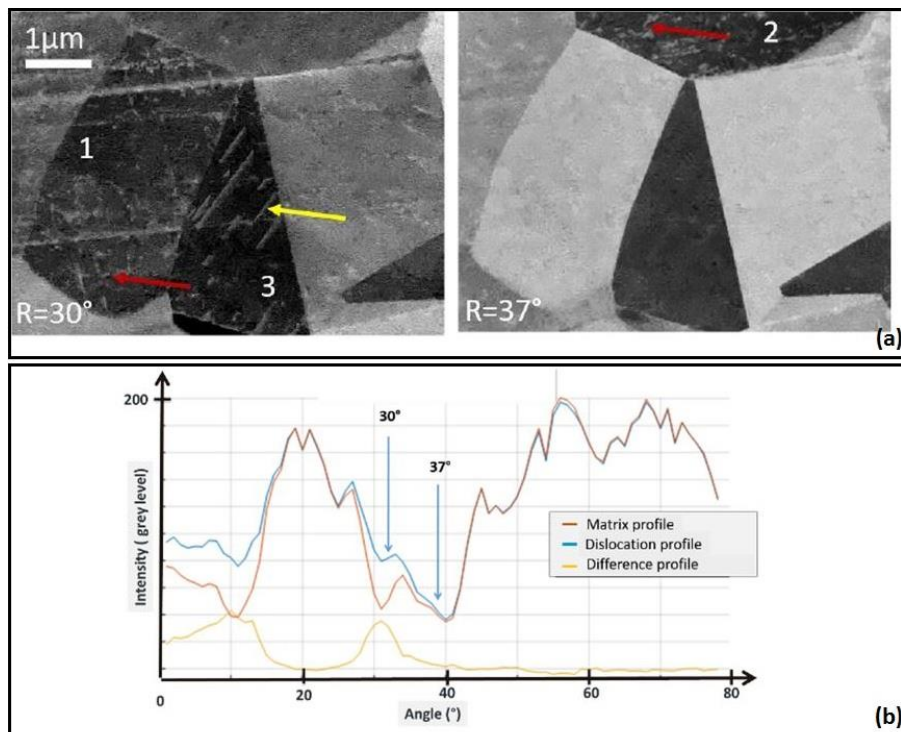


FIGURE 20: (A) IMAGES EXTRACTED FROM A ROTATIONAL SERIES, WHERE THE DISLOCATIONS (ORANGE ARROW) AND STACKING FAULTS (YELLOW ARROW) APPEAR IN DIFFERENT GRAINS FOR PARTICULAR ORIENTATIONS.(B) INTENSITY PROFILE RELATIVE TO THE GRAIN3, AS A FUNCTION OF THE ROTATION ANGLE FOR A SERIES OF IMAGES TAKEN ON A DUPLEX SAMPLE. (FROM L. CASIEZ REPORT (6))

Watching at profiles of the grain3, situation of contrast difference are achieved around 10° and 30° degrees of rotation where TB condition are met and defect are visible.

Moreover, at 37° of rotation (right part of Figure20a), stacking faults are not visible even if a TB condition is present (the matrix is dark), therefore an invisibility criterion is achieved for these defects. Knowing that a TB condition is crossed at 37° of rotation, this criterion is detectable with profiles because at 37° the gray contrast of defects is the same of matrix, this means that they are not visible.

These local differences between profiles allow to discriminate pixels belonging to defects and, when considering the whole intensity profile of a rotation stack, all dislocations should be detected. Indeed, when using conventional image analysis, performed on a given two beam condition, all dislocations in extinction conditions are not seen and therefore not taken into account in the dislocation density measurement. For instance, in the presented grain, stacking faults of grain 3 would not be seen in the TB condition met at 37° of rotation. The intensity profile analysis should allow detecting them.

Moreover, the  $g_{hkl}$  vector linked to different two beam condition can be deduced from the indexed ECP related to the profile. Knowing the  $g_{hkl}$  vector is crucial for the determination of the defect nature. Indeed, the nature of the defect can be determined if two invisibility criterion are crossed. Further studies are needed to determine the statistical number of crossed invisibility criterion for a random grain orientation, as a function of the used tilt, the accelerating voltage and crystal nature.

In parallel to this master thesis, G. L'hôte (22), from METEIS laboratory, also used such a kind of technique in order to study the evolution of dislocation structures after cyclic fatigue for pure Cu mono-crystals. In this work a rotational eCHORD stack, with an initial tilt of 6.5°, have been used in order to facilitate the determination of sample orientations where channeling occur, for showing that in this way it is possible to obtain ECC Images of dislocations overcoming the necessity of knowing the crystal orientation of the sample via EBSD or other analysis and so speeding up the process. Thanks to the acquired rotational stack, taken at a magnification which made impossible to see dislocations, angles in which crystallographic defects were expected to appear have been found. After that, the ROI have been indexed via eCHORD in order to obtain the linked simulated ECP, shown in Figure 23a, for determining interested diffracting planes in crossed TB conditions. Finally a high magnification BSE image has been taken in one of the detected rotation angles for studying dislocations structures visible in Figure 23b, even if the magnification haven't been enough to resolve individual dislocations.

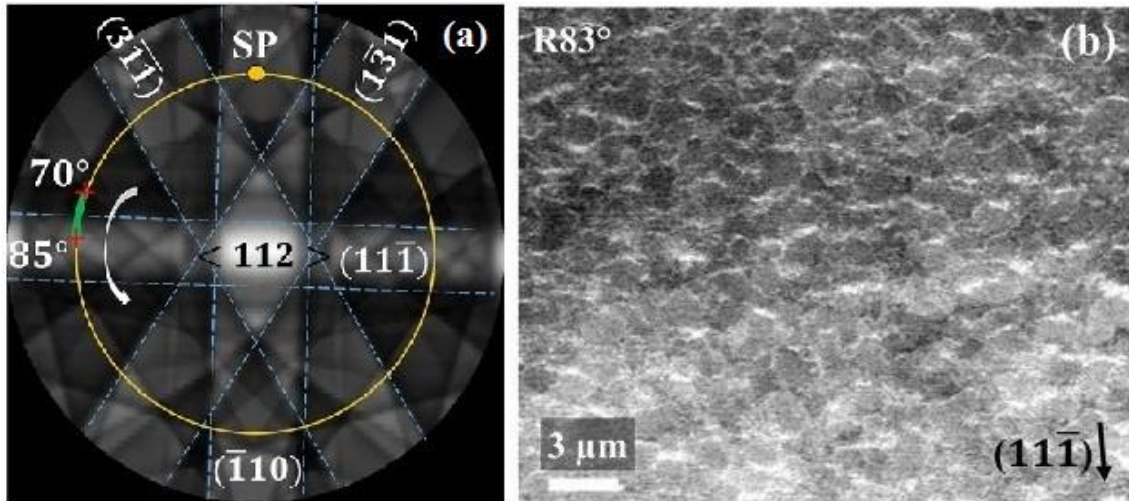


FIGURE 21: (A) INDEXED ECP RELATIVES TO THE STUDIED ROI. (B) THE ECC IMAGE OBTAINED THANKS TO THE ORIENTATION INFORMATION OF THE PRELIMINARY LOW MAGNIFIED STACK.

For improving the defects visibility, more ECC images have been taken in the studied angular range and have been summed via ImageJ, furthermore, an augmentation of the used magnification has led to the resolution of single dislocations.

A great advantage of this technique is that it needs no assumptions on the dislocation nature or on the crystallographic orientation of the considered grain. It is a great advantage in comparison to classical ECCI or TEM direct detection, as they require a significant theoretical knowledge on both defect imaging conditions and crystal structures (1). However, this work has also evidenced that the technique needs to be improved in order to get quantitative and qualitative information on dislocation characteristics (22), acting either via image processing or via optimization in experimental parameters. Moreover, the dislocation density characterization has been done just on single ECC images and therefore not taking advantage of the difference between rotational profiles belonging to defects and matrix. This technique takes the name of *rotational ECCI (R-ECCI)*.

In this context, it is worth trying to improve the experimental methodology in order to obtain useful rotational stacks, with a magnification with which defects are visible. Once done that, rotational profiles could be used to develop an automatic characterization (both quantitative and qualitative) of defects in bulk materials, applicable for any SEM and easy to set up, even for people that don't have a detailed background in that subject.

## D. EXPERIENCES

---

### I. OBJECTIVES

---

In this master's thesis R-ECCI stacks have been taken in order to try to further investigate on following objectives:

- To verify the possibility of achieving rotational stacks of 360 degrees useful for the crystallographic defects characterization.
- To optimize the experimental parameters in order to achieve a significant variation of the contrast between matrix and defects' pixels and to maximize the angular range in which defects appears.
- To optimize experimental parameters in order to maximize the number of crossed TB conditions in the rotational stack.
- To verify if it is possible to apply the clustering program to profiles linked to experimental stacks in order determine a dislocation density measurement and their Burgers vector.

Hence, two main sets of stacks have been done to accomplish as much as possible these targets.

### II. USED MICROSCOPE

---

The experimental acquisition of the stacks of images was accomplished with the Focused Ion Beam SEM ZEISS with a Gemini column equipped with a Field Emission Gun, shown in Figure22.



FIGURE 22: IMAGE OF THE FIB SCANNING ELECTRON MICROSCOPE USED IN THIS MASTER'S THESIS.

As previously said, a custom made sub-stage is implemented in the microscope in order to achieve a better angular precision, to obtain stacks of images with an improved quality of alignment and in shorter times.

### III. SAMPLE PREPARATION

---

An issue in *disCHORD* analysis is that the original dislocation density should be affected as least as possible during the sample preparation, in order to not affect the result. To achieve this goal no chemical etching is applied and, in the last steps of the polishing, light load has to be applied in order to avoid the onset of deformation.

A conventional EBSD polishing was performed on the sample: first a mechanical polishing using SiC papers, followed by a diamond paste polishing down to 1 $\mu$ m. A final vibratory polishing using a colloidal suspension was performed. A fraction of colloidal silica particles tends to remain attached to the sample surface and that will affect the image quality, hence the sample is finally passed under an ultrasonic bath for above 30 min.

The choice of the OPS solution used could be critical if the material used is particularly sensible to corrosion like in the case of TWIP steels, austenitic alloy rich in Mn. In fact the formation of an oxide layer was observed when the sample was submitted to not neutral chemical conditions, as shown in Figure23.



FIGURE 23: EXAMPLE OF FAILED POLISHING IN A TWIP STEEL, DUE TO AN OXIDATION OF THE SURFACE DURING THE VIBRATIONAL POLISHING IN AN OPS COLLOIDAL SOLUTION.

In order to easily find the region of interest, a frame of reference can be obtained using micro indentation on the surface, that could be really useful when the orientation indexation has been obtained via EBSD, and so a change of geometry is involved.

Once obtained a good surface quality, the sample has to be put on the SEM specimen holder taking care in assuring the continuity of the electrically conductive layer. In fact, if this condition isn't achieved, electrons from the primary beam will not flow as current through the sample and this would lead to a static charge accumulation on the sample surface, that will significantly affect the quality of eCHORD stacks. For this reason, no glue traces must be left on the unpolished side of the sample, that was attached to a plastic holder (similarly to Figure 23) during the polishing step. After this final cleaning, the sample is attached to the specimen holder (or on the implemented sub-stage for the stack acquisition) using an electrically conductive adhesive tape.

The choice of samples was done considering that for the first trials, very well-known materials were needed, for which a good knowledge on the crystalline microstructure and on the dislocation and stacking fault behavior exists. The cubic crystalline lattice of TWIP (twinning-induced plasticity) and DUPLEX (containing both austenitic and ferritic phases) steels was found to be a good candidate for that purpose. Moreover, the low stacking fault energy of TWIP steel and the austenitic phase of DUPLEX steel assure the presence of crystallographic defects in both types of materials

#### IV. ACQUISITION ISSUES

---

Ideally, while acquiring an eCHORD stack with the purpose of detecting crystallographic defects, a great magnification and the best possible resolution are needed, in order to observe the defects without having a blurred image. For a given microscope, once chosen the appropriate magnification, working distance, aperture diameter and beam energy the quality of the image is basically controlled by:

1. The scan speed (ns/pixel), which defines the total time for obtaining an image (and a stack of images).
2. The image size chosen by the operator (defined as number of pixel compounding the image).
3. The ability of the operator in adjusting focus and astigmatism.
4. Post treatment of the image: denoising.

Hence, the best images are obtained with a larger number of pixels ( namely 2048x1080 pixels instead of 1280x720 ) and with a slow scan speed. In fact, the signal/noise ratio can be estimated from the following formula (6):

$$\frac{Signal}{Noise} = \sqrt{i * t}$$

Where  $i$  is the beam current and  $t$  the acquisition time.

However, an important consideration is that in this way the sample is submitted to larger scanning times that can create charging effects on the surface. This phenomenon happens particularly in not conductive materials but exists also in conductive materials when they are exposed to an excessive quantity of electrons. For this reason it is really important to make sure that a highly conductive connection, as wide as possible, is present between the sample and the stage in order to improve the flux of electrons going out of the sample. Moreover, charging phenomena are amplified by surface contamination, which makes the

sample less conductive, and so this must be avoided taking care by avoiding to touch the sample without wearing clean gloves and by removing all solvent traces after the sample polishing. Unfortunately, another source of contamination is present during the scan, since the electron beam produces the cracking of gaseous hydrocarbons present in the microscope atmosphere. That will result in the deposition of carbon on the sample surface, that increases with the time of exposure to the beam. A plasma cleaner could eventually solve the problem of contamination during the scan, improving stacks quality.

It is known that a charged surface leads to phenomena of drift and deformation of the acquired image, since the beam is deflected by the electrostatic field on the surface, producing an error in the real position of the scanned pixel. Therefore, the scanned area seems physically moving during the scanning or local deformation are produced in a single image, as shown in Figure24.

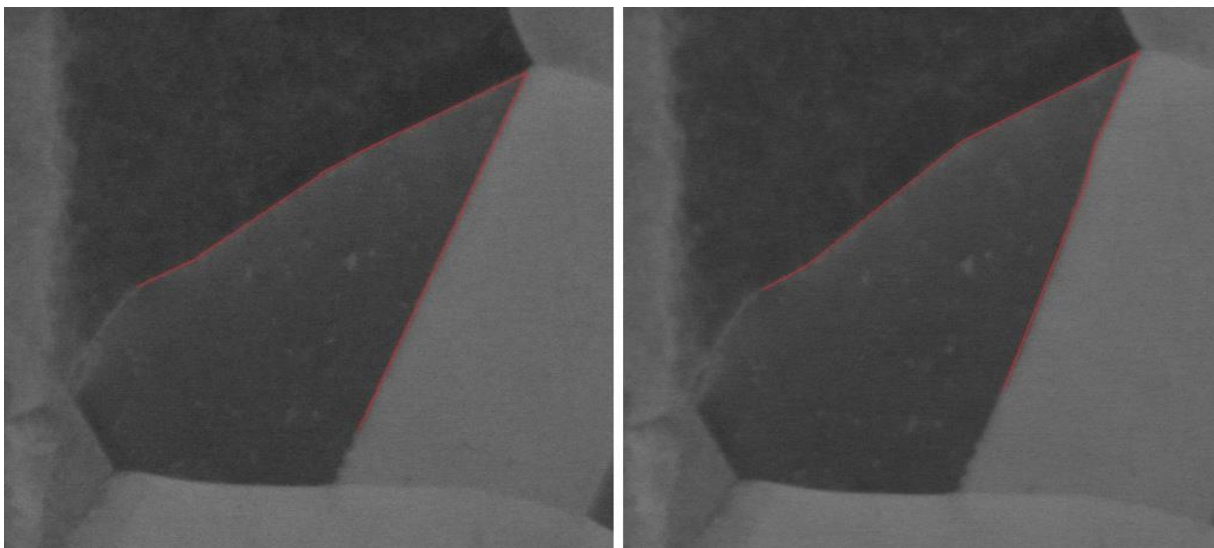


FIGURE 24: LOCAL DEFORMATION OF A GRAIN OF AUSTENITE IN A DUPLEX SAMPLE. THAT IS DUE TO A CHARGING EFFECT: THE ELECTROSTATIC CHARGE ACCUMULATED ON THE SAMPLE SURFACE LOCALLY DEFLECTS THE PRIMARY ELECTRON BEAM, PRODUCING AN ERROR IN THE DIGITAL BUILD UP OF THE IMAGE.

When drift occurs during the acquisition of an eCHORD stack, the region of interest will drift out from the scanned area and so it will be impossible to achieve a complete profile for every pixel of the ROI, making the stack useless. Alongside a local deformation of the image the risk is also of a bad alignment of the total stack, i.e. physical scanned pixels will not overlap perfectly each other among different images of the same stack, leading to not accurate pixels profiles. In fact, the matching between a virtual pixel of the stack and a physical point of the ROI will be lost. This “degradation” of profiles could be critical in detecting defects since these defects are very small and so even a small misalignment impacts on their profiles.

This technique requires conditions that enhance the presence of drift or deformation of the image such as high magnification, high resolution and consequently high scanning times. Thus, it is necessary to make the setup of the microscope (focus, astigmatism, centering of the rotation axis...) outside of the ROI, that must be contaminated as little as possible. This means, however, that the magnification, the pixel resolution and the acquisition time cannot be the best ones: trade-offs must be found. In addition, the piezo-

components of the sub-stage heats during the rotation series, which lead to some thermal expansion drift phenomenon.

Another point that must be taken into account is that during the stack acquisition the sample is submitted to a rotation; as already mentioned an image is taken every step that can be of  $0.5^\circ$ ,  $1^\circ$  or  $2^\circ$ . That means that, in every step of rotation, the scanned area loses the angular alignment with the initially chosen region of interest. Only after a post process rotation correction all images will have the same orientation of the first image, so that the corrected ROI will be circle shaped and much smaller than effective scanned area. To solve that problem a specific scan rotation correction correlated with the sample rotation step is used during image acquisition, in this way approximately the same area is scanned at each rotation step, and the final ROI is enlarged (6). Anyway, that correction isn't enough for a perfect alignment of the stack, in fact during the scansion not only a rotation is produced, but also deformations and translations are present for many reason like the drift effect or a not perfect centering of the rotation axis. Furthermore, even if it allows to solve the problem of the small ROI, the rotation correction during the stack acquisition is not perfect. For all these reasons, a specific and more precise digital alignment process will be done on the stack.

A little deformation is also produced by the fact that the sample is tilted during the rotation so the acquired image, which is a projection of the surface on the "0-tilted" plane, changes a bit its shape with the rotation around the Z axis (6).

One final issue that can happen in that kind of analysis is that the focus can get worse during the acquisition of a stack, hence it might be useful a random check on the quality of images done by the operator, that could eventually put in break the analysis and perform a focus correction if necessary



## E. RESULTS

---

### I. FIRST DUPLEX EXPERIMENTAL SET OF STACKS: STUDY OF PARAMETERS AND INVESTIGATION ON THE POSSIBILITY OF DETERMINING THE BURGERS VECTOR

---

This stack was acquired after a first essay on a TWIP steel where, at a magnification of 5kX, crystallographic defects weren't enough defined, probably because of a not perfect polishing. Indeed, as mentioned, this material presents some problems of oxidation and a surface oxide layer could be formed. Hence, the material was changed and DUPLEX steel was used.

After the polishing the sample was submitted to a series of micro-indentations in order to build a grid and so be able to find the ROI in successive analysis. This has been useful since that an EBSD orientation map of the same ROI was also taken on another microscope. Therefore it has been necessary to recognize the same area before starting the eCHORD stack acquisition, that is almost impossible without a system of reference, in fact the whole sample contains thousands and thousands of crystalline grains.

It is better to perform the EBSD analysis before the acquisition of the eCHORD stack, which requires long times of exposition to the beam and so can bring to the contamination on the ROI. In this work, however, the opposite was done and in order to obtain a good quality of the orientation maps, long times were needed. Luckily, for defect detection a high quality of the EBSD map isn't required. It acts just as a reference in order to check if the eCHORD orientation map is obtained with success. A satisfying result was obtained since that the same orientation map was obtained with both techniques.

The orientation map and the phase map showed in Figure 25 (left) were taken at a magnification of 1500X, that is too low for defects detection. Effectively, this preliminary stack of images has been acquired in order to give the orientation of a large area, which was then divided in 4 smaller areas used for the crystallographic defects detection, in which a magnification of 5kX has been used. This choice was done for two reasons, firstly because it was planned to acquire many eCHORD stacks and the risk of contamination was real, therefore the presence of 4 different zones on which was possible to work seemed a good solution. Moreover, working on a bigger area would allow to characterize a larger number of grains, obtaining more statistic results and studying more orientations. It is possible to have an idea of the contamination produced during the scan in Figure 25 (right), in which darker frames are visible just in the portions of the ROI that are the intersection between more zones, for that reason they have been submitted for longer times to the electron beam.

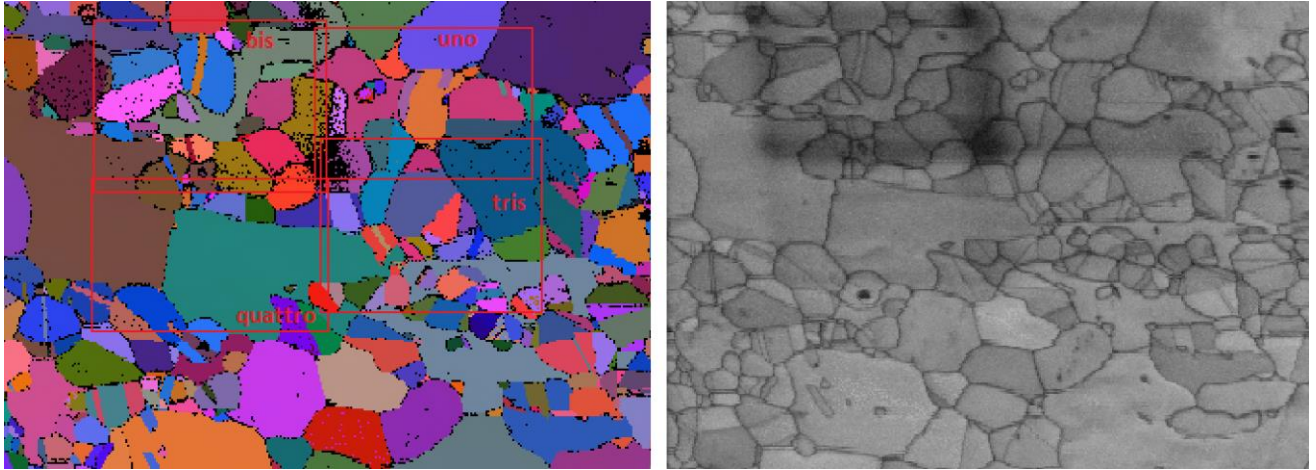


FIGURE 25: ON THE LEFT EULER' S COLORS ORIENTATION MAP OF THE ROI USED IN THE ANALYSIS. ON THE RIGHT A SEM IMAGE OF THE SAME ZONE (TAKEN UNDER THE SAME GEOMETRICAL CONDITIONS AS THE EBSD IMAGE). IT IS POSSIBLE TO SEE 4 SUB-ZONES IN WHICH OTHERS SERIES HAVE BEEN TAKEN WITH A GREATER MAGNIFICATION.

This set of stacks was used not just for the study of parameters, indeed also the study of defects detection via clustering was a purpose, unfortunately it has emerged that the quality of these stacks wasn't enough for that. Hence, it has been found that to achieve 360° rotational stack in which crystallographic defects can be detected via clustering is no easy thing, as a consequence other strategies for improving the quality of stacks were carried out, in order to avoid charging and contamination problems, bringing to a second set of stacks. However, the high number of analyzed grains and the experimental conditions in these stacks were also used for further investigating the possibility of detecting the Burgers vector with this technique.

---

### ACQUIRED ROTATIONAL SERIES

---

The total region of interest is divided into 4 sub-zones, in which eCHORD stacks was acquired with a magnification of 5000X, in order to have a set of data useful for the study of the technique. With that purpose, some parameters were changed between a stack and another, in order to confront results. As showed in Figure 26, that is taken directly from the preliminary stack, with a magnification of 1500X, the sub-zones have been called respectively 'uno', 'bis', 'tris' and 'quattro'. Red points represent the center of each sub-zone, around which the sample has been rotated during the analysis in order to vary the contrast. Alongside, the green center of the grid is the rotation center used in the preliminary series that concerns the whole ROI.

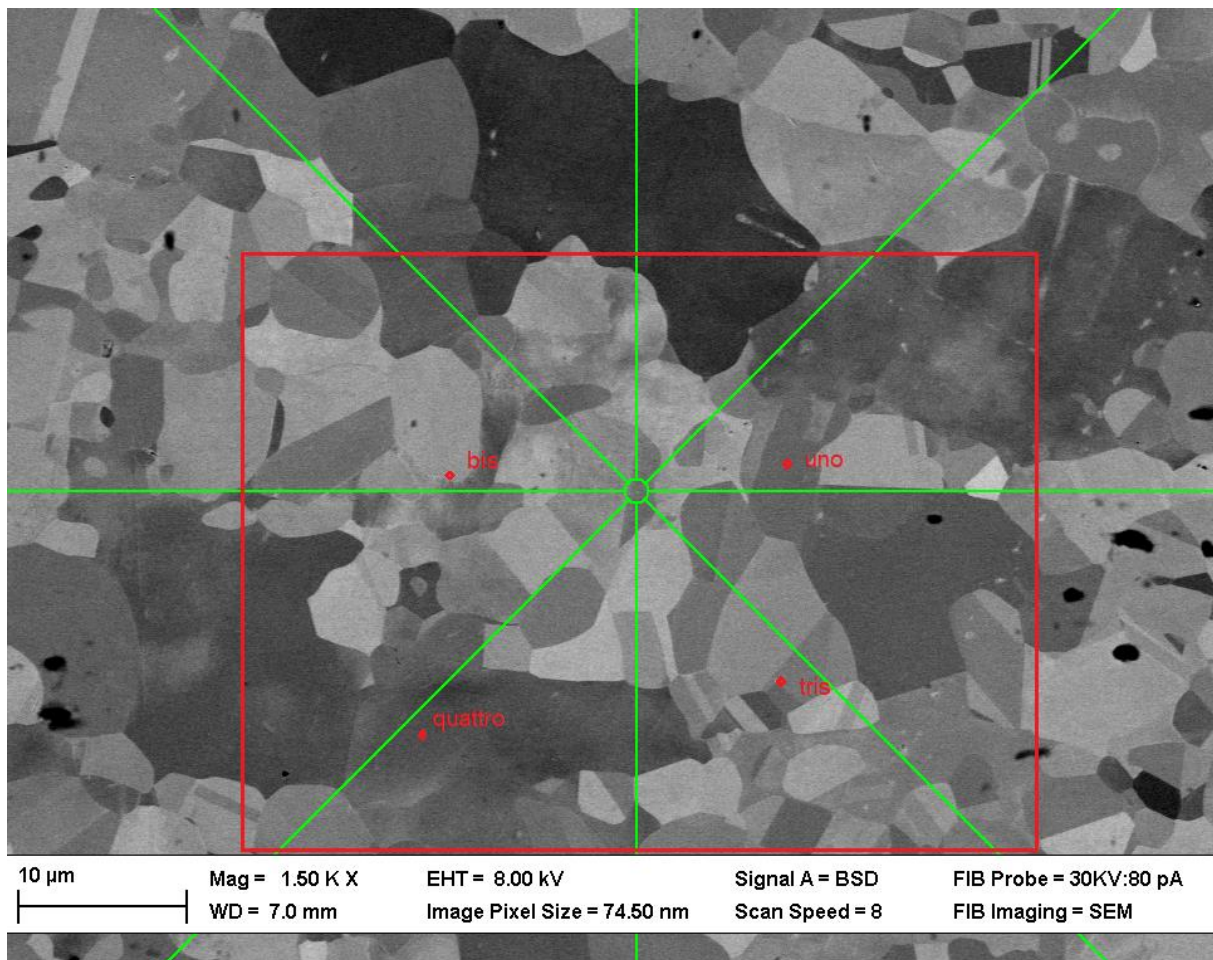


FIGURE 26: A BSE SEM IMAGE REPRESENTING THE WHOLE AREA USED IN THIS ANALYSIS. SINCE THAT THE MAGNIFICATION ISN'T ENOUGH FOR SEEING CRYSTALLOGRAPHIC DEFECTS, 4 SUB-ZONES ARE DRAWN INSIDE IT.

It must be considered that the material present two different phases: the ferrite (body centered cubic) and the austenite (face centered cubic), notably the last one is more deformable and so more crystallographic defects are formed. For this reason, just austenitic grains have been considered; another motivation is that, for the moment, the software and the technique itself are in development and so initially just the FCC geometry is considered. Indeed, it is reasonable that to develop a new technique it is better to start with the easier scenario and explore the rest when the first results are achieved. Figure 27 shows the phase map that was used to recognize the two different phases, the austenitic phase is colored in blue. However, a preliminary and fast way for recognizing austenitic grains, even if much less accurate, is to find the greatest concentration of dislocations and twins boundaries, since it is well known that the FCC geometry has a lower stacking fault energy, that leads to a higher formation of these crystallographic defects.

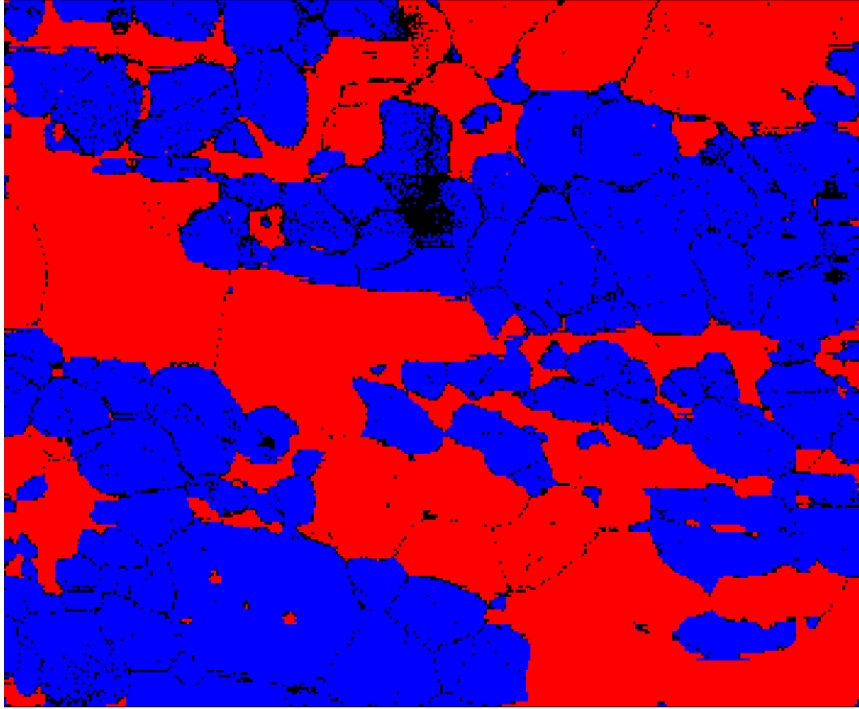


FIGURE27: A PHASE MAP OF THE WHOLE ROI, OBTAINED BY AN EBSD ANALYSIS. IN BLUE AUSTENITIC GRAINS, IN RED FERRITIC ONES.

Finally, eight useful stacks were acquired. The preliminary stack was taken with a low beam energy in order to have a smaller volume of interaction and therefore remain closer to the surface. In this way the risk of considering the contribution of grains that are deeper under the surface is minimized. Stacks 2, 3 4 and 5 are all taken with same parameters but each one on a different sub-zone, they are used as a reference for other acquired stacks, in which some parameter have been modified in order to study the technique.

Table2 shows how parameters were changed between different stacks. The other parameters were kept constant referring to the ECC theory developed by Zaefferer et al. (2) and to the eCHORD team experience, they are all shown in Table3.

Table2: experimental parameters varied between different analysis.

STACK	MAGNIFICATION [KX]	BEAM ENERGY [KeV]	TILT ANGLE [DEGREES]	SCANNED SUB-ZONE
Preliminary stack	1.5	8	10°	Whole zone
stack 2	5	20	10°	uno
stack 3	5	20	10°	bis
stack 4	5	20	10°	Tris
stack 5	5	20	10°	quattro
stack 6	5	20	15°	uno
stack 7	5	20	6.5°	bis
stack 8	5	30	6.5°	bis

Table3: fixed parameters used in the acquisition of stacks.

Parameter	value	reference
DIAMETER APERTURE [ $\mu\text{m}$ ]	120	Zaefferer et al.
WORKING DISTANCE [mm]	7	Zaefferer et al.
RESOLUTION	1K	eCHORD team
ANGULAR PATH	$1^\circ$	eCHORD team
SCAN SPEED [ns/pixel]	from 6485 to 25685	eCHORD team

In every sub-zone, analyzed austenitic grains were selected and named, in the zone *tris* and *quattro* no grains were analyzed since just one stack with reference parameters was taken, therefore it was useless for comparing different parameters. Moreover, the zone *tris* have been used to study the possibility of determining the Burgers vector, work that will be mentioned later.

Hereafter there will be shown sub-zones *uno* and *bis* (Figure28) and their analyzed grains, moreover the indexed ECP linked to each of these grains will be represented (Figures 29 and 30).

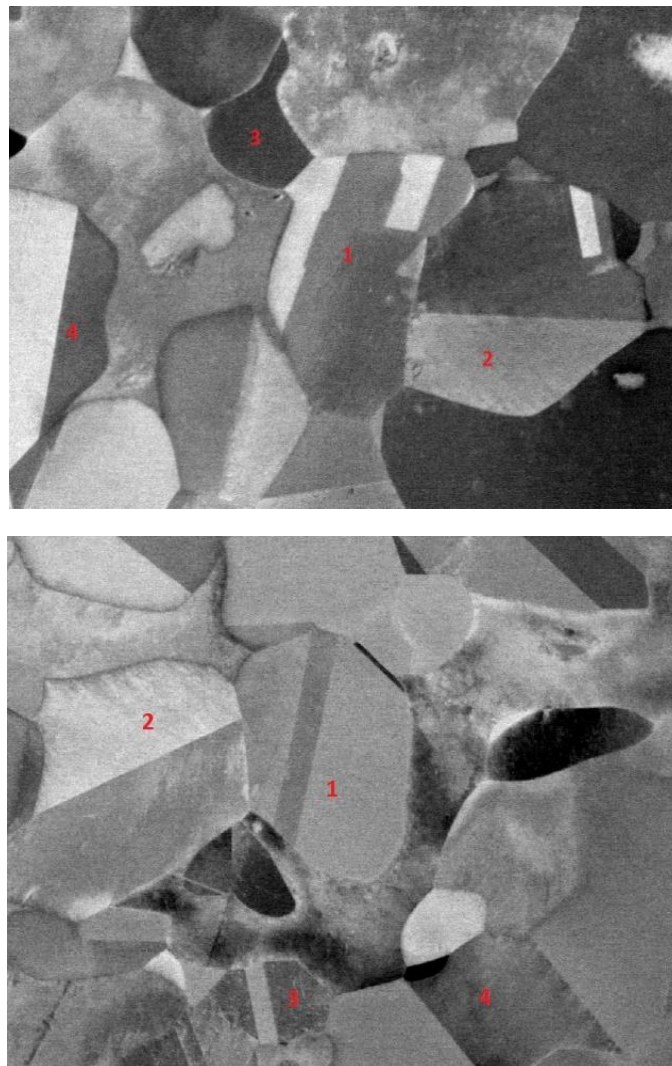


FIGURE 28: BSE IMAGE OF THE SUB-ZONE 'UNO' (ON THE TOP) AND 'BIS'(ON THE BOTTOM).

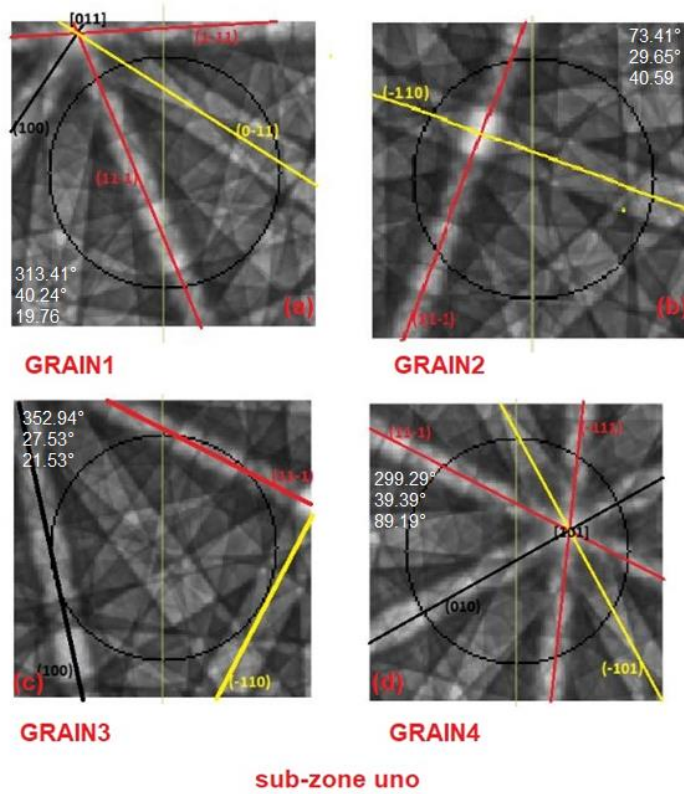


FIGURE 29: ECPS CENTERED IN THE ORIENTATION OF EACH GRAIN, CIRCLES REFER TO A 10° TILT. (A) REFERS TO THE 1<sup>ST</sup> GRAIN, (B) TO THE 2<sup>ND</sup>, (C) TO THE 3<sup>RD</sup> AND (D) TO THE 4<sup>TH</sup>. ON EVERY ECP, EULER'S ANGLES ARE WRITTEN IN WHITE.

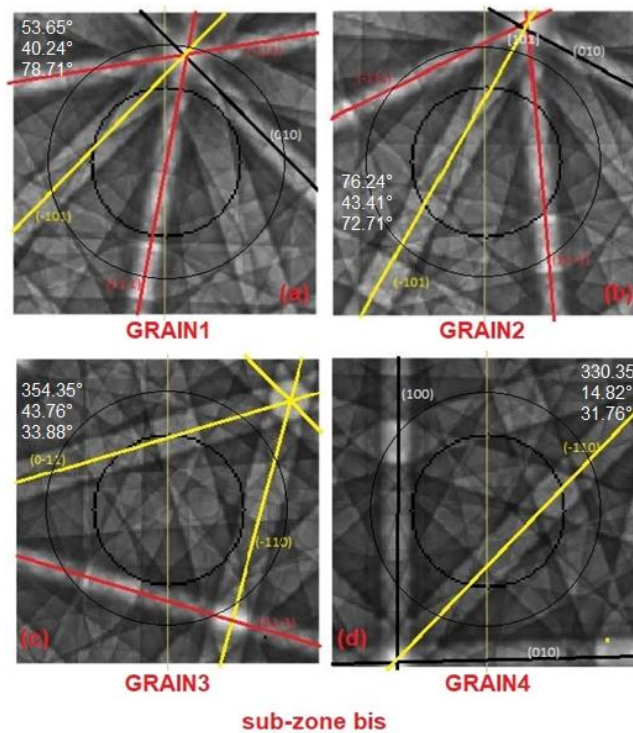


FIGURE 30: ECPS CENTERED IN THE ORIENTATION OF EACH GRAIN, CIRCLES REFER TO BOTH 6.5° (THE TINNER) AND 10° TILT. (A) REFERS TO THE 1<sup>ST</sup> GRAIN, (B) TO THE 2<sup>ND</sup>, (C) TO THE 3<sup>RD</sup> AND (D) TO THE 4<sup>TH</sup>. ON EVERY ECP, EULER'S ANGLES ARE WRITTEN IN WHITE.

---

## PARAMETERS CONSIDERATIONS

---

In order to respect the objectives that have been set, experimental parameters should maximize the visibility of crystallographic defects and thus the contrast achieved with the matrix. Alongside, also the angular range in which a TB condition is achieved should be maximized.

Furthermore, the number of crossed TB condition should be as high as possible for increasing the probability of meeting invisibility criteria through the rotation of the sample, which is essential for determining the nature of crystallographic defects by characterizing their Burgers vectors. Considerations about the achieved defects resolution will also be done.

This first analysis allowed to make an evaluation of the parameters that are used while acquiring rotational stacks, which are summed up hereafter.

### SCAN SPEED

---

Choosing the scan speed value is choosing the right compromise between the fastest acquisition possible and enough signal/noise ratio to visualize the defects. Using a fast scan speed is also important to limit the charge/drift issue.

Table 4 gives the equivalence between the scan speed given by the SEM and the relative physical speeds in ns/pixel for the used instrument.

*Table4: Equivalences between Scan Speeds*

Scan Speed (Zeiss)	Scan Speed (ns/pixel) for resolution 1k	Scan Speed (ns/pixel) for resolution 2k
3	479,4	445,0
4	929,5	858,3
5	1780,2	1653,0
6	3306,1	3242,5
7	6485,0	6453,2
8	12970,0	12842,8
9	25685,6	24795,5
10	61925,3	57220,5
11	114440,9	
12	213623,0	
13	419617	
14	831604	
15	1647949	

Figure31 allows to visualize how the dislocations contrast evolves with the scan speed. The noise is reduced when the scan speed gets slower. In intensity profiles are indicated the values of the mean intensity of the noise and the values of the intensity of the defects peak, values that are then used for evaluating the visibility of defects for each used scan speed.

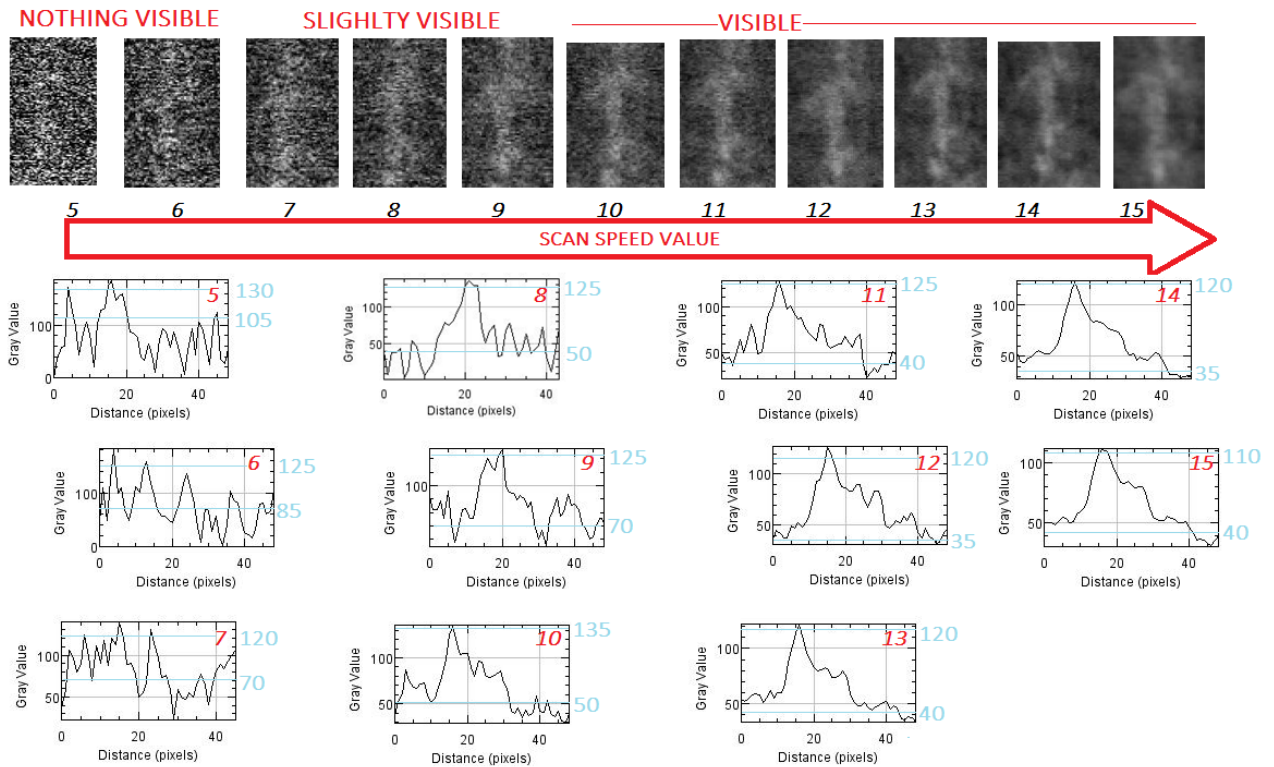


FIGURE 31: REPRESENTATION OF ONE CRYSTALLOGRAPHIC DEFECT AND IN AN ECCI IMAGE AND HOW IT CHANGES WHEN THE SCAN SPEED IS CHANGED. TO EVERY VALUE OF SCAN SPEED, A GRAY INTENSITY PROFILE COLLECTED ALONG A LINE WHICH CROSS THE DEFECT IS LINKED.

When analyzing profiles, it is possible to see that the noise hides the peak related to defects, with the peak starting to be distinguishable from the noise when the scan speed value exceeds 8. It can also be observed that it is not worth exceeding the value of 10, where the peak is already completely distinguishable.

Figure 32 shows how the ratio between the intensity of defects peak and the mean intensity of noise changes with the value of scan speed. It can be seen that over the value of 11 the defect visibility does not change, but that it is important to use values significantly higher than 6 to distinguish the peak from the noise.

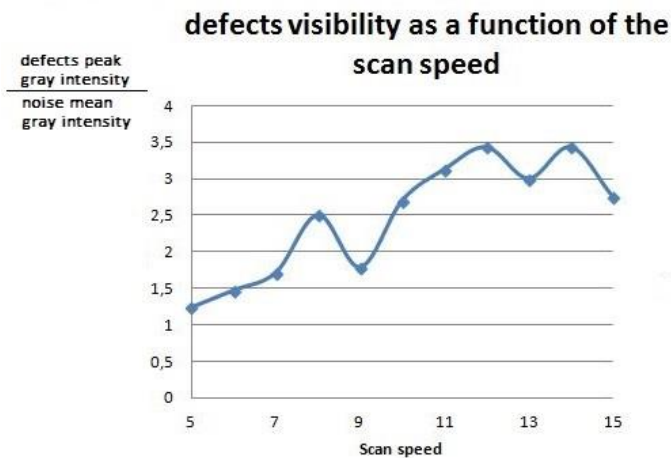


FIGURE 32: HOW THE VISIBILITY OF DEFECTS EVOLVES WITH THE SCAN SPEED

The evolution of this ratio is not linear and quite specific, therefore this parameter should be analyzed case by case. Moreover, in the studied images single dislocations cannot be resolved and it would be worth to repeat this study with a better image quality.

Keeping in mind the first evaluations and considering the presence of charging problems during the acquisition of rotational stacks, the best strategy for setting this parameter seems to be to verify the presence of the drift before starting to acquire the stack. This is done by scanning more or less five times the same area and checking if any drift is produced with such a scan speed. If no drift is observed, then the acquisition can start, otherwise another try must be done with a lower scan speed (less ns/pixel).

In this work a scan speed of 8 was used, always checking if it causes drift phenomena.

### MAGNIFICATION

This parameter plays a very important role in defect detection, in fact magnification is strictly related to the number of analyzed grains but it has to be high enough to resolve dislocations and stacking faults. If the analysis purpose is to make crystallographic defects characterization, the most important target is to obtain a stack with profiles that can be used in clustering programs, therefore the magnification should be improved even if less grains would be analyzed simultaneously. Since alignment is not perfect, the width of any defect must be sufficient to keep the most part of the defect pixels in the same position even if small translations are produced in the aligned stack, thus obtaining profiles useful for clustering. Obviously, the only way to increase the defect width is to augment the magnification. Moreover, in this way not only it is possible to observe a larger number of defects (also the fraction of smaller defects is detected) in the ROI but their shape is more defined, as shown in Figure 33, where the same zone is observed at a magnification of 5kX and 15kX.

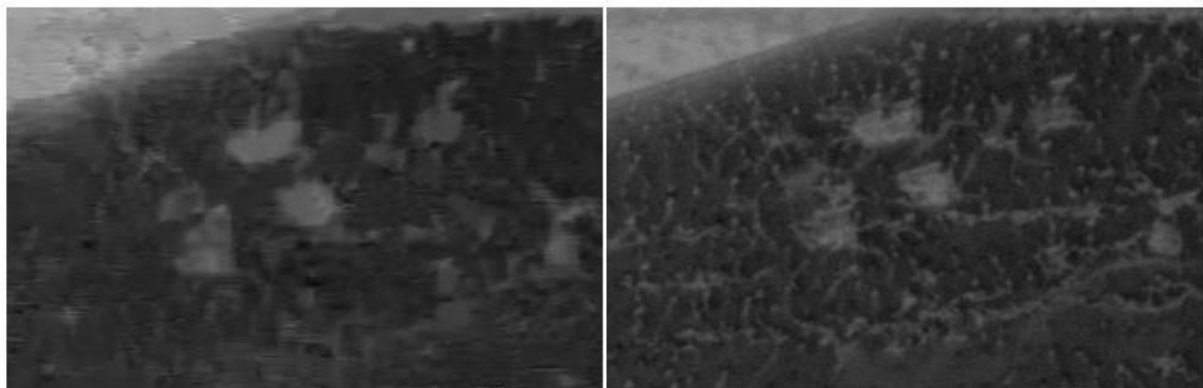


FIGURE 33: SOME ZONE OF A DUPLEX STEEL, OBSERVED WITH TWO DIFFERENT MAGNIFICATION: 5KX AT LEFT AND 15KX AT RIGHT. IS EVIDENT HOW THE LOWER MAGNIFICATION SHOWS JUST BIGGER DEFECTS AND HOW THE SHAPE OF DEFECTS IS MORE PRECISE IN THE IMAGE TAKEN WITH A GREATER MAGNIFICATION. (FROM L. CASIEZ RAPPORT (6)).

In Figure 34 are shown two different grains, one obtained from one of the analyzed stacks, with a magnification of 5kX and an average defect width higher than 2 pixels, the other obtained with a magnification of 20kX and with the main defect width higher than 10 pixels. It can be easily seen that defects in the 5kX grain are too thin and not enough resolved for clustering purposes, in fact the not perfect alignment, leading to a small

translation of defects, causes a deterioration of profiles. However, this effect is not impacting in the grain observed with a greater magnification, in which defects appear larger.

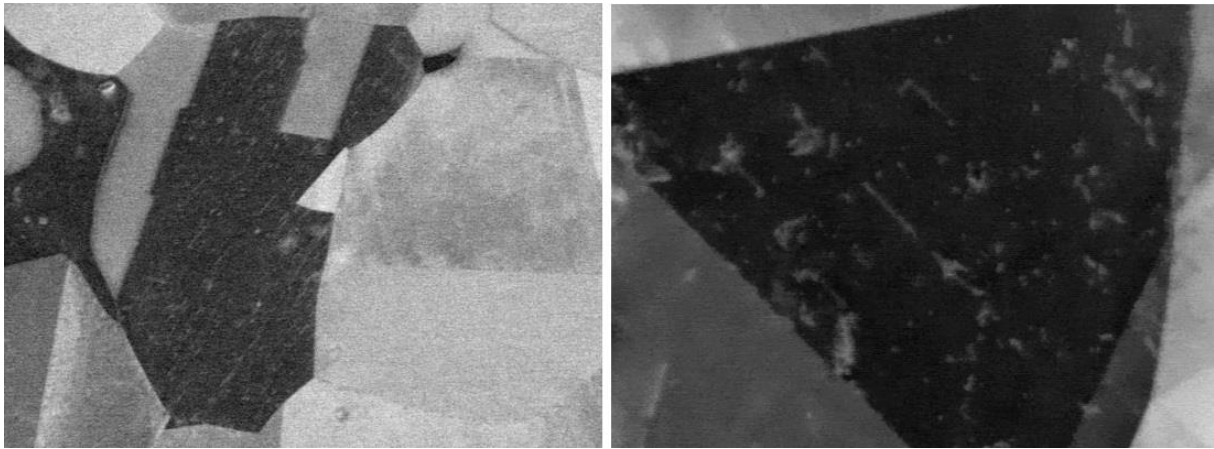


FIGURE 34: COMPARISON BETWEEN TWO DIFFERENT GRAINS, THE ONE AT LEFT IS OBTAINED WITH A MAGNIFICATION OF 5KX, THE ONE AT RIGHT WITH ONE OF 20KX. IS POSSIBLE TO HAVE AN IDEA ON HOW DEFECT WIDTH CHANGES WITH THE MAGNIFICATION.

A magnification of x5k is the very low limit to observe dislocations. Working at higher magnitude is required to observe all the present dislocations and to let the clustering program to work.

As mentioned, the drift and deformation problem has to be considered, in fact a higher magnification causes a larger density of electrons that impacts on the analyzed ROI (if other parameters are kept constant), and charging effects could become important.

Since, by now, a precise alignment at the pixel size is still impossible to achieve, a problem in crystallographic defects detection is produced. In fact, the same pixel could act as a defect in a part of the stack and as the matrix in the rest of the stack. This has an impact on the minimum magnification that must be used; in fact, to overcome this problem it is necessary that the dislocation width measures more than five pixel and this value corresponds to a magnification greater than the ones used in this first set of stacks.

### TILT

Since the tilt defines the radius of the circle along which the eCHORD profile is collected, anticlockwise, it is important to discuss further this parameter in order to optimize it. It must be said that a minimum tilt of  $4^\circ$  is needed in order to achieve a profile from which is possible to obtain the orientation of the relative grain via eCHORD (17).

The smaller is the tilt circle, the smaller is the probability of crossing a large number of Kikuchi bands and therefore TB conditions, as can be seen in Figure 35, in which ECP linked to the 1<sup>st</sup> grain of the sub-zone *bis* is showed. Both  $6.5^\circ$  and  $10^\circ$  tilt circles are represented but the higher tilt allows to include also TB conditions related to the (-111) family of planes, which are not detected with the smaller tilt. Therefore it would be impossible to identify the eventuality of an invisibility criterion in TB conditions missed in the less tilted ( $6.5^\circ$ ) rotational stack.

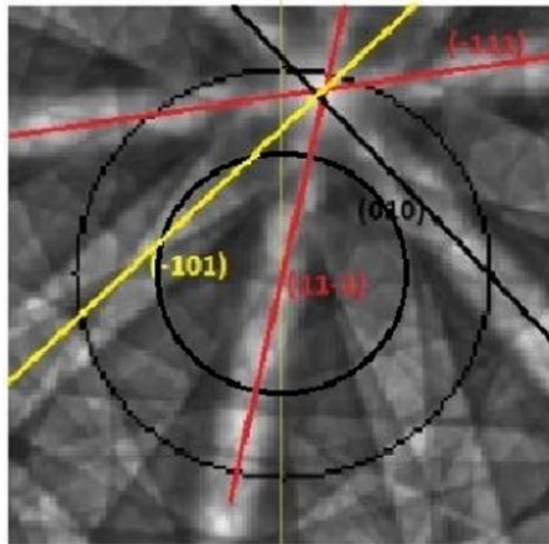


FIGURE 35: ECP OF THE 1<sup>ST</sup> GRAIN OF THE SUB-ZONE 'BIS'. THE SMALLER TILT CIRLE IS RELATED TO A TILT OF 6.5° DEGREES, THE BIGGER TO A TILT OF 10° DEGREES.

In the case of defects analysis, not only Kikuchi bands must be crossed but especially TB conditions, the dark edges of these bands (so called Kikuchi lines), must be achieved. It is in fact in these conditions that dislocations appear.

A zone-axis, where more Kikuchi bands intersect, could be a good opportunity for crossing a large number of TB conditions, but the tilt plays a role in that. In the case of a grain oriented close to a zone axis, the tilt value needed should be large enough to avoid including in the tilt circle the bright part of the ECP, that is related to the center of the zone-axis. This will allow to include more TB conditions. Figure36 is an example of this, indeed the same oriented ECP, centered near to the [101] zone-axis, is represented with two different tilt circles, respectively 10° and 15°, and it is evident how the bigger tilt allows to meet more TB conditions on its tilt circle.

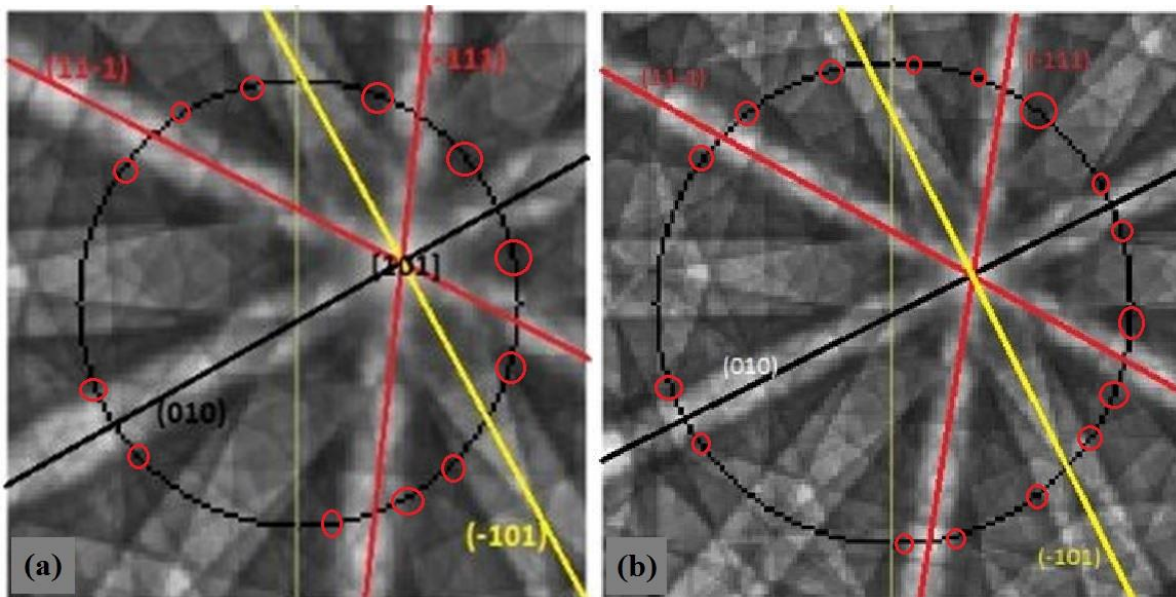


FIGURE 36: ECPS RELATED TO THE 4<sup>TH</sup> GRAIN OF THE SUB-ZONE 'UNO' ARE SHOWN, THE CONCERNED ORIENTATION IS CLOSE TO THE [101] LOW INDEX ZONE-AXIS. TILT CIRCLES REFERE TO AN INCLINATION OF 10° (A) AND 15° (B).

On the other side, by observing the profiles it can be noticed that, keeping the orientation constant, a smaller tilt circle is linked to a greater angular range in which crystallographic defects are visible, in fact the same band covers a larger angular range in smaller circles, obtained with a smaller tilt, simply for geometrical reasons. This can be seen for example watching the portion of the rotational profile that concerns the (11-1) Kikuchi band of the 1<sup>st</sup> grain of the sub-zone *bis* (see Figure 35 for the linked ECP). Figure 37 confronts the profile achieved with a tilt of 6.5° with the one achieved with a tilt of 10°, where the red curves correspond to simulated data and the blue ones to experimental data. Since the band cross perpendicularly both tilt circles, is possible to see how the angular ranges that characterize both TB conditions and bright Kikuchi bands are bigger with a smaller tilt.

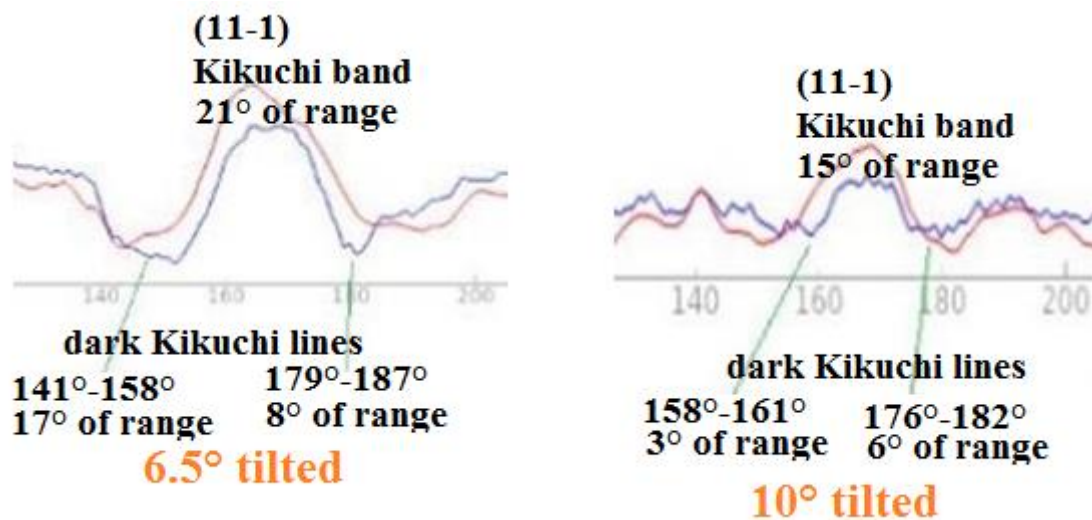


FIGURE 37: PORTION OF ROTATIONAL PROFILES OF THE SAME GRAIN (1<sup>ST</sup> GRAIN OF THE SUB-ZONE 'BIS') BUT OBTAINED WITH TWO DIFFERENT TILT (6.5° AT LEFT AND 10° AT RIGHT). ANGULAR RANGES CHARACTERIZING TB CONDITIONS BECOME BIGGER IF THE TILT IS SMALLER.

Anyway, it must be pointed out that the angular range in a crossed TB condition is not only dependent by this factor; in fact, what mostly affects this range is how the Kikuchi band cross the tilt circle, and this depends on the ECP and therefore on the initial grain orientation.

In the studied scenario, there is only one situation where a tilt of 10° degrees doesn't allow to individuate all invisibility criterions found with a greater tilt (see grain 3 of the sub-zone 'uno'). To achieve a greater probability of crossing many TB conditions a 15° tilt is suggested, but a 10° tilt is enough most of the times. Greater tilts would make the angular range, in which TB conditions are found, too small for defect detection purposes. It must be said that this result is relative to the studied material that has a fcc geometry, therefore further investigations must be done for other geometries.

The contrast between defects and matrix varies a lot when different TB conditions are studied but it is not influenced by the value of tilt. In fact, higher contrast is achieved in specific orientations of the sample that could be met for a given value of tilt or for another, depending on the initial orientation of the sample, which defines the ECP.

Further studies should be done in future in order to give results which statistically describe the number of crossed TB conditions for a given tilt angle.

## BEAM ENERGY

The energy beam is another important parameter to set in order to obtain a satisfying channeling contrast and therefore being able to see crystallographic defects in TB conditions. In fact, as Zaefferer et al. says, with the used instrument channeling conditions improves augmenting the acceleration voltage (2). Indeed, augmenting the energy beam means to have thinner Kikuchi bands in the ECP, but for what concerns darker Kikuchi lines at edges of the bands, which are responsible of the darker contrast of TB conditions, they seems to be more defined and thicker with higher energy beams, as showed in Figure38.

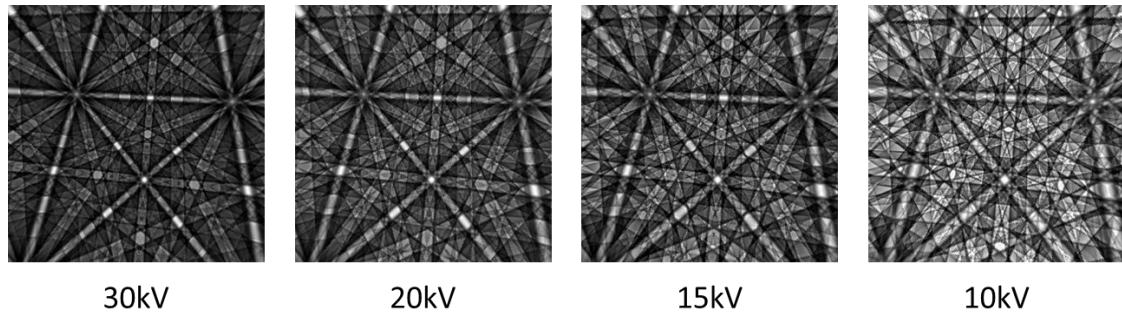


FIGURE 38: HOW ACELERATING VOLTAGE INFLUENCE ECPS ON FCC MATERIAL (AUSTENITE). ECPS OBTAINED SIMULATING HIGHER VOLTAGES SHOW MORE DETAILS AND SEEMS TO ENNANCE THE CHANNELING CONTRAST ON KIKUCHI LINES, WHICH APPEAR DARKER THAN ECP SIMULATED AT LOWER ACELERATING VOLTAGES.

In order to verify this effect, stacks concerning grains of the sub-zone *bis*, analyzed under two different beam energies (20 and 30 keV), have been compared and it was deduced that, in the studied scenario, the angular range in which defects are visible is not influenced by this factor. Figure 39 shows the ROI in the two different stacks; the evaluation of the contrast between defects and matrix demonstrates that working with 20 or 30 keV has no significant effect on the results. Therefore, in order to reduce the charging problems, a value of beam energy of 20 keV should be preferred.

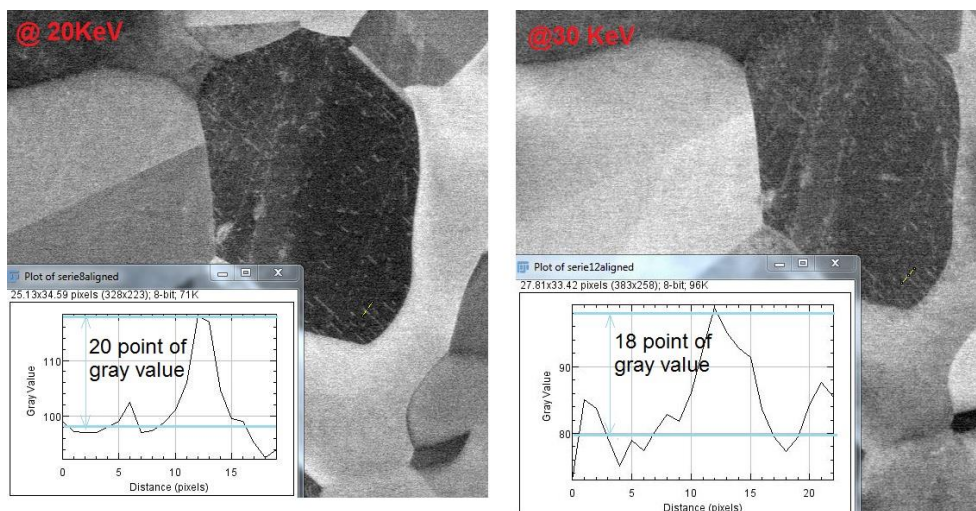


FIGURE 39: THE GRAIN1 OF THE SUB-ZONE 'BIS' SEEN WITH DIFFERENT BEAM ENERGIES (20KEV AT LEFT AND 30 KEV AT RIGHT). A PLOT OF THE GRAY INTENSITY VALUE ALONG A LINE WHICH CROSSES A CRYSTALLOGRAPHIC DEFECT IS LINKED TO EACH IMAGE.

However, it must be taken into account that, in this set of stacks, only two stacks present different energy beam and can be compared together, therefore further investigations should be done. Moreover, the stack taken with 30 keV has been the 4<sup>th</sup> stack taken on the sub-zone 'bis' and so results could be influenced by contamination.

Higher beam energy allows also to hide surface defects left during the polishing, such as dusts and scratches, in fact the interaction volume get higher and deeper with the accelerating voltage and surface details are lost. On the other hand, with higher volumes of interaction there is the risk of collecting information from deeper grains, as already mentioned.

It has to be considered that augmenting the beam energy causes also a worsening of rotational stacks quality, in fact, in that case more contamination and charging phenomena are present.

A work on single ECC Images, similar to the one done for testing the scan speed, has been done with the beam energy. What it has been firstly deduced is that 15 keV are not enough for a good visibility of defects. Furthermore, higher values of beam energy seem to augment the resolution of defects but, on the other hand, values too big causes a diminution of the contrast between defects and matrix. This could explained either for the changed geometry between electron beam and crystal or for an augmented backscattering ratio of the matrix, if higher beam energies are used.

As a consequence, to use a beam energy of 30 keV might be useful only when the aim is to perfectly resolve single dislocations, and for that aim very high magnifications are needed (order of 60kX); unfortunately, this is not possible with the instrument used in the thesis. Figure 40 shows the same ROI visualized at different beam energies and the gray intensity profiles collected along a segment which crosses a group of dislocations, that have been used to evaluate the contrast between matrix and defects in the same way as in the work described previously on the evaluation of the effect of scan speed.

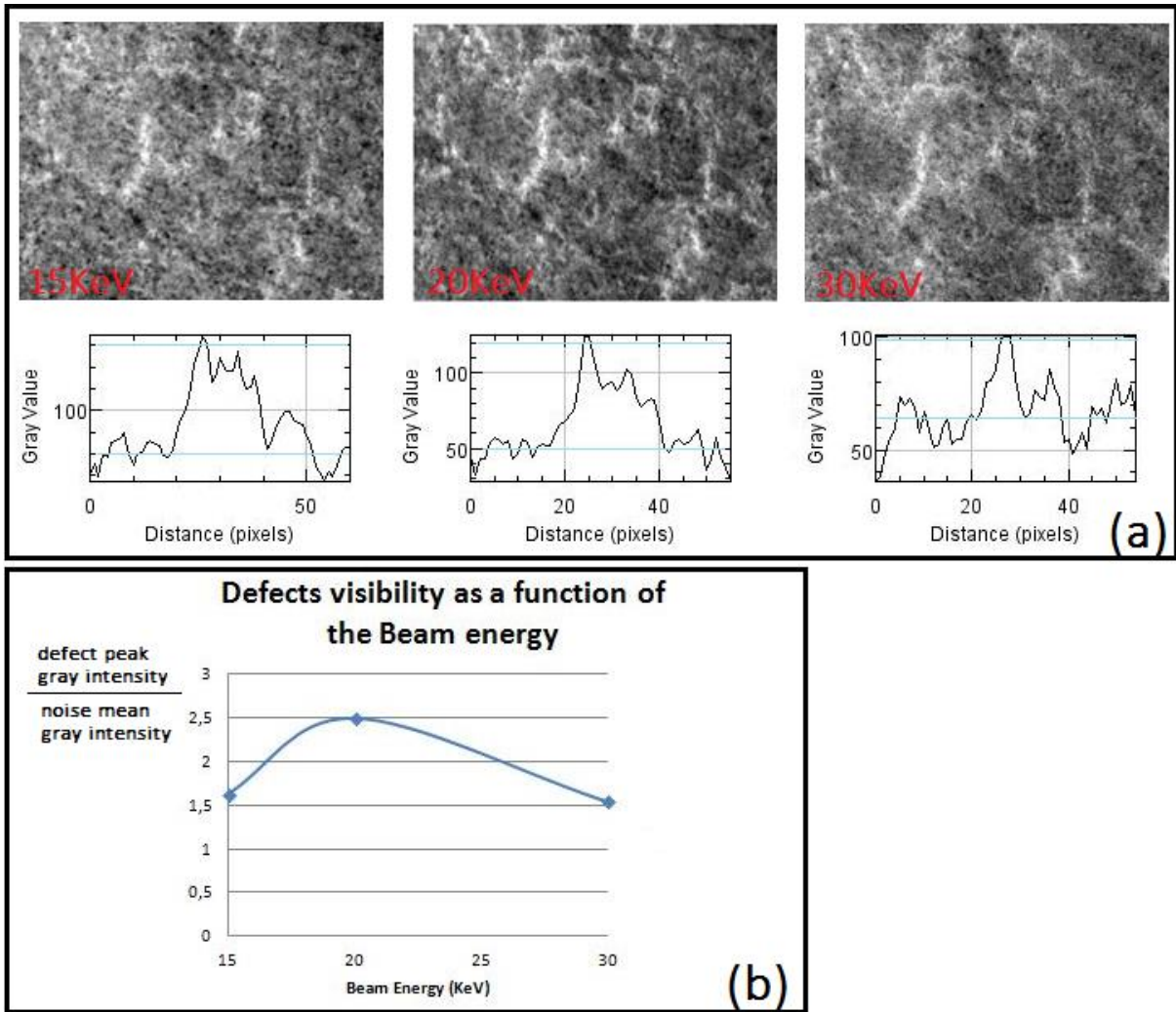


FIGURE 40: (A) THE INFLUENCE OF THE BEAM INTENSITY ON THE VISIBILITY OF DISLOCATIONS, INTENSITY PROFILES COLLECTED ALONG A SEGMENT WHICH CROSSES DEFECTS ARE LINKED TO EACH IMAGE . (B) HOW THE CONTRAST BETWEEN MATRIX AND DEFECT VARIES WITH THE STUDIED PARAMETER.

Hence, 20 keV seems to be the best value to use for the purpose of this master' thesis.

### APERTURE DIAMETER

The last parameter that has been studied is the aperture diameter, also in that case the used strategy was to confront ECC Images achieved with different values of this parameter. Figure41 shows these images and the relative profiles collected along a line which crosses a zone rich of dislocations (circled in red).

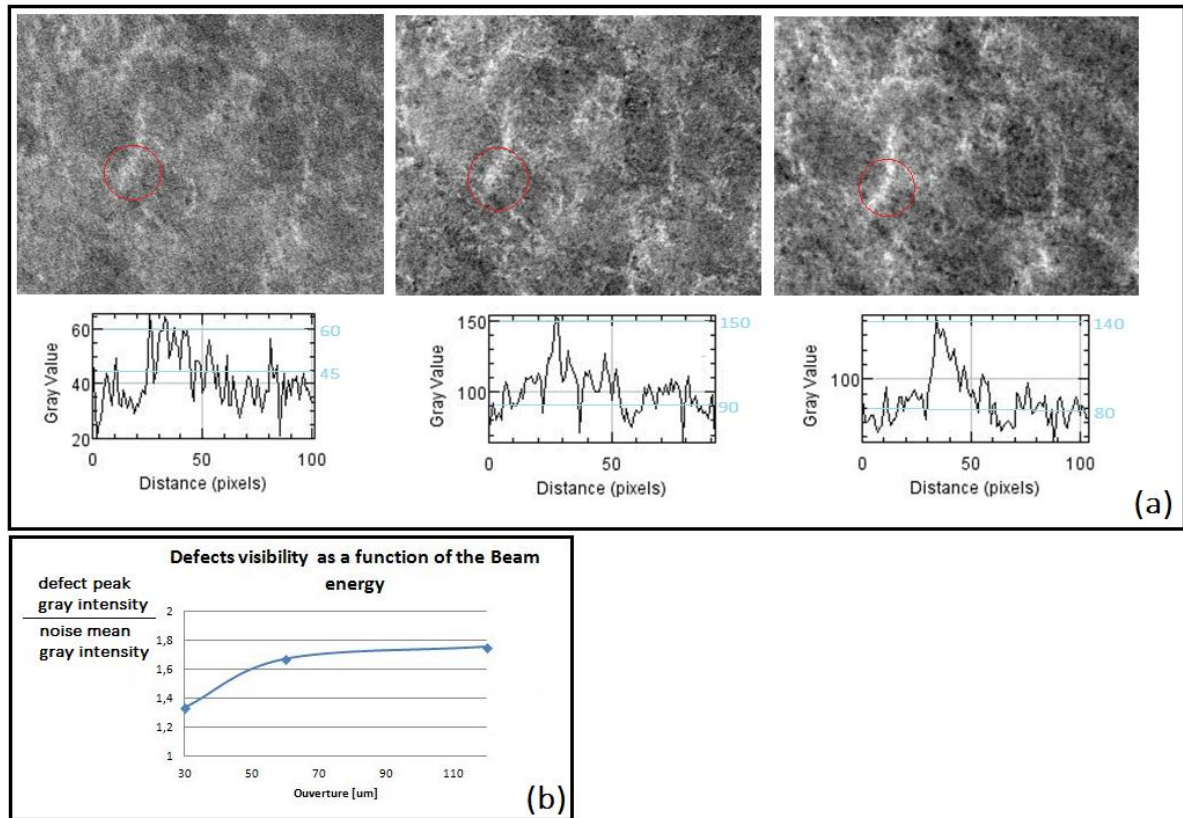


FIGURE 41: (A) THE INFLUENCE OF THE DIAMETER APERTUREY ON THE VISIBILITY OF DISLOCATIONS, INTENSITY PROFILES COLLECTED ALONG A SEGMENT WHICH CROSSES DEFECTS ARE LINKED TO EACH IMAGE . (B) HOW THE CONTRAST BETWEEN MATRIX AND DEFECT VARIES WITH THE STUDIED PARAMETER.

It is evident that the dislocations are more visible if the diameter aperture is higher, since this maximizes the signal to noise ratio. The maximum value (120  $\mu\text{m}$ ) is found to be the best one, as also suggested by Zaefferer et al. (2).

## EXPERIMENTAL PARAMETERS CONCLUSION

Looking at these first results, it is clear that the initial orientation of the grain mostly influences results and that is a random factor.

The gray level depends on the position of a TB condition on the ECP since it could overlap with other brighter or darker bands. Again, this is orientation dependent.

TB conditions often presents short angular ranges (above  $5^\circ$ ), but sometimes it is possible to observe much bigger angular ranges (above  $20^\circ$  and more) and that is due to a particular disposition of a Kikuchi line, which has to be tangent to the tilt circle. An example is shown in the ECP of Figure42 in which the ECP of the 4<sup>th</sup> grain of the sub zone *bis* is represented with the relative experimental and simulated profiles: (100) oriented planes present a Kikuchi line that is tangent to the  $10^\circ$  tilt circle, widening the TB angular range up to  $34^\circ$ .

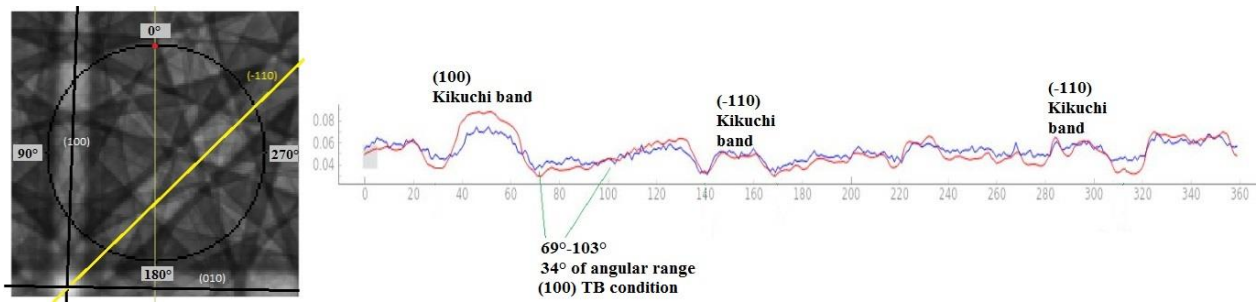


FIGURE 42: AT LEFT, A REPRESENTATION OF THE ECP OF THE 4<sup>TH</sup> GRAIN OF THE STACK3, AT RIGHT RELATIVE PROFILES, BOTH EXPERIMENTAL AND THEORETICAL. THE (100) KIKUCHI BAND IS ORIENTED SO AS TO EXPANDING THE ANGULAR RANGE OF THE RELATIVE TB CONDITION.

To characterize the Burgers' vector of a dislocation, at least two invisibility criteria have to be crossed, and such a situation happens sometimes but isn't predictable. For this reason it is important to select grains where more Kikuchi bands cross the tilt circle. Moreover, crossing a larger number of these conditions would also improve the number of images in which defects are presents, and this would certainly help the defects recognition via clustering.

An orientation close to a *zone axis*, namely a high symmetrical direction that is shared by many families of planes, could be the most promising solution. Anyway, it is not certainly linked to the presence of invisibility criteria. A faster and less magnified preliminary stack, with a worst quality of images, is therefore useful for firstly indexing a larger number of grains, on order to analyze relative ECPs and to chose the best ROI in which to work and the optimal tilt. However it has to be said that this would limit the choice of grains to be analyzed and that is a problem. A solution to this issue might be to change the sub-stage of the microscope with one composed of two axis of tilt, so that it would be possible to change the initial orientation of any grain to be analyzed, in order to put it close to a zone-axis, similarly to the case of TEM analysis.

It is important to remind that the visibility of dislocations and therefore their quantitative characterization via clustering is possible even without an eCHORD indexation and a previous analysis of ECPs. In fact, this has been done just in order to better understand and study the technique. On the other side, a qualitative analysis of the nature of dislocations, to characterize the Burgers vector, needs an indexation of the analyzed grains.

The image quality can also get worse during the analysis for contamination problems, for example the sub-zone *bis*, that has been submitted to three stack acquisition, has shown a deterioration in image quality during the time, as a consequence also the best alignment was observed in the first acquired stack.

---

## INITIAL APPROACH TO THE BURGERS VECTOR DETERMINATION VIA ROTATIONAL STACKS

---

As mentioned, in order to characterize the Burgers vector of dislocations it is essential to achieve at least two invisibility criteria in TB conditions that concern different families of planes. This set of stacks has also been used for investigating toward this direction, in

order to understand if disCHORD could open the possibility of a qualitative analysis of dislocations too.

Anyway, with this magnification it is not possible to resolve single dislocations and therefore the hypothesis that all dislocations in a given grain have the same Burgers vector was made. This would allow to search the eventuality of invisibility criterions on a whole grain, overcoming the problem of trying to resolve single dislocations. Therefore, the results achieved with that method are not reliable entirely, but they can give an idea on the feasibility of a characterization of the Burgers vector via disCHORD.

### ANALYSIS STEPS

---

It is necessary to link each two beam condition crossed during a stack with specific family of crystallographic planes and then to study how often the invisibility criterion is achieved.

The steps done on each analyzed stack, that has obviously to be already denoised and aligned, are the following:

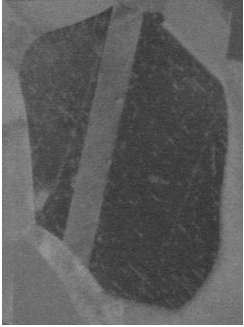
1. *Indexation of the ROI* by EBSD analysis and eCHORD analysis, in order to know Euler's angles for each analyzed grain.
2. *Selection of grains that have to be analyzed*, it is better to choose ones with more *two beam* (TB) conditions, in which crystallographic defects are expected to appear.
3. *Indexation optimizing with CHORD program* (developed by C. Lafond) which, starting by known Euler's angles, is able to find the orientation that gives the best superposition between theoretical and experimental profiles. This have to be done for every analyzed grain.
4. *Production and indexation of Pole figures centered in the optimized orientation of every analyzed grain*. In these figures it is represented the stereographic projection of principal families of crystallographic planes, furthermore they can be superposed to the ECP characterizing the same orientation and, consequently, Kikuchi bands are indexed too.
5. *Identify the diffracting plane linked to every TB condition crossed in the stack*. Knowing the rotational angle in which a Kikuchi line (where channeling conditions are achieved) crosses the tilt circle on the ECP, it is possible to characterize the  $g_{hkl}$  vector for the corresponding TB condition in the stack.
6. *Check the presence of an invisibility criterion in some crossed TB condition*. All crossed TB conditions must to be seen in the stack in order to verify the visibility of dislocations.
7. *Determinate the Burgers vector if two invisibility criterions are found*.

For better understanding this procedure, Annexe1 shows a detailed example of these steps applied on the 4<sup>th</sup> grain of the sub-zone *uno*.

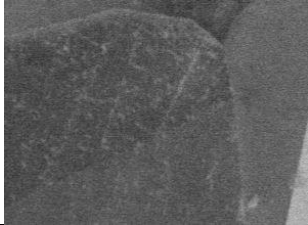
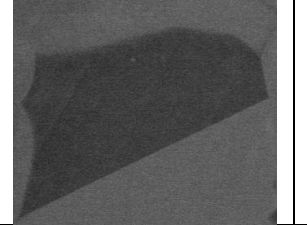
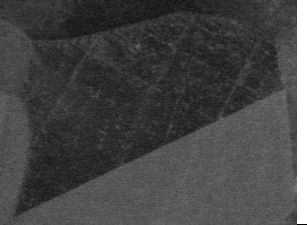
## RESULTS

An overview on different situation of orientations and used parameters has been achieved, the Burgers vector has been found for two out of eight analyzed grains.

Here following two examples of achieved results.

TB GRAIN1 subzone <i>bis</i>	(-111)	(-101)	(11-1)	(010)
images				
Defects visibility	visible	not visible	visible	not visible
notes	This Kikuchi band is crossed just with a tilt of 10°, therefore it is not present in stack 7 and 8.	Visible just in stack 3 (10° tilt) and 8 (6.5° tilt).		Not visible in stack 7. Certain Kikuchi bands overlap each other and so the invisibility is lost.

Since that two invisibility criterion are met, it is possible to give a value to the Burgers vector for the analyzed grain. Considering that in (-1 0 1) and (0 1 0) diffracting planes the equation  $g_{hkl} * \bar{b} = 0$  is respected (invisibility criterion present), and that  $\bar{b}$  is the same, with some analytical calculus the Burgers vector is found to be  $\bar{b} = \frac{1}{2}(\mathbf{101})$

TB GRAIN2 subzone <i>bis</i>	(-111)	(-101)	(11-1)
images			
Defects visibility	visible	not visible	visible
notes	This Kikuchi band is crossed just with a tilt of 10°, therefore it is not present in stack 7 and 8.		With a tilt of 6.5° the TB has a very big angular range (see the concerned ECP)

Achieved invisibility criterions are not enough to determine the Burgers vector for this analyzed grain.

This analysis has highlighted that:

- A higher magnification is needed (more than 5000x) to better image dislocations individually.
- Not enough TB conditions are met in a random matter in order to determine the Burgers vector nature. Each grain should then be observed with different orientations, ie several rotation series are needed for each grain. To do this, the use of a double tilted sub-stage would be necessary.
- Not indexed TB conditions are crossed through the stack, and the eventuality of an invisibility criterion is sometimes met also there. It would be useful a better indexation of ECPs, considering a larger number of families of planes.

For all these reasons automation in searching invisibility criterions via disCHORD might be very complicated and requires for sure a better quality of images.

All other results of this analysis are showed in the annexe2.

---

## DISLOCATION DENSITY VIA CLUSTERING

---

The clustering program can be used to calculate the fraction of defect pixels and then the dislocations density since it is able to discriminate the behavior of each pixel in the stack, cataloguing it as a part of the matrix or as a defect.

The program was run on these stacks in order to discriminate the matrix by crystallographic defects. The detection is made confronting the pixels profiles of a single grain and discriminating the ones relative to a matrix profile with respect to the ones relative to a feature profile.

As already mentioned, by analyzing the results achieved with these stacks, it can be observed that the program is not able to distinguish crystallographic defects from the matrix. This is due to the fact that defects are not enough resolved with the chosen parameters. Basically, with a magnification of 5kX, defects are very small and poorly resolved and this fact, added to a not perfect alignment, makes impossible to have profiles with enough precision for defects detecting purposes. It is therefore necessary to improve image quality if dislocation density is to be detected. This can be reached either by augmenting the magnification and the time of scansion, or by using an image size of 2k. However, drift and deformation problems must be avoided during the stack acquisition. If in the future significant improvements will be done in the alignment strategy, these stacks could be re-aligned in order to obtain cleaner profiles that could finally be used for the clustering.

## II. SECOND DUPLEX EXPERIMENTAL SET OF STACKS: A STRATEGY TO IMPROVE STACKS QUALITY FOR CLUSTERING PURPOSES

To achieve a good resolution of the image in a reasonable amount of time, it has been chosen to split the total rotational range ( $0^{\circ}$ - $360^{\circ}$ ) into many, smaller mini-stacks. Since, as already said, dislocations' and matrix's profiles differ just in some angular conditions (TB conditions), it was thought to acquire mini-stacks just in these conditions keeping just the "interesting" part of the stack, for what concern the defect detection, and dropping the rest. For this purpose, a quick complete stack was done for detecting TB conditions and, after that, miniseries were taken, denoised, aligned and stocked. Finally, stacks relative to the same ROI but in different TB conditions were stuck together to form the final stack, which had to be re-aligned. It was observed that collecting these smaller stacks of images (above 15 images instead of 360) reduced by far charging and de-focusing problems and opens the possibility of improving magnification and scan speed in order to achieve better results in the quality of images.

Also this time a DUPLEX steel sample was used, the ROI of the preliminary stack is shown in Figure 43, taken with a magnification of 5kX, an energy beam of 20 keV and a scan speed of 5. In the figure are indicated two grains, on which other mini-stacks at higher magnification and scan speed were taken, and that will be used in order to verify the usefulness of rotational profiles for defects detection. For these mini-stacks, it was chosen to use a magnification of 20kX, an energy beam of 20 keV and a scan speed of 9, always verifying the presence of drift before to start the acquisition. All other parameters are the same of the Table 3 except for the used *angular path* that has been changed to  $0.5^{\circ}$ .

For what concern other parameters, the fixed parameters shown in Table 3 were used.

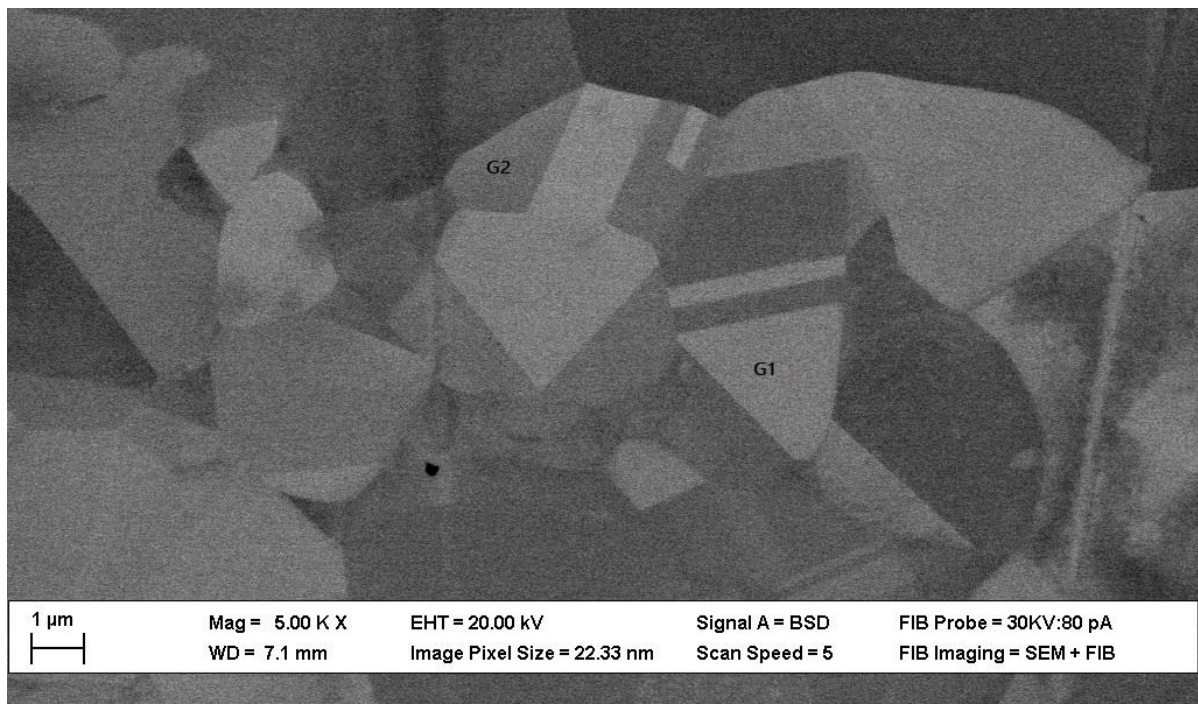


FIGURE 43: ROI OF THE PRELIMINARY STACK, DUPLEX SAMPLE. ANALYZED GRAINS G1 AND G2 ARE SHOWN.

By using the preliminary stack, an eCHORD indexation of ECPs belonging to analyzed grains was done, in order to link a diffracting plane to crossed Kikuchi bands. Results for Grain1 are shown in Figure44.

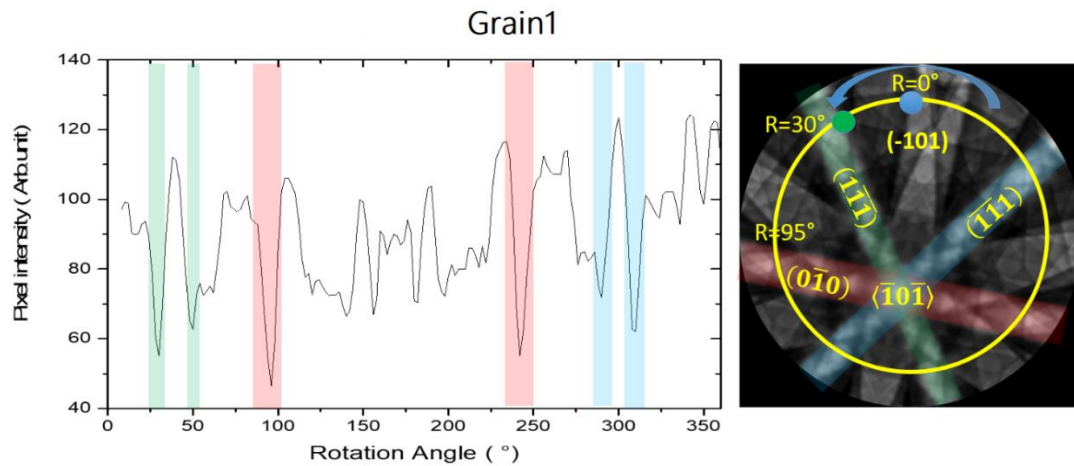


FIGURE 44: INTENSITY PROFILE OF THE GRAIN1, LINKED TO THE CORRESPONDENT ECP, THEREFORE CENTERED IN ITS ORIENTATION. DIFFRACTING PLANES OF KIKUCHI BANDS ARE INDICATED TOO.

Thanks to this analysis, angular ranges in which to achieve mini-stacks were chosen:

Angular range	24.5° - 33.0°	44.5° - 52.0°	91.5° - 100.0°	285.5° - 295.0°	305.5° - 315°
Concerned Kikuchi line	(1-1-1)	(1-1-1)	(0-10)	(-1-11)	(-1-11)

Observing mini-stacks, a visibility of defects coherent with the concerned type of diffracting plane was obtained and can be visualized in Figure45.

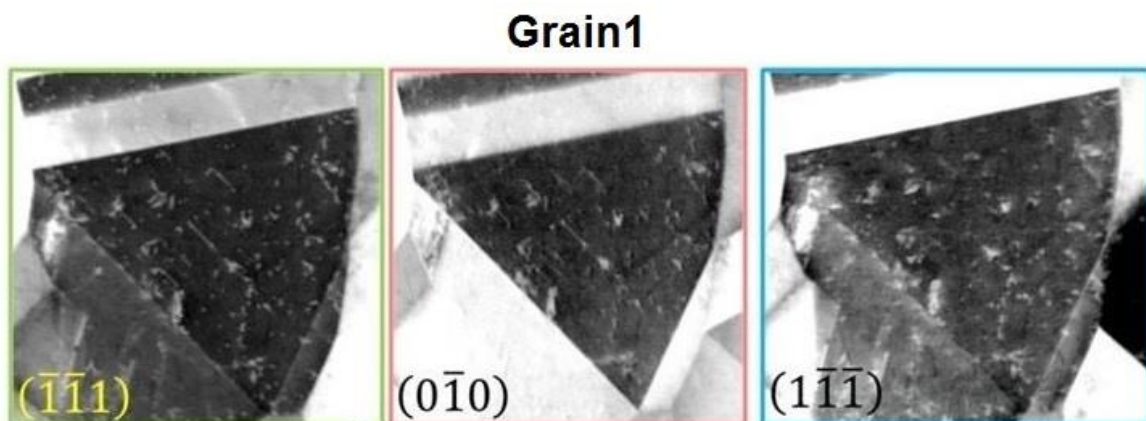


FIGURE 45: REPRESENTATION OF THE DIFFERENT TB CONDITIONS CROSSED DURING THE ROTATIONAL STACK.

The grain2 has also been studied and results are stocked in the Annexe3.

## ROTATIONAL PROFILES OF MINI-STACKS

Mini-stacks concerning different TB condition were stuck together. A better quality of images was reached.

Three zones of the analyzed grain, for which different behavior are expected, were chosen in order to verify if their rotational profiles are enough different to allow a clustering detection of defects. Figure 46a shows the zones, the one circled in blue is a dislocation, the one circled in red is a stacking fault and the one circled in black is the matrix. Profiles of these zones are in Figure 46b.

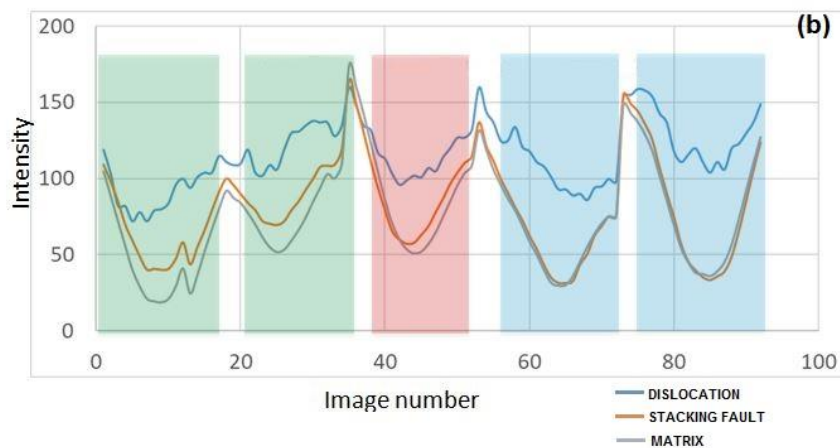
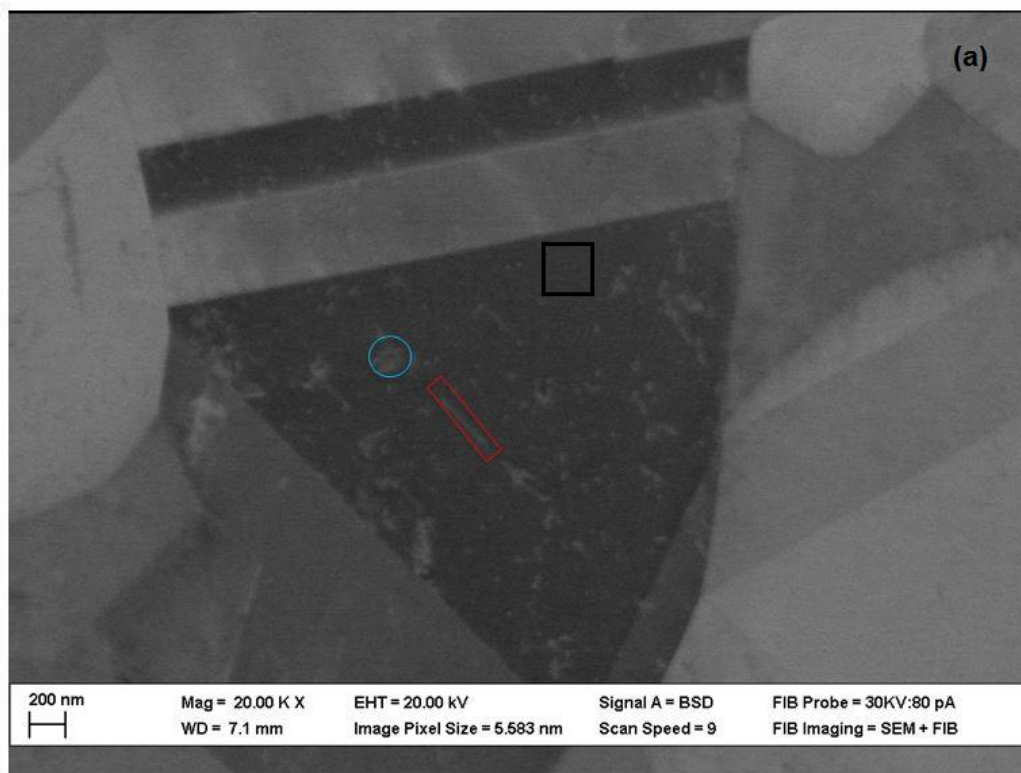


FIGURE 46: INTENSITY PROFILE OF THE DIFFERENT PIXEL TYPES ( MATRIX, STACKING FAULT AND DISLOCATION).

Promising results were obtained, indeed achieved profiles effectively refer to a precise physical zone in the analyzed grain with a good approximation. Profiles of crystallographic defects are effectively brighter than the profile of the matrix, even if the difference is less pronounced for stacking fault profiles.

When looking at the red profile, which refers to a stacking fault, it can be noted that an invisibility criterion is achieved in last two TB conditions, referring to the  $(-1 -1 1)$  diffracting plane

To conclude, thanks to the use of mini-stacks, there is enough difference in intensity profiles to discriminate between the different pixels type. Therefore, it is worth to try to analyze the stack with the clustering program for detecting crystallographic defects and for trying to develop an alternative way to characterize them.

Anyway, it must be noted that the used magnification doesn't allow to analyze more than one grain for each acquired stack therefore, for having statistic results, lots of mini-stacks have to be taken. Anyway, the acquisition of a mini-stack is faster than the acquisition of a total stack, and it is easily affordable to achieve experimental data for analyzing at least 3 grains in above 3 hours.

## F. DATA PROCESSING WITH CLUSTERING PROGRAMME

---

Thanks to the achieved good quality of images, resolution and alignment, the discrimination between matrix and crystallographic defects using differences between profiles is now possible. It has to be noted that profiles do not refer to the complete rotation, such as eCHORD profiles, but just some portions, in which TB conditions are achieved.

Since the clustering program is custom made, was never used before and presents some bugs, time for understanding how it works and which problems it presents was necessary. Briefly, the program starts to separate grains with an initial clustering, recognizing profiles that are different in the totality of the angular range. Selecting just one grain, the program is able to discriminate the matrix from crystallographic defects with a finer clustering, always using profiles associated to each pixel.

### I. CLUSTERING THEORY

---

To get closer to the ambitious objective of this master's thesis, a key point is to discriminate crystallographic defects pixels from matrix pixels using differences between profiles. For such a purpose a clustering program has been coded by C.A.Roth and T. Dreyfus, even if some bugs have still to be fixed, that should allow this discrimination. Furthermore, this program showed a potential also in discriminating zones with different families of intensity profiles such as different grains, different phases, precipitates, porosities and dusts.

Clustering is a Machine Learning technique that involves the grouping of data points. Given a set of data points, we can use a clustering algorithm to classify each one into a specific group. Once the clustering is finished, data points that are in the same group should have similar properties and/or features (in the studied case similar intensity profiles), while data points in different groups should have highly dissimilar properties and/or features. Clustering is a method of unsupervised learning and is a common technique for statistical data analysis in many fields. This kind of analysis is used to gain valuable information from our data by seeing into which groups the points fall when a clustering algorithm is applied (23).

The custom-made program, written in Python programming language, is made for discriminating different areas in a sample using a stack of several images of the same zone. Every image of the stack is taken with different experimental conditions achieved with different angles between sample and electrons beam or with different analysis (SE, BSE...), that will lead to different contrasts between different images. In fact, if the alignment between images was done successfully, to each pixel of a stack corresponds an experimental profile characterizing the variation of the contrast with the variation of experimental conditions. Consequently every profile will characterize the behavior of the single pixel concerned.

The program will analyze a selected portion of the region of interest comparing N - dimensional vectors associated to the profile of each pixel each others, where N is the images number of a stack. That will lead to the creation of clusters made of pixels having a similar profile and therefore a similar behavior. Since the program analyze profiles and not pixels themselves, the notion of similarity between two pixels relies on the similarity of profiles associated to them, and so a cluster could initially include pixels that are physically not linked each others in the stack.

In this kind of analysis, the first issue concerns the size of the data. In the most extreme cases, an input image might contain more than 3 million pixels, and usually the dataset for eCHORD contains 360 images. This means that running the clustering over the whole dataset requires processing  $\sim 1$  billion values. However, the information is highly redundant in the profiles over a grain and so a Principal Component Analysis (PCA) can be run in order to project the data onto a lower dimensional space, in which projected coordinates represent just high variance dimensions in the original space (24). This significantly reduces the size of the data to process. Note that, while running PCA over the input, those  $\sim 1$  billion values have anyway to be processed. To circumvent this difficulty, an approximation of PCA known as Incremental PCA has been used: this approximation allows to build the principal components incrementally by batches of a given size, leading to a speeding up of the process (24).

Once the dimension of the given file was reduced, a primary clustering is done for separating different grains present in the stack. The simplest approach consists in using the Euclidean distance between profiles, since all dimensions will be considered with an equal weight. K-means algorithm is used, it is a knowledge-based algorithm, meaning that the number of clusters searched must be given as an input. This is not a problem since the number of grains is usually countable from the images, and some post-processing might help merging or splitting undesirable clusters (24). However, this might be an issue if this clustering step has to be fully automated. Even if k-means is the best candidate, for comparing purposes, other clustering algorithms are provided.

Given a single cluster representing a single grain or given a manually selected area, which has to be chosen within a grain, the program can try to recognize defects contained in it with a finer clustering. Pixels within a grain sharing a similar profile along all the dimensions are catalogued as the matrix. When a profile is dissimilar to the average matrix profile only on some specific sets of consecutive dimensions, which correspond to TB conditions, it is discriminated as a feature profile and it represents a defect. Some profiles which are almost flat could also been observed and they are catalogued as dust. Finally, profiles that do not enter any of these categories are called noise. Note that the matrix is considered to be the largest cluster.

A feature should differs the most from the matrix on a window of consecutive dimensions and to compute this difference a variant of the Chebychev distance is used, where averages of the coordinates over consecutive dimensions are used rather than the coordinates directly:

$$d_{k_c}(x, y) = \max_{1 \leq i \leq n-k} \left| \frac{1}{k} \sum_{j=i}^{i+k-1} x_j - \frac{1}{k} \sum_{j=i}^{i+k-1} y_j \right|$$

where  $k$  is the window size. We call such a variant the  $k$ -window-Chebyshev distance, when  $k = 1$  it fits to the usual Chebyshev distance (24).

The bigger cluster is considered as the matrix and other are then catalogued. It's important to keep in mind that the clustering was done on the profiles and not on the pixels and so several features are initially engulfed in the same cluster. To overcome that, connected components of pixels are computed for each cluster of profiles and then separated in single feature clusters (24). Afterwards, each independent set that is too small to be considered as a feature will be discarded and listed as noise while others will be catalogued as features or dust (if the profile is flat).

Note that the clustering algorithm can be chosen just for the primary step: the clustering of different grains. Indeed for the clustering of defects the DBscan algorithm is used and no information about the number of clusters is needed as an input.

## II. HOW TO USE THE PROGRAM AND HOW RESULTS ARE SHOWN

The final result will be a grain in which matrix pixels are colored in green, defects' in blue and noise's pixels in gray, as shown in Figure47. It is possible to obtain also information about profiles. Moreover a file '.txt' can be saved, in which to every pixel  $XY$  is associated a specific number in order to classify it:

- '0' if the pixel is part of the matrix
- '1' if the pixel is part of a feature (crystallographic defect)
- '-1' if the pixel is considered as a noise
- '2' if the pixel is part of a dust (the contrast is constant along the angular range)

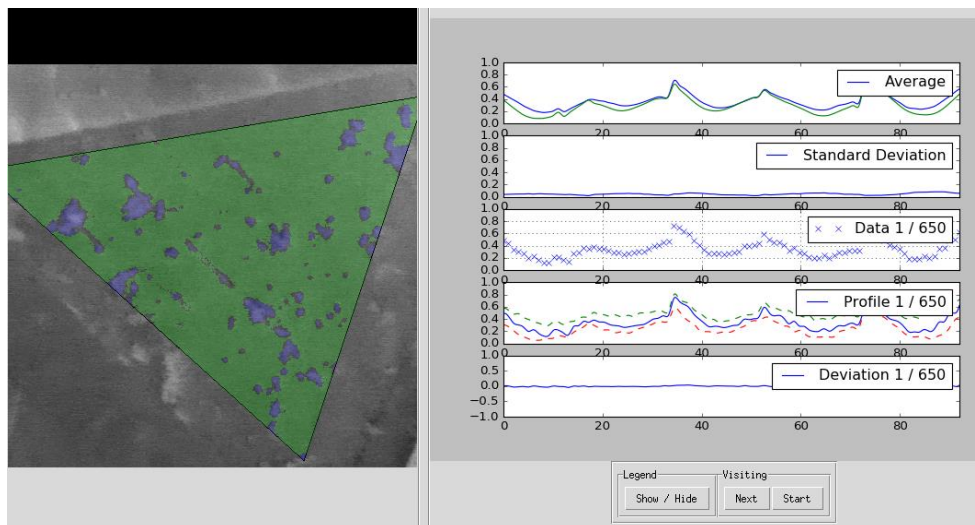


FIGURE 47: EXAMPLE OF A CLUSTERING ANALYSIS RESULT. IN THE ANALYZED GRAIN MATRIX (GREEN) AND FEATURES (BLUE) ARE SEPARATED. OBSERVING PROFILES, IT CAN BE SEEN THAT THE AVERAGE

PROFILE OF DEFECTS SHOWS AN INTENSITY HIGHER THAN MATRIX'S IN SPECIFICS ANGLES (TB CONDITIONS).

Moreover, if a pixel is part of a feature, in the file '.txt' are noted all angles in which there is effectively a significant difference with the matrix profile, that is taken as a reference. In this way is possible to know in which TB conditions the pixel of a feature is visible through the matrix and in which TB conditions it is not. That could effectively lead to an automatic characterization and recognition of invisibility criterions.

An example of an output file '.txt' is shown in Figure48. It is possible to save similar files which concern each single feature, in which all pixels belonging to the selected defect are written with their discriminating angles.

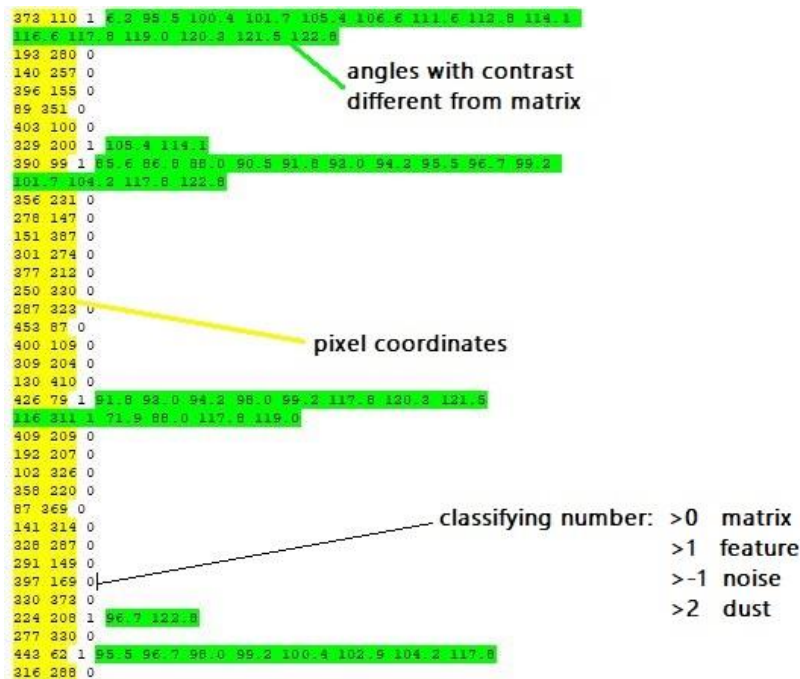


FIGURE 48: EXAMPLE OF AN OUTPUT FILE '.TXT' REFERRING TO PIXEL OF AN ANALYZED GRAIN. INFORMATION ABOUT COORDINATES, TYPE OF THE PIXEL ARE GIVEN, IF THE PIXEL BELONGS TO A PIXEL THE DISCRIMINATING ANGLES ARE ALSO NOTED.

It has to be noted that TB conditions crossed during a rotation owns an angular range larger than one degree and many times a feature pixel shows to be bright just in a fraction of this angular range. It is therefore difficult, watching at these files, to define if this pixel is effectively visible or not in this TB condition. Another issue is that in the file '.txt' referring to a single defect, it is found that its pixels don't present exactly the same angles in which there is a difference with matrix's profile, even if in theory all pixels of a single feature must behave in the same way. For these reasons an investigation needs still to be done in order to verify the efficiency of the clustering method.

While using the clustering program, many parameters can be varied in the used algorithm, and thus hereafter a brief overview on the main parameters and their meaning is given.

Let's firstly explain the main parameters in the preliminary clustering, in which different grains are detected. The 'detecting features' part will analyzed later.

- *Number of clusters*: for choosing the number of clusters that will be obtained, the program analyze profiles in order to distinguish the selected number of ‘different families’.
- *PCA number features*: Represent the number of dimensions (size) which the representation of a profile is going to have after having filtered the non-significant dimensions (see chapter ‘*Clustering theory*’). It can not exceed the dimension of the stack analyzed.

Once the results are obtained, it is possible to modify them; the operator can check if it is necessary to merge two different kinds of cluster, to split a ‘profiles family’ into smaller families, to re-cluster or to eliminate an entire family. In that way, the grain separation should reach acceptable results.

Once separated different grains, each one can be chosen to be analyzed, so that a ‘deeper’ clustering can be done for detecting features. It must be kept in mind that the analyzed area can also be ‘hand-selected’ by the operator with the command ‘*select region*’. Also in this step some parameters can be modified such as:

- *Epsilon*: Represents the maximal vectorial distance (between profiles) so that two profiles are considered similar. The bigger this distance is, the more the program is going to consider "similar" different profiles while detecting the matrix (that is the first to be detected) and so fewer pixels of defects will be detected. Currently, it seems that the results are not very sensitive to this parameter.
- *Noise size*: it defines boundaries between the matrix and defects. The smaller it is, the less noise will be obtained.
- *Window size*: Represents the size of the angular window used for calculating the distance between two profiles during the detection of the dislocations (the angular range of TB conditions used by the program).
- *Feature deviation <1*: considering the “epsilon circle” (in the profiles space), it defines the fraction of pixels similar to the analyzed one that must be achieved for considering the analyzed pixel one of them. (If it is low a bigger cluster will be obtained).

It must be said that the most impacting parameters in feature detection are the last two: *Feature deviation* and *Window size*. While analyzing stacks 9 and 10, these parameters were set in order to achieve the better superposition of detected features, (in blue in Figure47) with crystallographic defects in TB conditions, brighter than the matrix. Then several values of *noise size* were used in order to obtain the relative files ‘.txt’, in order to obtain different values of *dislocation density* and to compare them with the *dislocation density* obtained with the traditional method of intercepts.

---

## A STRATEGY FOR AUGMENTING THE QUALITY OF CLUSTERING

---

Once the mini-stacks of this last analyzed grain were aligned and concatenated in the right order, a first essay with the clustering program has been done. The first result was discouraging, since features were badly detected and lot of noise was produced (see

Figure 49 left). This is produced because, during the rotation, the matrix darkens not homogeneously, a gradient contrast change is observed in the first and last images of every mini-stacks, where the grain starts to change its channeling conditions.

In order to fix that problem some images have been deleted at the beginning and the end of mini-stacks even if the continuity of the angular range was maintained. After removing those images, the detection is largely improved (see Figure 49 right).

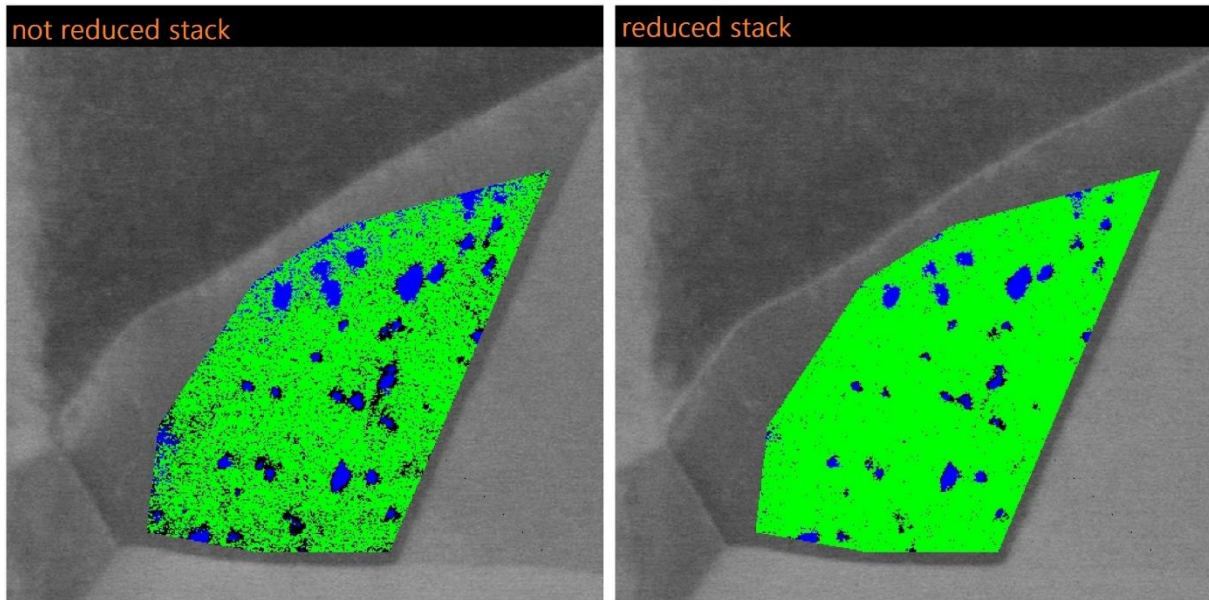


FIGURE 49: A COMPARISON OF THE CLUSTERING DEFECT DETECTION MADE FROM THE STACK10 (RIGHT) AND FROM THE MODIFIED STACK10BIS. A VALUE OF NOISE SIZE=1 HAVE BEEN USED IN BOTH ANALYSIS.

Therefore, the initial choice of angular ranges which characterize mini-stacks is impacting on the quality of clustering analysis. In the same way, to delete worst images from a rotational stack could also lead to improvements.

### III. OTHER CLUSTERING POSSIBILITIES

---

While performing the clustering program, it was thought to take advantage of it also for another purpose, in particular, the potential of the program of detecting and then characterizing precipitates or porosities was studied.

In fact, it is sure that the behavior of precipitates is different from the one of the matrix, and the same for porosities. Hence, the same ROI, taken under different experimental conditions, shows a characterizing variation of contrasts and produces useful profiles for their detection. For that purpose, it would not be necessary to use stacks with many images, but just a little number should be enough for the detection. Moreover, not just the variation of the angle between the electron beam and the sample could be used, since just the variation of the detector or other parameters would let the clustering program to find differences in profiles.

An essay was done in order to verify the feasibility of the method. Two images (shown in Figure 50) were taken on the same ROI using two different detectors, aligned and then

used in the clustering program. Note that these images have been provided for a first test and there are no information about the nature of the sample and of defects. In the images two families of defects are individuated, one of darker and bigger precipitates (or porosities) and one other of brighter precipitates really small and homogeneously dispersed in the sample.

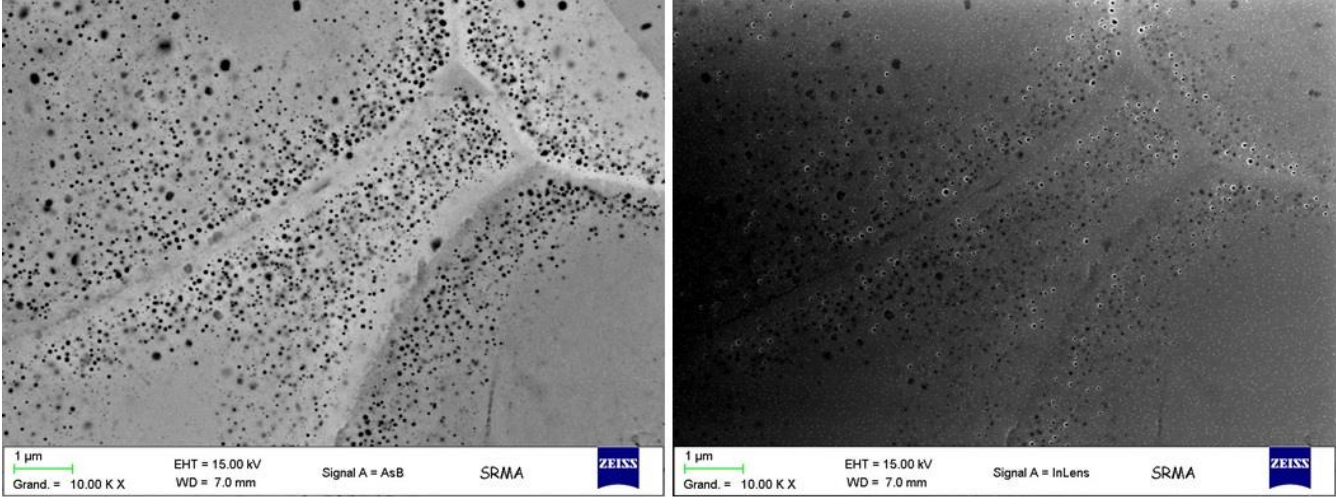


FIGURE 50: EXPERIMENTALE IMAGES OF THE SAME ROI, TAKEN WITH DIFFERENT DETECTORS.

Since the matrix presents a not homogenous contrast in single images, it is split into more clusters by the program, as showed in Figure 51.

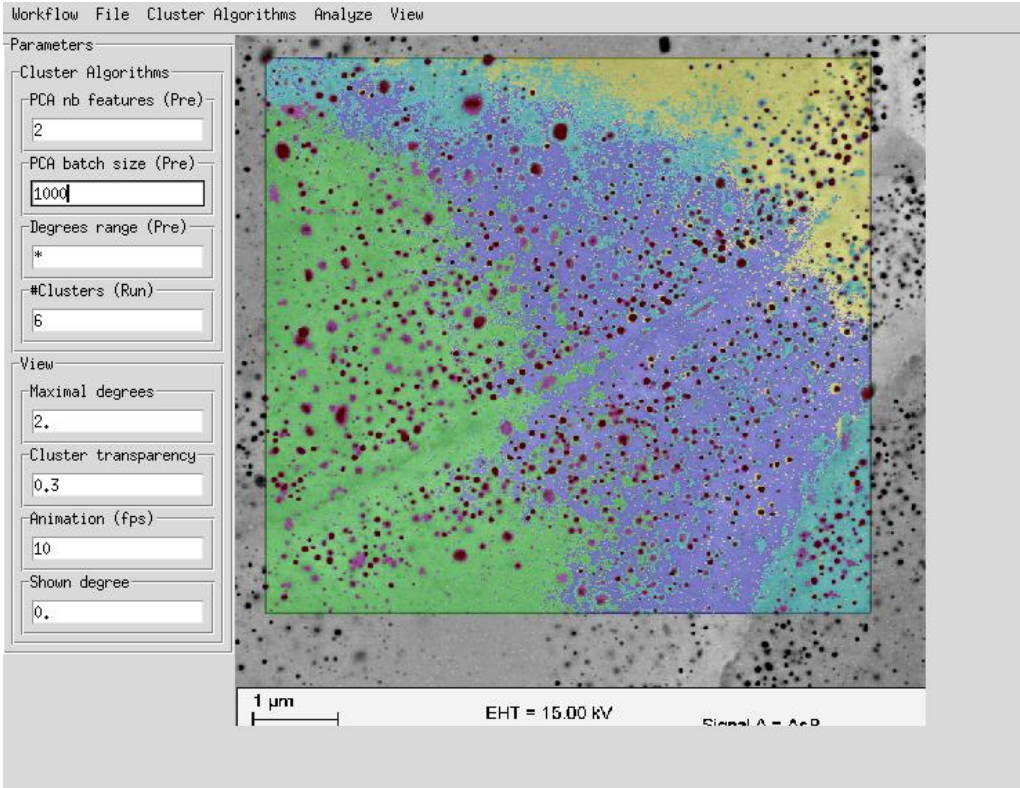


FIGURE 51: INDIVIDUATED CLUSTERS IN A SELECTED REGION. 6 CLUSTERS HAVE BEEN SELECTED AS INPUT PARAMETERS IN ORDER TO ACHIEVE AN ACCEPTABLE DETECTION OF DEFECTS.

Another test was done choosing a smaller clustered region, in which the matrix shows a homogeneous contrast. Results are showed in Figure 52, this time both two families of defects are detected (in red and yellow) by the clustering, choosing a minimum of 4 clusters as an input parameter. The matrix still remains not completely homogeneous, however this not affects the precipitates (or porosities) detection.

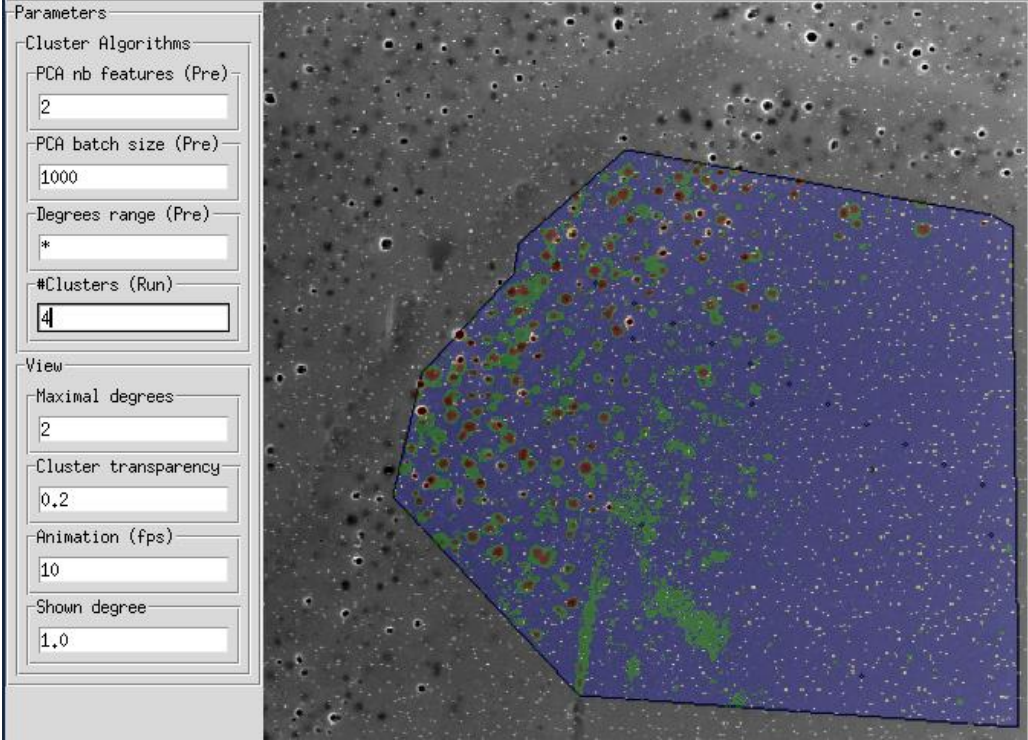


FIGURE 52: DETECTED CLUSTERS IN A SMALLER SELECTED REGION OF THE SAME ROI. TWO FAMILIES OF DEFECTS ARE WELL DETECTED (IN RED AND IN YELLOW) IF A NUMBER OF CLUSTERS OF 4 IS CHOSEN AS PARAMETER.

For every cluster, the program provides an output file '.txt' in which every pixel of the concerned cluster is noted. A Matlab script was written in order to exploit these data and to analyze the properties of defects. Precisely, the surface fraction, the number of defects and their size distribution were calculated. Results are showed in Figure 53.

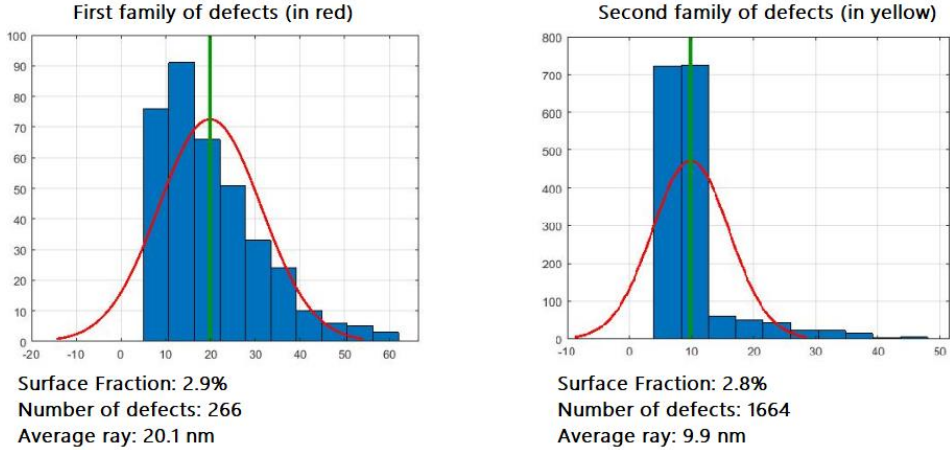


FIGURE 23: FINAL RESULT ACHIEVED WITH A DATA TREATMENT VIA MATLAB ON FILES '.TXT' CONCERNING CLUSTERS OF FAMILIES OF DEFECTS.

This first essay showed that also precipitates and porosities could be detected via clustering and with a very small number of images, it is therefore worth to further investigate in this direction.



## G. DEVELOPMENT OF A MATLAB AUTOMATIC METHOD WHICH USE CLUSTERING DATA FOR CHARACTERIZING DISLOCATIONS

---

---

A Matlab script for the analysis of output data coming from the clustering analysis on stacks 9 and 10bis was written in order to provide values of dislocation density and see if results were reasonable.

### I. DISLOCATION DENSITY OBTAINED VIA CLUSTERING

---

As mentioned, in the clustering output data, to every analyzed pixel a number is associated in order to classify it. By recognizing the classification of all the pixels and with some simple analytical calculation, the Matlab program is able to estimate the density of dislocations in the analyzed cluster. The formula for dislocation density is the following:

$$\rho_{dist} = \frac{L}{S * t}$$

Where:

- ' $L$ ' is the total length of dislocations in the analyzed area, obtained by the product of the number of features' pixels ' $P_f$ ' and the physical length of a single pixel (' $p$ '), this length is stocked in the information associated to the images taken with the SEM (open the image comments and find "AP\_IMAGE\_PIXEL\_SIZE").
- ' $S$ ' is the total surface of the analyzed area, obtained from the product of the total number of pixels ' $P_T$ ' and the area of a single pixel (' $p^2$ ').
- ' $t$ ' is the thickness of the volume concerned by the experimental analysis when the stacks is taken via SEM, that depends on the voltage used in the analysis and can be calculated theoretically with a Montecarlo simulation of electrons paths through the sample. It must be said that the "orientation information" could be related only to the surface part of the volume of interaction, in fact interactions between BSE and the sample could lead to the loss of the "deeper information". Anyway 75 nm is considered a good estimate in the case of an image taken with a 20 kV electron beam, as suggested by Zaefferer et al. (2).

With the chosen magnification, dislocations have a thickness bigger than one pixel and so, to estimate the total length of the dislocations, the total number of dislocations' pixels must to be divided by the average width of dislocations ' $D_w$ ' (in pixel) that have to be analyzed case per case. A characteristic image of the stack, in which defects are visible, must be analyzed with the software ImageJ, in order to measure the width of dislocations and, after a significant number (*e.g.* 10) of measurements, the final result is obtained by taking the average of the obtained values.

It must be said that, for now, the analyzed region must be selected manually in order to avoid the presence of grain boundaries within it. In fact, they are detected as features by the clustering program since the not perfect alignment ruins the profiles in these zones, where different grains are close, and a difference with the matrix is therefore found.

A correction factor should be added for taking into account a source of error. In fact, looking closely to ' $L$ ' it can be realized that it is not the real length of dislocations but the *projected* one, dislocations aren't always parallel to the sample surface. Then, on the assumption that dislocation segments are randomly oriented with respect to the plane of the sample surface, the factor of correction will be  $\frac{4}{\pi}$  (25).

The final formula will be:

$$\rho_{disl}^{clust} = \frac{4}{\pi} \frac{\frac{P_f}{D_w}}{P_T * t * p}$$

As said, many results are obtained by changing the value of *noise size* in the clustering program, and these different results are then compared with the dislocation density obtained by a standard approach, the intercepts method.

For obtaining the *dislocation density* with the intercepts method, some lines are firstly drawn on a significant image and their total length (' $L_{tot}$ ') is measured. Secondly, the number of intersections between these lines and the dislocations is counted (' $n$ '). The chosen image must show all the crystallographic defects, and this can be achieved using *ImageJ* for doing the '*standard deviation*' on all the stack, obtaining a single and significant image. Finally, by considering that the thickness (' $t$ ') is evaluated at about 75 nm, the following equation has been used to determine the density:

$$\rho_{disl}^{int} = \frac{2n}{L_{tot} * t}$$

The formula can be used since that it has been shown that if a set of random lines, with total length  $L_{tot}$ , is marked on a surface  $S$  and the number of intersection  $n$  is measured, then the projected length will be  $L = \frac{\pi * n * S}{2 * L_{tot}}$ , giving the above formula when the value of  $L$  is used in  $\rho_{disl} = \frac{4}{\pi} \frac{L}{S * t}$ . Uncertainty is calculated considering an error of  $\pm 1$  while counting ' $n$ '.

In order to give another reference, the dislocation density have also been calculated with the ratio between the number of features detected via clustering and the total surface analyzed (in  $m^{-2}$ ). This value is used in the literature and it has the advantage of not considering the uncertainty given by the dislocation width value and by the thickness value. The used formula has been:

$$\rho_{disl}^N = \frac{N}{P_T * p^2}$$

Where  $N$  is the number of features detected via clustering.

## VALIDATION OF THE MATLAB PROCEDURE (ON COPPER IMAGES)

To ensure a good fit between the studied method and the intercept one, an initial test was done on ECC Images used in the work of G. L'hôte (22), which studies dislocations structures in Cu mono-crystals. Since in this work rotational stacks were not used, single images were transformed in binary images, as shown in Figure 57a, thanks to a threshold filter in ImageJ. This was done in order to give a quick discrimination between dislocations and matrix, obtaining exploitable data. The Matlab script was modified in order to analyze binary images and dislocation density was calculated with both this method and the intercepts one. Images are taken from two samples of Cu differently oriented ([110] and [111]) which were submitted to cycles with increasing tensile stress. The results show a good fit between the methods, as shown in Figure 54b.

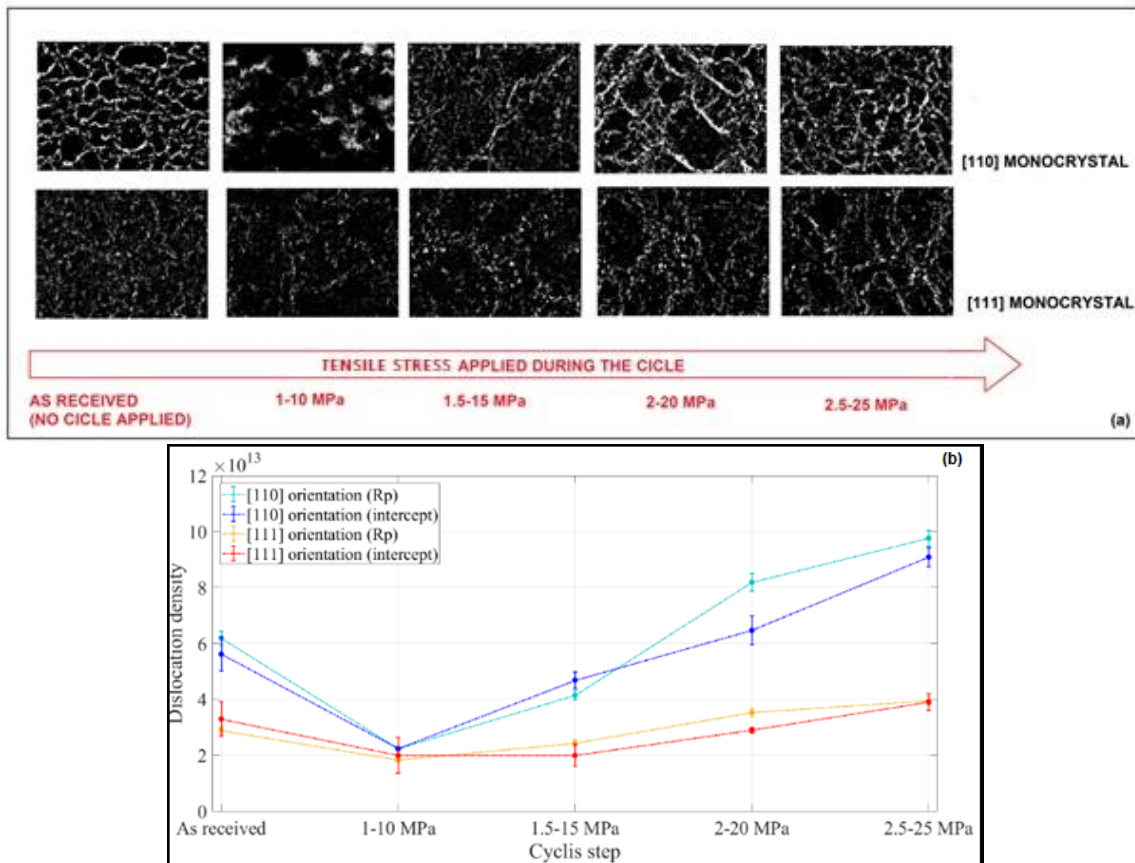


FIGURE54: (A) BINARY IMAGES OF COPPER DISLOCATIONS STRUCTURES IN COPPER MONOCRYSTAL SUBMITTED TO DIFFERENT FATIGUE CYCLES (22). (B) DISLOCATION DENSITY ( $m/m^3$ ) VALUES OBTAINED WITH THE INTERCEPT METHOD AND THE MATLAB SCRIPT ON BINARY IMAGES. ON [110] AND [111] ORIENTED COPPER SAMPLE.

It is important to consider that these results are obtained from R-ECC images and so a fraction of dislocations could be under the invisibility criterion in these conditions, leading to an error in the obtained value. Furthermore, more uncertainty is added in the process of binarization of the image. In fact, the threshold value of gray used for discriminating the final color (black or white) of a pixel is selected manually, indeed a human error affects the result that depends on the operator choice. All of these problems are overcome using eCHORD profiles and the clustering program for discriminating defects. Therefore, this initial result just shows that it is worth to use this approach for calculating the dislocation density. Values of dislocation density are similar between our

Matlab method (Rp) and the Intercept one (Intercept) and so further calculations will be performed, using data obtained by rotational analysis.

---

### DISLOCATION DENSITY UNCERTAINTY: DISLOCATION WIDTH

---

It was observed that one of the input parameters particularly affects the results of dislocation density. Indeed, when changing the value of *dislocation width* a not negligible variation is produced. Moreover, it is the operator who makes the evaluation of this parameter, and this means that the measurement is not reproducible and can change with different persons.

In order to try to overcome this issue, ten measures of dislocation width was taken via ImageJ and the average value and standard deviation on that set of values have been calculated:

average disl. width (pixel)	standard deviation of disl. width
4.37	0.79

These values for calculating the dislocation density were then selected as: 3.58 pixels (average minus standard deviation), 4.37 pixels (average) and 5.17 pixels (average plus standard deviation). In this example, the used data were those with a noise size of 1 pixel, giving the following results:

disl width (pixels)	$\rho_{disl}^{clust}$ [m <sup>-2</sup> ]
3.58	5.93*10 <sup>13</sup>
4.37	4.85*10 <sup>13</sup>
5.17	4.11*10 <sup>13</sup>

The dislocation density is lower when the dislocation width increase and, on average, changing the dislocation width of around 1,5 pixels brings a variation of results of above 50%.

To give a final result, the dislocation density was calculated with the average dislocation width, while the uncertainty was calculated as half the difference of the two values obtained with the lower (3.58 pixels) and the higher (5.17 pixels) value of dislocation width:

$\rho_{disl}^{clust}$ [m <sup>-2</sup> ]
(4.85± 0.91)* 10 <sup>13</sup>

This method is the one that was used to give all the results of dislocation density in this work.

RESULTS OF DISLOCATION DENSITY VIA MATLAB

The clustering program was run on the grain1. For comparing results and analyze the influence of parameters, values of 1, 10, 50 and 100 pixels of *noise size* were used. Figure55 shows the region on which the clustering was made (a) and a representation of the achieved detection, build up with the Matlab script (b). In that case the used noise size was 1pixel.

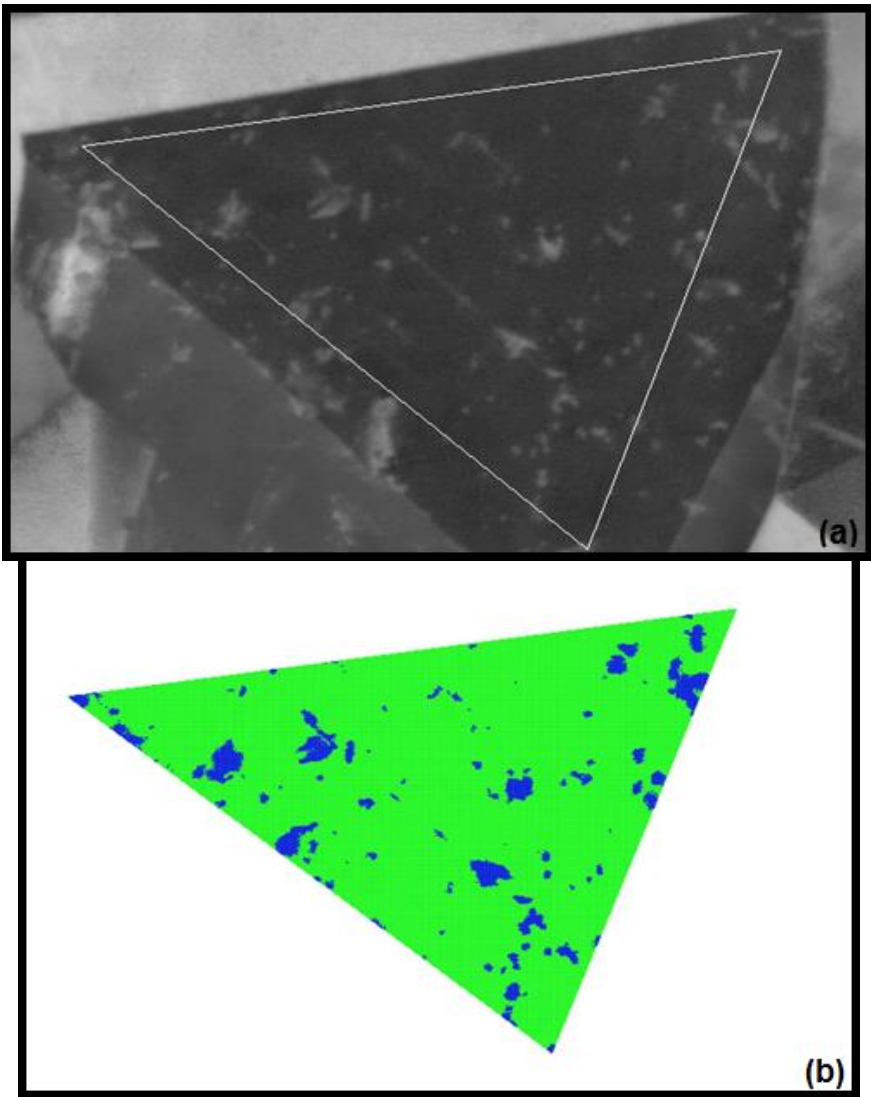


FIGURE 55: CRYSTALLOGRAPHIC DEFECTS DETECTION VIA CLUSTERING (B) AND THE RELATIVE SELECTED REGION IN THE GRAIN1 (A).

After that, clustering data, formatted as a file ‘.txt’, were analyzed with the Matlab using the following parameters:

Pixel size	Dislocation width	thickness
5.8 nm	4.37±0.79 pixels	75 nm

Results are showed in Figure56. Note that also the grain2 has been studied and those results are showed in the annex3.

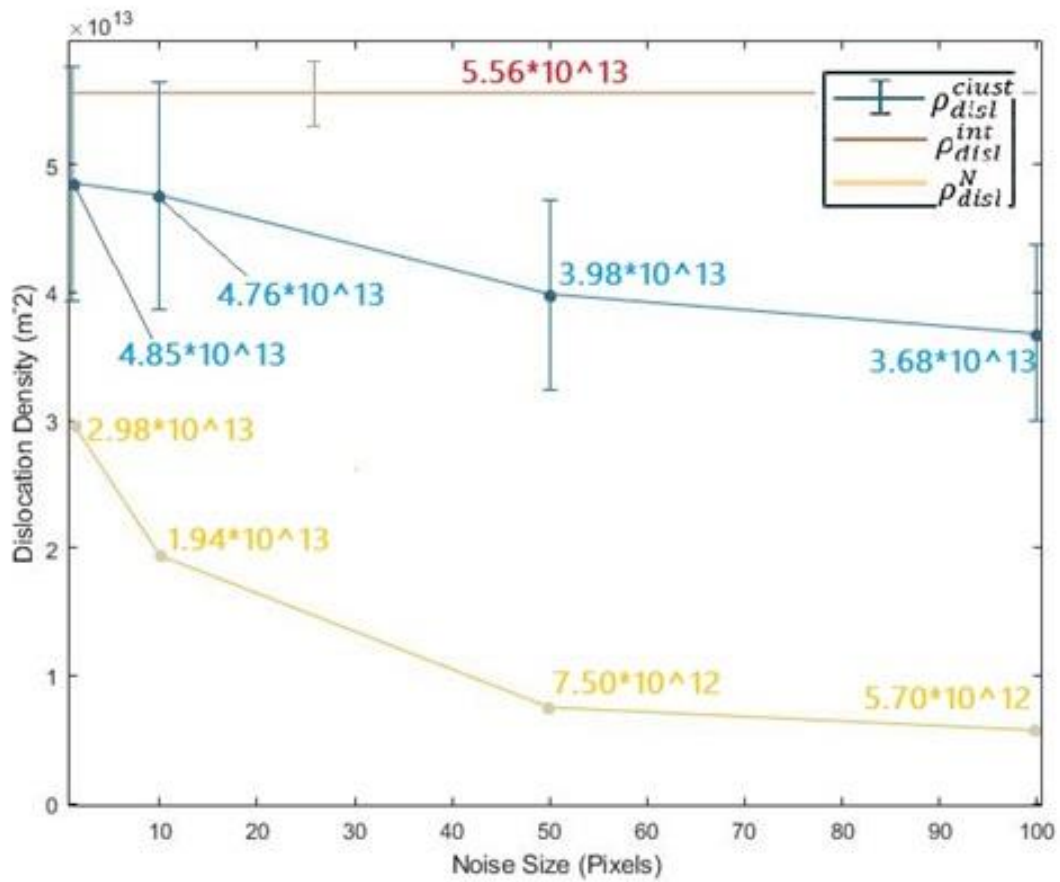


FIGURE 56: DIFFERENT VALUES OF DISLOCATION DENSITY FOR THE GRAIN1. IN RED THE VALUE ACHIEVED WITH THE TRADITIONAL METHOD OF INTERCEPT. OTHER COLORS REPRESENT VALUES OF DISLOCATION DENSITY OBTAINED VIA CLUSTERING(IN BLUE) AND THE N/SURFACE DISLOCATION DENSITY (IN YELLOW). NOTE THAT LAST TWO DISLOCATION DENSITIES TYPES VARY WITH THE USED VALUE OF NOISE SIZE.

For what concerns  $\rho_{dist}^{clust}$  and  $\rho_{dist}^N$ , it was observed that using an high value of noise size brings to the disappearance of many features, as shown in Figure57, where it is represented the evolution of the number of features as a function of the *noise size*, in the case of the Grain1:

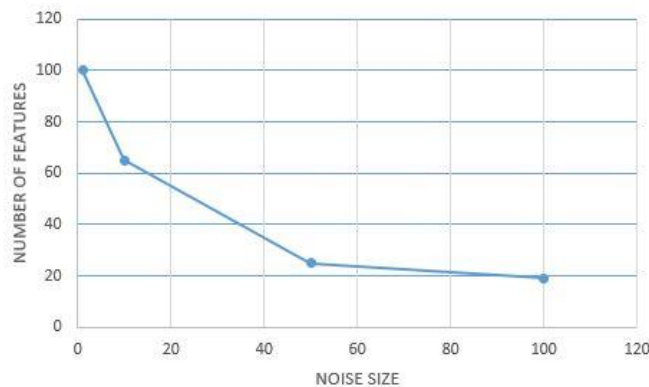


FIGURE 57: HOW THE NUMBER OF DETECTED FEATURES CHANGES WITH THE NOISE SIZE.

This is due to the fact that, if the value of *noise size* is too high, there are many features that can actually present an area smaller than this value and therefore they are detected as noise. For this reason, the perfect value of noise size depends on the used magnification, which influences the main number of pixels in a feature. With the used magnification it has been observed that if this value cannot exceed 10 pixels if defects details must be maintained. Using 10 pixels instead of 1 pixel brings to a significant decrease of the number of detected features but only very small ones are effectively deleted, therefore the value of  $\rho_{disl}^{clust}$  is not affected that much, the same cannot be said for  $\rho_{disl}^N$ , that is strictly correlated to the number of detected features ( $N$ ). Watching at results of the grain 2 (see annex 3) it is evident that with a noise size of 1 pixel the number of detected features increase too much since some noise is detected as a feature. Instead, for the grain 1, that has a rotational stack with less drift and therefore a better alignment and image quality, a noise size of 1 pixel can be used.

As said, the dislocation density calculated via intercepts method was used as a reference. Also in this case, in order to see dislocations as better as possible during the manual detection of  $n$ , an image treatment was done with the software “ImageJ”. The standard deviation of all the stack was taken, resulting in a single image in which dislocations are more visible, as shown in Figure 58.

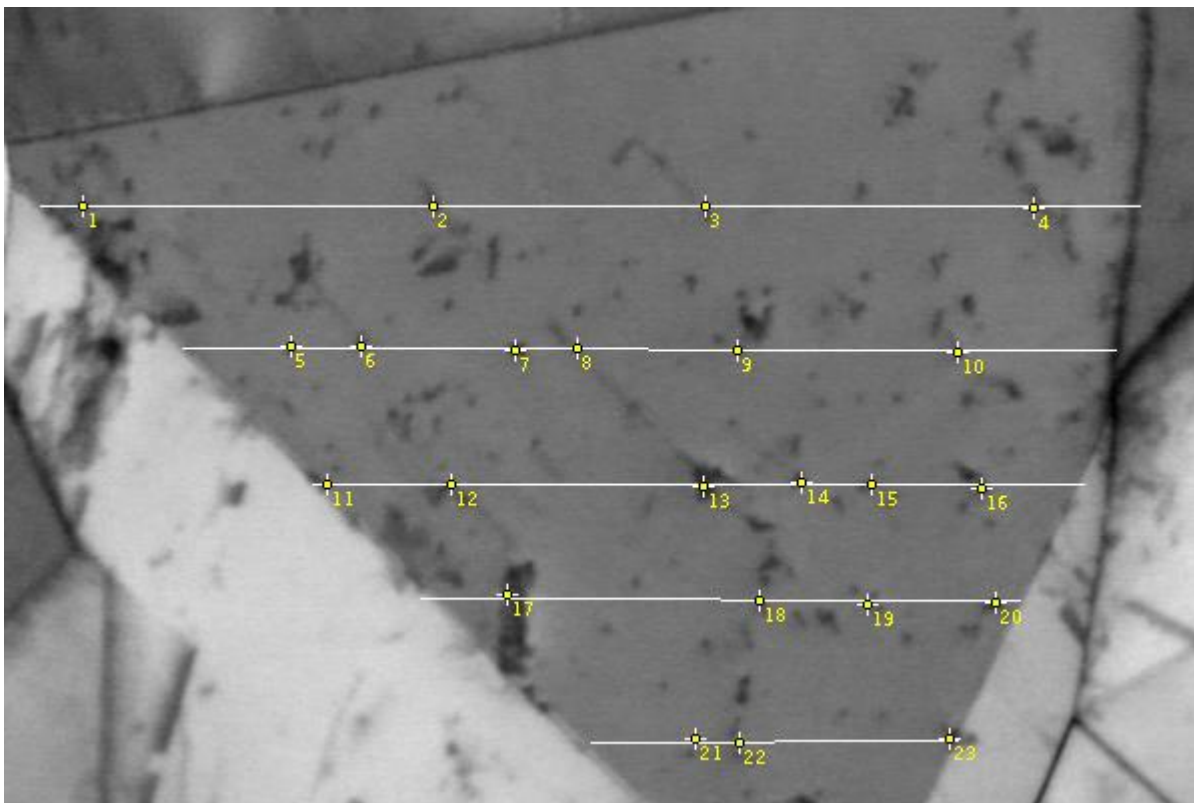


FIGURE 58: THE RESULT OF THE STANDARD DEVIATION OF THE STACK9. IN THIS WAY, ALL CRYSTALLOGRAPHIC DEFECTS ARE VISIBLE AND IT IS POSSIBLE TO COUNT THE NUMBER OF INTERSECTIONS BETWEEN DEFECTS AND DRAWN LINES, WHICH IN THIS CASE IS 23.

The results obtained fit perfectly the order of magnitude of dislocation density obtained via Intercepts method. Clustering dislocation density, in which the noise size is taken into account, seems to have a good fitting if the value of noise size is smaller than 10 pixels, but

the best value depends on the used magnification. Moreover, values achieved with the intercept method don't have a perfect precision, as an example, how the operator puts lines on the grain could change a lot the number of intersected defects. Therefore it is deemed sufficient to obtain the same order of magnitude.

Also in this case results achieved for the Grain2 are stocked in the Annex3.

## II. DETECTION OF CRYSTALLOGRAPHIC DEFECTS VISIBLE FOR SPECIFIC CROSSED TB CONDITIONS: TOWARD THE AUTOMATIZED DETECTION OF DISLOCATIONS' NATURE

---

Considering that the main objective of this master' thesis is to give a reliable value of dislocation density and to obtain in parallel a crystallographic information about defects, an effort was made in order to exploit as better as possible the output data of the clustering program. As mentioned, for every detected features, the clustering program creates a file called *'feature\_i'*, where *'i'* represents the number of the analyzed feature, in which to all pixels of the feature are associated rotational angles where a pixel is brighter under a TB condition. Using such information it is possible to catalogue every crystallographic defect via Matlab, briefly, a structure that contains all defects is created and, for each of them, five fields are filled:

- *'X'*: a vector with all *'x'* values of pixels concerned in the feature.
- *'Y'*: a vector with all *'y'* values of pixels concerned in the feature.
- *'gb'*: a vector in which are shown the fractions of the analyzed feature' s pixels that are bright in angular ranges characterizing TB conditions. [0.68 0.33 0.15 0.98] can be an example, in this case, just the 68% of pixels in the analyzed feature are effectively visible under the TB condition of the first angular range considered.
- *'area'*: a number representing the total amount of pixels for a feature.
- *'gbtr'*: a vector that represents which angular ranges are effectively considered characterizing for the feature. Basically, a *threshold fraction* is chosen by the operator, then the totality of the feature will be considered visible in a particular angular range if the relative fraction showed in *'gb'* is greater than the threshold. In the example used in the field *'gb'*, if 0.64 would be chosen as a threshold, the resulting *'gbtr'* vector would be [1 0 0 1].

Particularly, thanks to the information stocked in *'gbtr'*, it could be possible to study invisibility criterions of every detected crystallographic defect in order to determinate its Burgers vector.

Figure59 shows an example of a real structure in which 18 features are mentioned, a threshold fraction of 0.64 has been used. It can be noted that there are features with an area of just few pixels and that other features are much bigger. Moreover, the used *noise size* is 1pixel since that there are features with an area of just 2pixels, that would have been considered as noise with a larger value of this parameter.

...	X	Y	gb	area	gbtr
1	[202;201;200;201;201;202]	[189;191;190;190;189;190]	[0 0 0 0 1]	6	[0 0 0 0 1]
2	449x1 double	449x1 double	[0.8196 0.2116 0.3586 0.1203 0.6704]	449	[1 0 0 0 1]
3	22x1 double	22x1 double	[0 0 0 0 1]	22	[0 0 0 0 1]
4	56x1 double	56x1 double	[0.2321 0 0 0 0.9821]	56	[0 0 0 0 1]
5	713x1 double	713x1 double	[0.9467 0.2777 0.2693 0.2412 0.5245]	713	[1 0 0 0 0]
6	36x1 double	36x1 double	[1 0.1389 0 0 0.4722]	36	[1 0 0 0 0]
7	25x1 double	25x1 double	[0.6000 0 0 0 0.4800]	25	[0 0 0 0 0]
8	[329;329]	[284;283]	[1 0 0 0 0]	2	[1 0 0 0 0]
9	40x1 double	40x1 double	[0.5500 0.1250 0 0.0750 0.8500]	40	[0 0 0 0 1]
10	148x1 double	148x1 double	[0.5541 0.0811 0.5405 0.2432 0.6757]	148	[0 0 0 0 1]
11	[63;62]	[115;115]	[1 0 0 0 0]	2	[1 0 0 0 0]
12	[93;93;92;92;94;91;93]	[155;154;154;155;157;154;156]	[0 0 0.4286 0 0.8571]	7	[0 0 0 0 1]
13	213x1 double	213x1 double	[0.2066 0.0939 0.7230 0.1315 0.6573]	213	[0 0 1 0 1]
14	[98;98;97;97]	[146;145;146;145]	[0 0 0 0 1]	4	[0 0 0 0 1]
15	[67;67;66]	[118;117;118]	[1 0 0 0 0]	3	[1 0 0 0 0]
16	[60;61]	[112;112]	[1 0 0 0 0]	2	[1 0 0 0 0]
17	[76;77]	[130;130]	[0 0 1 0 0]	2	[0 0 1 0 0]
18	121x1 double	121x1 double	[0.2975 0 0 0.3306 0.8264]	121	[0 0 0 0 1]

FIGURE 59: A STRUCTURE OBTAINED VIA MATLAB, IN WHICH INFORMATION ABOUT 18 FEATURES ARE CONTAINED. FOR EACH FEATURE ARE SHOWED THE COORDINATES OF ITS PIXELS, ITS AREA, AND TWO VECTORS CHARACTERIZING ITS CRYSTALLOGRAPHIC BEHAVIOUR.

Because of this choice, the selection of the *threshold fraction* becomes a not negligible issue. In fact, each feature will be considered part of the population of a TB condition only if the chosen threshold is smaller than the real fraction of pixels effectively lighted up in this angular range. This obviously affects the building up of the 'gbtr' vector and therefore which invisibility criterions are detected for such a feature.

## FURTHER STUDIES ON BEST THRESHOLD TO USE

In order to study how the *threshold fraction* affects results and what could be the best value to use, it has been thought to compare the dislocation density achieved via clustering for singles TB conditions, with the intercepts method value of dislocation density obtained on mini-stacks portions concerning just the single angular range.

To do this the Matlab script has been improved to calculate the dislocation density relative to a population of crystallographic defects characterizing just a selected angular range and therefore a TB condition. For each angular range, results achieved with different *threshold* have been compared with relatives intercept results.

Mini-stacks with best image quality were used for that purpose (stack 9, (24.5° to 33°) and (305.5° to 315°) ), a noise size of 10 pixels have been used in the clustering program. Results are showed in Figure 60.

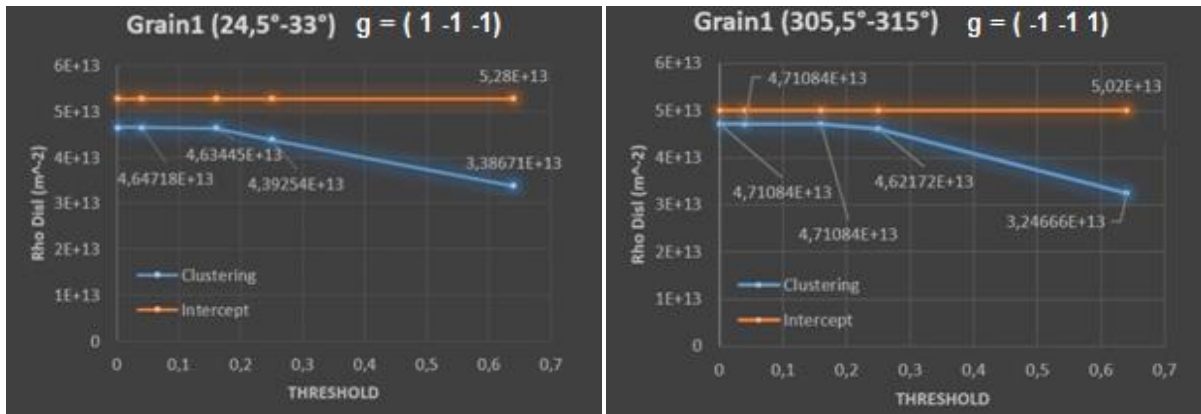


FIGURE 60: .IN BLUE: LOWER DISLOCATION DENSITY CALCULATED IN SINGLE TB CONDITIONS USING CLUSTERING DATA AND THE MATLAB SCRIPT; DIFFERENT THRESHOLD VALUES HAVE BEEN USED. IN ORANGE: INTERCEPT DISLOCATION DENSITY FOR THE CONCERNED ANGULAR RANGE. GRAIN1 HAS BEEN USED IN THE CLUSTERING PROGRAM WITH A NOISE SIZE VALUE OF 10 PIXELS, (24.5° TO 33°) AND (305.5° TO 315°) ANGULAR RANGES HAVE BEEN SELECTED WITH THE MATLAB SCRIPT.

For what concern the *threshold fraction*, values of 0.64, 0.25, 0.16, 0.04 and 0.001 have been used and it is evident how reducing this value up to 0.16 leads the dislocation density get closer to the intercepts method value. With this quality of stacks, it is not worth to use values smaller than 0.16 since the dislocation density remains constant.

In theory, with a perfect alignment, *threshold fraction* wouldn't affect the value of dislocation density, since that, in every angular range, each crystallographic defect would occupy exactly same pixels (unless the presence of an invisibility criterion) and so the totality of pixels of a detected defects would be concerned for all characterizing angular ranges. The reality appears different, and that is due to the fact that the shape and the position of features changes a little within a stack, therefore some pixels of a clustered defect would be bright just in some angular ranges and not in others. As a consequence, this leads to an over-estimation of the real area of a defect by the clustering program and to the fact of having just a fraction of a feature's pixels in specific angular ranges.

The chosen *noise size*, *threshold fraction* but also the quality of a stack itself, represent a source of error when the dislocation density of single TB conditions want to be measured.

Figure 61 allows visualizing the effect of changing the abovementioned parameters, referring to a particular of the analyzed ROI, a threshold value of 0.64 remains too high and a not negligible part of defects is not detected. The same goes for a value of noise size of 50 pixels, but in this case the applied magnifications plays an important role.

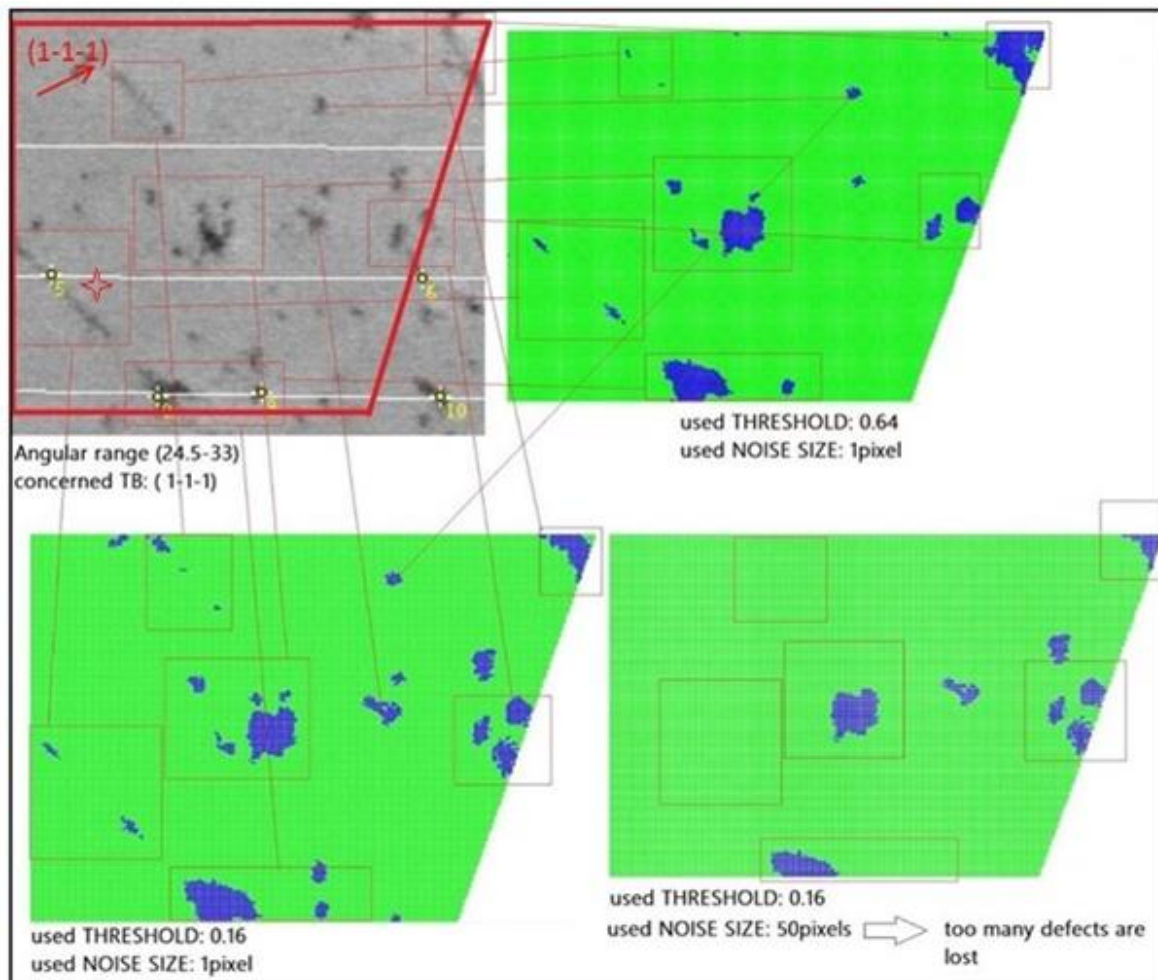


FIGURE 61: A DETAIL OF THE ROI, SEEN UNDER A TB CONDITION CONCERNING THE (1 -1 -1) DIFFRACTING PLANE. CLUSTERING RESULTS VARY WITH DIFFERENT USED THRESHOLD AND NOISE SIZE VALUES.

---

## RESULTS

---

The Matlab script has showed to work efficiently and it has effectively been possible to characterize each feature detected by the clustering. For every diffracted plane concerned in the rotational stack, crystallographic defects visible (in blue) and invisible (in red) can be catalogued, as the Figure 62 shows.

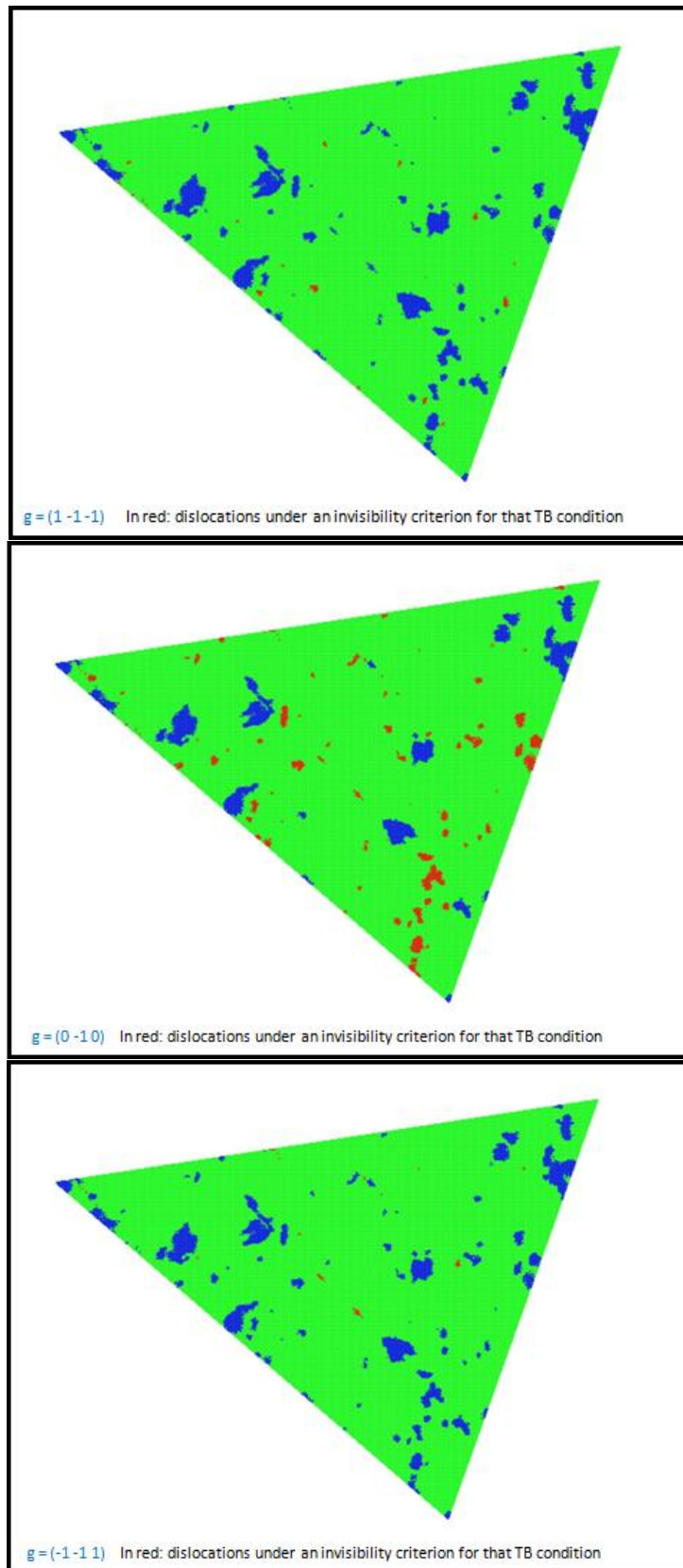


FIGURE 62: REPRESENTATION OF THE ANALYZED REGION UNDER DIFFERENT TB CONDITIONS. FEATURES UNDER AN INVISIBILITY CRITERION ARE HIGHLIGHTED IN RED.

Figure 63 shows an enlargement zone of the ROI under all analyzed diffracting planes, a threshold of 0.001 and a noise size of 10 pixels have been used, both experimental images and clustering representations are present in order to verify performances.

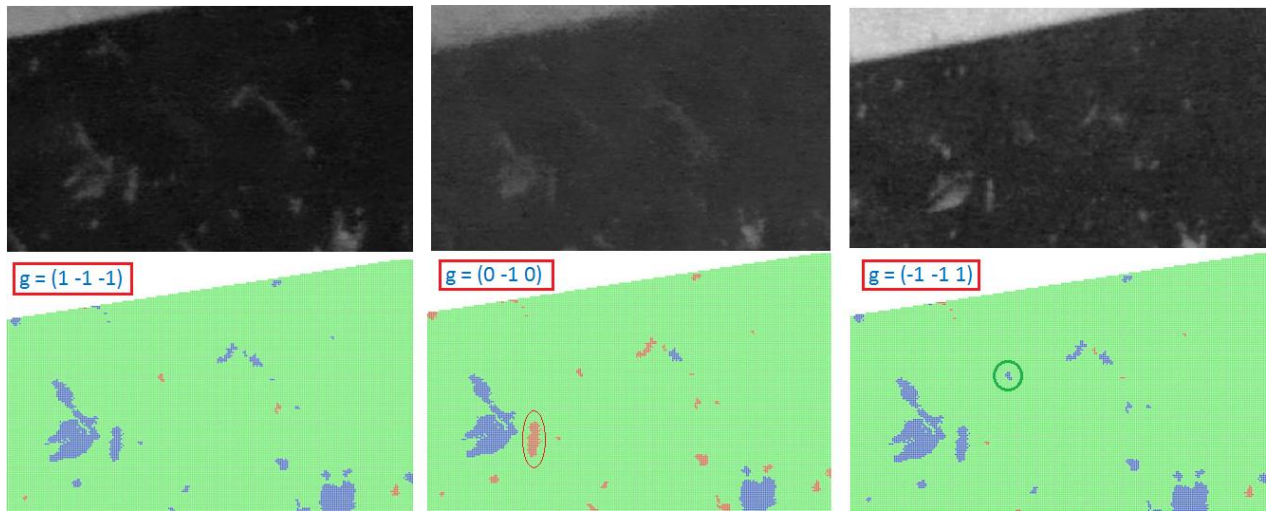


FIGURE 63: A PARTICULAR OF THE GRAIN1 (STACK9), SHOWED UNDER DIFFERENT TB CONDITIONS CROSSED ALONG THE ROTATION. THE SAME ROI IS REPRESENTED ALSO WITH THE MATLAB REPRESENTATION OF THE CLUSTERING FOR SHOWING DEFECTS WHICH HAVE BEEN DETECTED.

Some errors are still produced and an example is circled in red, that features is not detected in (0 -1 0) even if it is present in correspondent experimental image. Anyway, there are many features for which the correspondence between the clustering detection and the experimental evidence is found. Particularly, for the one circled in green, two invisibility criterions are found, indeed its 'gbtr' vector corresponds to:

(24.5°-33°)	(44.5°-52°)	(91.5°-100°)	(285.5°-295°)	(305.5°-315°)
0	0	0	0	1

Considering that  $g_{hkl} * \bar{b} = 0$  is respected in invisibility criterions of (1 -1 -1) and (0 -1 0), and that  $\bar{b}$  is the same, with some analytical calculus the Burgers vector is found to be  $\bar{b} = \frac{1}{2}(\mathbf{101})$ .

However, also in this case not enough TB conditions are met in a random matter and the determination of the Burgers vector remains influenced by the crystallographic orientation of the analyzed grain.

Since that, with the used quality of stack and alignment, a little fraction of smaller crystallographic defects are not detected by the clustering program, it could be better to use the smaller value as possible of noise size (1 pixel) in order to preserve ones that have been detected. On the other hand, it must be said that with the lower quality of alignment found in Grain 2 (see annex 3), some detected features are for real just noise. Moreover, the not perfect alignment always leads to an over-estimation of the area of defects. Hence, it is always important to do a visual check and see if the used *noise size* and *threshold* allows to well detect crystallographic defects.

Another time, what emerges by this study is that the image quality of experimental stacks and of the alignment have still to be improved in order to achieve perfect results,

furthermore the orientation of the analyzed grain is critical for finding two invisibility criterions and characterizing the Burgers vector.

However, it has to be considered that all detected features, for any crossed TB conditions, are detected by the clustering and therefore used in the Matlab script for the determination of the total dislocation density, which is found to work with the used quality of rotational stacks. The advantage of taking into account crystallographic defects invisible in certain TB conditions is still present.

## H. CONCLUSIONS AND PERSPECTIVES

---

To conclude, this Master's thesis confirmed the potential of dislocations and stacking faults characterization via *disCHORD*. The innovation of using rotational profiles, associated to pixels in rotational stacks, for characterizing the behavior of different zones via clustering was shown to be an excellent strategy.

During this work, more than few difficulties were encountered. Experimental issues initially brought to the conclusion that discriminating crystallographic defects with this method might be impossible with the used instruments. However, the idea of using mini-stacks led to an augmentation of rotational stacks quality enough to complete this ambitious task. In fact, the possibility of achieving rotational series with a magnification of 15KX and a scan speed of 9, without an excessive presence of charging problems, largely allows to associate to each pixel of the ROI a specific behavior.

Then, an effort was done in order to exploit as better as possible clustering output data. Thanks to a Matlab script, it is easy to achieve values of *dislocation density* for a rotational stack. As said many times, the great advantage is that more than one TB condition is considered and this allows not to neglect all crystallographic defects under invisibility criterions in single TB conditions. Achieving a rotational stack is quite easy to do and TB conditions are always crossed, therefore it is not necessary to have a specific knowledge in crystallography in order to find specific orientations where dislocations are visible, consequently shorter time is needed and more people could be able to investigate on dislocation density. It was found that the dislocation density via intercepts method is often slightly higher than the one measured via *disCHORD*, so other essays should be done in order to confirm this trend and to understand which technique predicts the parameter with better precision.

Even if the used magnification doesn't allow to study more than one grain in a rotational stack, many series can be taken in half a day. *DisCHORD* is less time-consuming and this let to easily achieve statistic results in dislocations characterization.

The characterization of the Burgers vector with rotational profiles of dislocations was another target of this thesis and in order to reach it, a strategy for individuating TB conditions in which every clustered dislocation is visible was developed successfully. Unluckily, in the course of the work it emerged that it is not common to achieve the requisite to found the Burgers vector. In fact, the presence of more than one invisibility criterion is required and this is not always possible.

The grain orientation plays a very important role in this sense and it must be such that two TB conditions, in which dislocations are invisible, are met in the oriented ECP. Since this fact cannot be anticipated, it would be necessary to check its presence before to start a rotational stack acquisition. In order to assure the possibility of characterizing the Burgers vector for every dislocation in every grain of a ROI, it is necessary to modify the sub-stage used during the rotation, in fact the presence of a *double tilt* is necessary in order to modify the initial orientation of the analyzed grain, changing therefore the linked ECP. Anyway, sometimes the Burgers vector can be determined just with the initial orientation of the grain.

It is interesting to consider that many improvements can be done to improve the image quality in rotational stacks.

A strategy is for sure to use a next generation BSE detector, this would augment the resolution and the magnification, therefore single dislocations could be easily resolved and the alignment would be improved for the higher number of present details to which the algorithm refers. Consequently the clustering precision would be also improved. Figure 64 shows an ECC Image taken on the Thermo Scientific™ Quattro E-SEM, as said the image quality is outstanding.

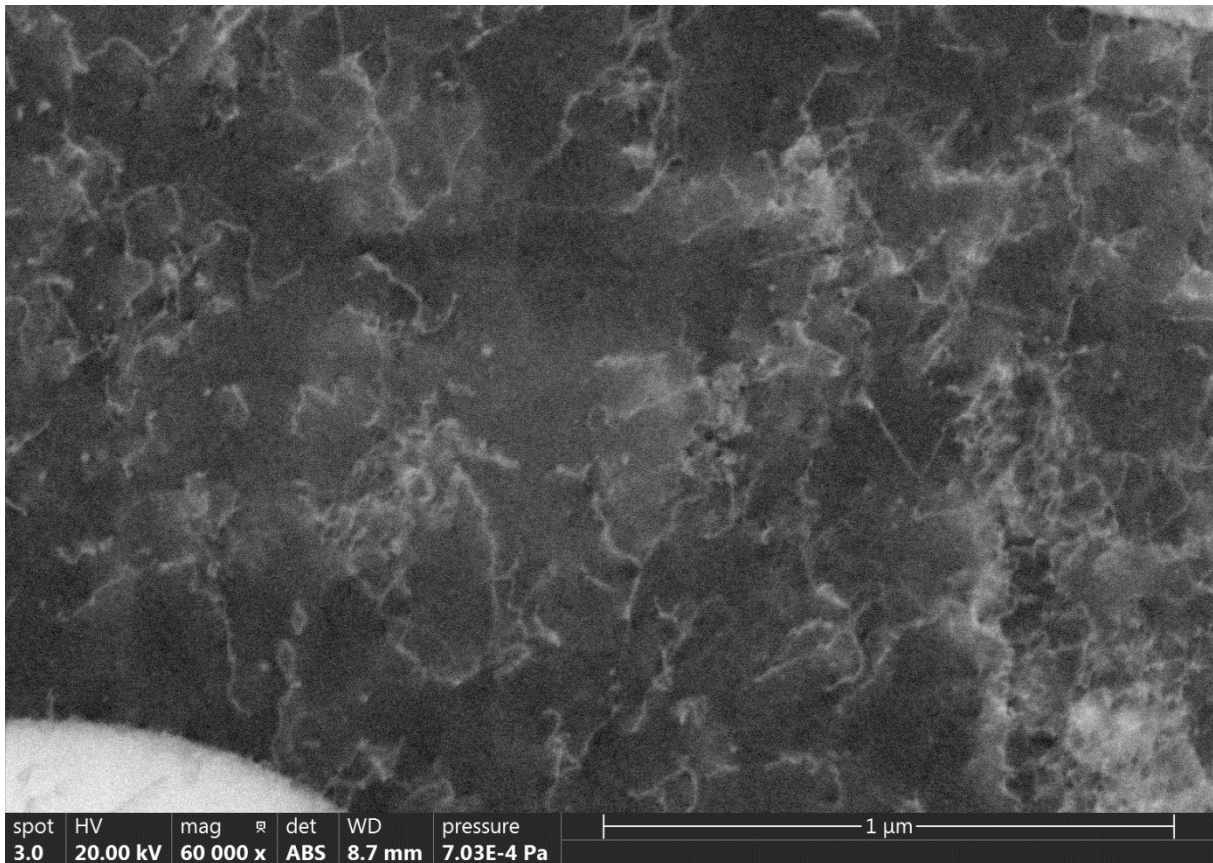


FIGURE 64: ECC IMAGE TAKEN IN A SEM WITH A NEXT GENERATION BSE DETECTOR. GRATER MAGNIFICATION CAN BE USED AND A GREATER RESOLUTION IS ACHIEVED.

For this reason, it would be interesting to implement a sub-stage for performing sample rotations and achieving rotational stacks in such a kind of instrument. Further studies should be done on the presence of charging issues and on the best parameters to use in order to avoid them.

Another way to improve the stacks quality is to improve the image treatment, in particular the denoising and the alignment. Many algorithms are present and better options could be found. For example a new strategy of alignment showed a good potential, that uses a *Bspline* algorithm, which is able to perform not local deformations, unlike the *affine* transformation used in this master's thesis.

Hence, it is important to continue investigating on *disCHORD* technique in order to improve its potential and to reach all of the ambitious objectives that have been fixed.

Moreover, it is important to study other kinds of steels and crystallographic geometries for widening the scenario in which this technique can be useful.



## I. ANNEXES

### ANNEX 1: EXAMPLE OF TOTAL PROCEDURE FOR FINDING BURGER VECTOR IN THE FIRST SET OF STACKS(ON THE 4<sup>TH</sup> GRAIN STACK6)

Starting from the orientation map obtained from the EBSD analysis, Euler's angles correlated to the orientation of the analyzed grain have been obtained, precisely they are:

$\varphi_1$	$\Phi$	$\varphi_2$
299.3°	39.9°	89.0°

After an alignment of the orientation map with the rest of the stack, starting by these Euler's angles and using the CHORD program developed by C. Lafond, an optimization of angles has been done in order to find the orientation that gives the best superposition between experimental and theoretical profiles. The following result has been obtained:

$\varphi_1$	$\Phi$	$\varphi_2$
296.5°	39.4°	89.2°

Note that:

- The same grain produces different optimized angles if different stacks are used, in fact different stacks produce profiles that are not identical, and therefore the CHORD program will find solutions that differ a bit one from another.
- The alignment between the stack and the orientation map is harder than a normal alignment process because the orientation map is colored. It is necessary to split it into its three RGB components and to align them singularly with the total stack, after that the three aligned component are fused together in order to obtain the colored and aligned orientation map.

Using this result, a Pole figure, representing the stereographic projection of main families of planes ( {100}, {110} and {111} ), oriented according to these angles, was computed using a program developed by C. Langlois. This program is designed for a fcc geometry, therefore it is important to verify that the analyzed grain is austenitic. The obtained Pole figure is indexed as represented in Figure 65, where black square brackets represent crystallographic directions and green round parenthesis are  $g_{hkl}$  vectors associated to crystallographic planes, described by a stereographic projection, which is a single line.

Even if the whole figure is used for the indexation step, just a very little portion of the Pole figure is then used for characterizing Kikuchi bands contained in the ECP representing the orientation of the analyzed grain. The circle along which is collected the simulated



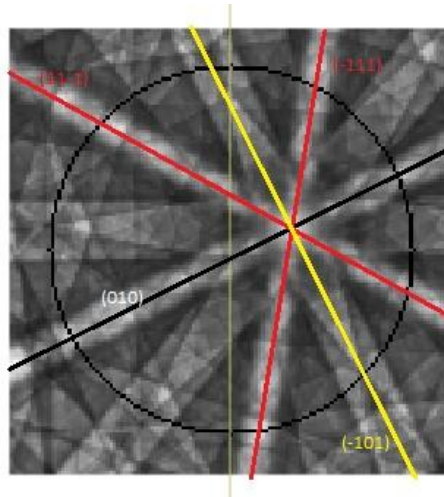


FIGURE 66: ECP CENTERED IN CENTERED IN EULER'S ANGLES ( $\varphi_1=296.5$  ;  $\Phi=39.4$  ;  $\varphi_2=89.2$ ). THE REPRESENTED CIRCLE REFERES TO A ROTATION OF THE SAMPLE TILTED WITH  $15^\circ$ . MANY KIKUCHI BANDS CROSS THE CIRCLE FOR THE PRESENCE OF A ZONE AXIS IN ITS ORIENTATION RANGE.

Figure67 shows both the experimental (in blue) and theoretical (in red) profile of the analyzed grain. Peaks around which the contrast intensity falls are present, they are actually the projection of bright Kikuchi bands and of dark Kikuchi lines on their boundaries (see Figure11 in the chapter “*ECCL, theory behind the BSE channeling contrast*”). TB conditions are achieved on Kikuchi lines, which correspond to these zone of reduced intensity in the profiles. Once recognized TB conditions, their correspondent rotational angles are observed in the rotational stack, in this way it is possible to verify the presence of crystallographic defects or the eventuality of invisibility criterion.

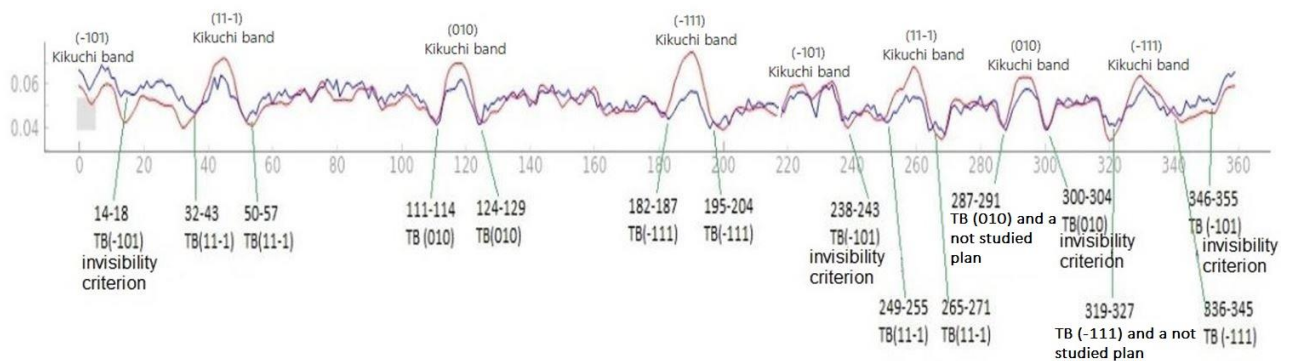


FIGURE 67: CHANNELING CONTRAST PROFILES, IN BLUE THE EXPERIMENTAL ONE, ACHIEVED FROM A MATRIX PIXEL OF THE ANALYZED GRAIN. IN RED THE EXPERIMENTAL ONE, OBTAINED FROM AN ECP CENTERED IN THE SAME ORIENTATION AS THE GRAIN.

The rotational angle in ECP varies counterclockwise, therefore picks corresponding to  $45^\circ$  and  $120^\circ$  degrees of rotation correspond respectively to (11-1) and (010) Kikuchi bands.

For every crossed TB, the operator checks if an invisibility criterion is achieved. It has to be said that in some TB conditions crystallographic defects are characterized by a low visibility and therefore many times is not easy to define if the criterion is effectively achieved. In Figure68 it is possible to see the analyzed grain under two different TB conditions, in one of them the criterion is achieved and crystallographic defects are not visible.

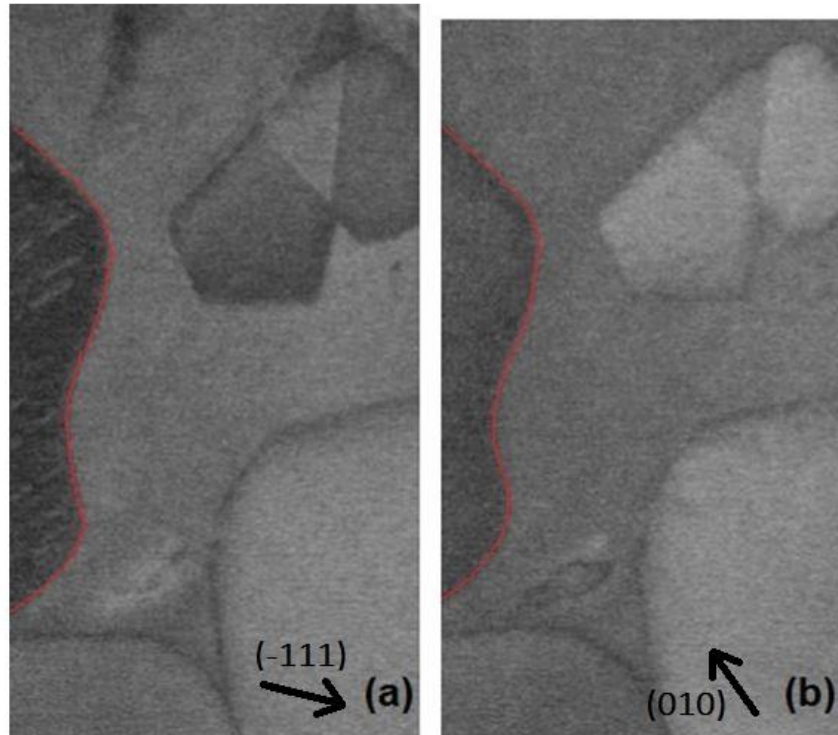


FIGURE 68: THE ANALYZED GRAIN UNDER TWO DIFFERENT TB CONDITIONS. IN (A) CRYSTALLOGRAPHIC DEFECTS ARE VISIBLE, IN (B) THEY ARE NOT AND THEREFORE THE INVISIBILITY CRITERION  $\vec{g} \cdot \vec{b} = 0$  IS ACHIEVED.

Considering all crossed TB conditions and observing the visibility of dislocations the following result have been obtained:

TB	(-101)	(11-1)	(010)	(-111)
Invisibility criterion	present	Not present	present	Not present

Sometimes a TB condition could present an invisibility criterion but its Kikuchi line is too close or superposed to another Kikuchi line (in which the criterion is not achieved) and defects will be visible anyway. For example, for the (010) diffracting plane, the criterion is found just in one angular range, even if others are concerned by its Kikuchi band.

Since that two invisibility criterion are met, it is possible to give a value to the Burgers vector that in this case is  $\vec{b} = \frac{1}{2}(\mathbf{101})$ .

## ANNEX 2: RESULTS OF THE RESEARCH OF BURGERS VECTOR FOR THE FIRST SET OF STACKS

Analyzing all grains of all the acquired stacks in the same way of the 4<sup>th</sup> grain of the sub-zone *uno*, an overview on different orientations was made. Results concerning sub-zones *uno* and *bis* will be summed up hereafter.

### SUB-ZONE UNO

Two stacks have been acquired on this zone, the 2<sup>nd</sup> and the 6<sup>th</sup>, both taken with an energy beam of 20 keV, an aperture of 120  $\mu\text{m}$  and a magnification of 5kX. What changes between the stacks is only the used tilt, set at 10° in the 2<sup>nd</sup> stack and at 15° in the 6<sup>th</sup>.

In the following table are indicated the EBSD orientations of each grain of the analyzed sub-zone.

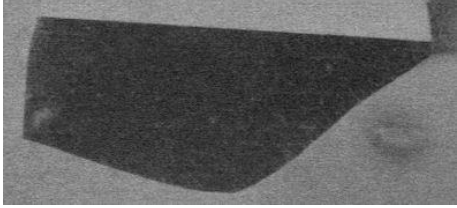
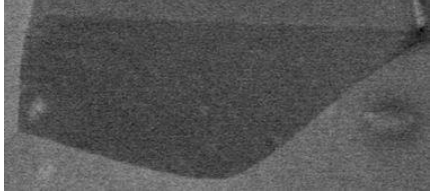
	$\varphi_1$	$\Phi$	$\varphi_2$
Grain1	313.41°	40.24°	19.76°
Grain2	73.41°	29.65°	40.59°
Grain3	352.94°	27.53°	21.53°
Grain4	299.29°	39.39°	89.19°

In the following a table for each analyzed grain of the sub-stack is shown, where all crossed TB condition are noted, with the possible presence of an invisibility criterion. It must be considered that the scenario might change between the two stacks that are tilted differently, in fact this changes if and how Kikuchi lines are crossed.

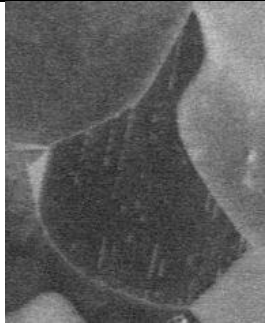
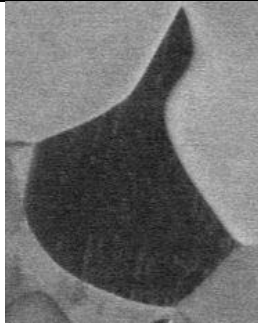
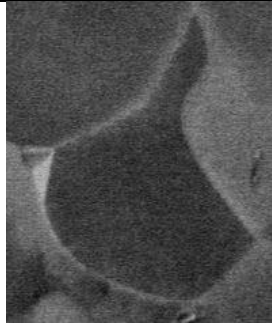
TB GRAIN1	(11-1)	(0-11)
Images		
Defects visibility	visible	not visible
Notes	-	-

The achieved invisibility criterions are not enough to determine the Burgers vector.

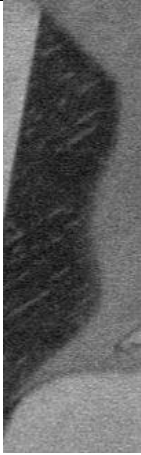
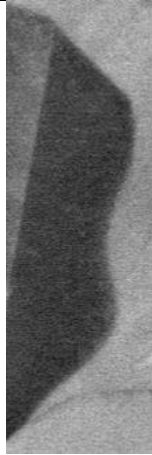
TB GRAIN2	(11-1)	(-110)
-----------	--------	--------

Images		
Defects visibility	not visible	not visible
Notes	-	-

Even if two invisibility criteria are present, the solution does not respect the form that a Burgers vector should comply to (modulus of the vector bigger than 1). This probably means that it has been an error in the detection of invisibility criterions.

TB GRAIN3	(11-1)	(100)	(-110)
Images			
Defects visibility	visible	not clear	not visible
Notes		Not present in the stack2 tilted at 10°	Not a good visibility in the stack6 tilted at 15°

The achieved invisibility criterions are not enough to determine the Burgers vector.

TB GRAIN4	(11-1)	(010)	(-111)	(-101)
Images				

Defects visibility	visible	not visible	visible	not visible
Notes		Visible just in stack6 tilted at 15°, but not enough resolution		In the stack2 certain Kikuchi bands overlap each other and so the invisibility is lost

Since two invisibility criterion are met, it is possible to give a value to the Burgers vector that in this case is  $\bar{b} = \frac{1}{2}(\mathbf{101})$ .

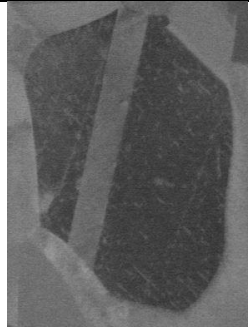
### SUB-ZONE BIS

Three stacks were acquired in this sub-zone, the 3<sup>rd</sup>, the 7<sup>th</sup> and the 8<sup>th</sup>. An energy beam of 20 keV was used in the 3<sup>rd</sup> and the 7<sup>th</sup>, instead in the 8<sup>th</sup> stack a 30 keV beam was used. For what concerns the tilt angle, it was 10° only in the 3<sup>rd</sup> and for both the other stacks a 6.5° tilt was used.

In the following table are indicated the EBSD orientations of each grain of the analyzed sub-zone.

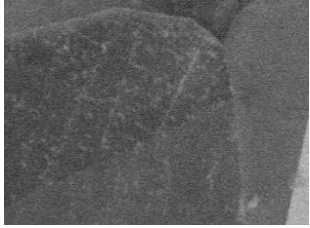
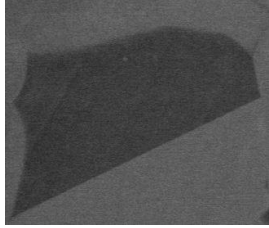
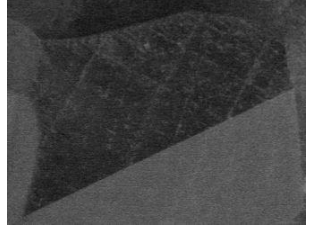
	$\varphi_1$	$\Phi$	$\varphi_2$
Grain1	53.65°	40.24°	78.71°
Grain2	76.24°	43.41°	72.71°
Grain3	354.35°	43.76°	33.88°
Grain4	330.35°	14.82°	31.76°

Also in this case, for each analyzed grain, a table was made, in which are indicated the crossed TB and if an invisibility criterion is met.

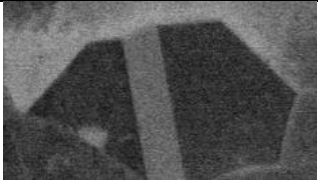
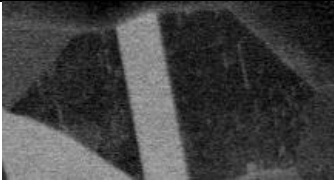
TB GRAIN1	<b>(-111)</b>	<b>(-101)</b>	<b>(11-1)</b>	<b>(010)</b>
Images				

Defects visibility	visible	not visible	visible	not visible
Notes	This Kikuchi band is crossed just with a tilt of 10°, therefore it is not present in stack 7 and 8.	Visible just in stack 3 (10° tilt) and 8 (6.5° tilt).		Not visible in stack 7.  Certain Kikuchi bands overlap each other and so the invisibility is lost.

Since two invisibility criterion are met, it is possible to give a value to the Burgers vector that in this case is  $\bar{b} = \frac{1}{2}(\mathbf{101})$ .

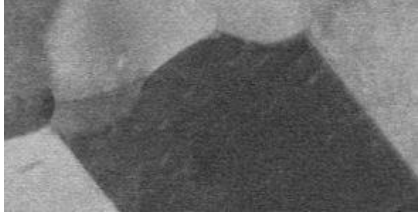
TB GRAIN2	<b>(-111)</b>	<b>(-101)</b>	<b>(11-1)</b>
Images			
Defects visibility	visible	not visible	visible
Notes	This Kikuchi band is crossed just with a tilt of 10°, therefore it is not present in stack 7 and 8.		With a tilt of 6.5° the TB has a very big angular range (see the concerned ECP)

The achieved invisibility criterions are not enough to determine the Burgers vector.

TB GRAIN3	<b>(0-11)</b>	<b>(11-1)</b>	<b>(-110)</b>
Images			
Defects visibility	not visible	e visible	not visible

Notes	Visible just in stack3, in other stacks tilted at 6.5° the Kikuchi band overlap with others.	With a tilt of 6.5° the TB has a very big angular range (see the ECP)	
-------	--	---	--

The achieved invisibility criterions are not enough to determine the Burgers vector.

TB GRAIN4	<b>(100)</b>	<b>(-110)</b>
Images		
Defects visibility	visible	not visible
Notes	With both used tilts the TB has a very big angular range (see the ECP)	Not visible in stack 8, tilted at 6.5° and with a beam energy of 30 KeV.

The achieved invisibility criterions are not enough to determine the Burgers vector.

## ANNEX 3: GRAIN2 OF THE SECOND SET OF STACKS

This grain has been analyzed exactly in the same way of the first, Figure69 shows the relative rotational profile and ECPs.

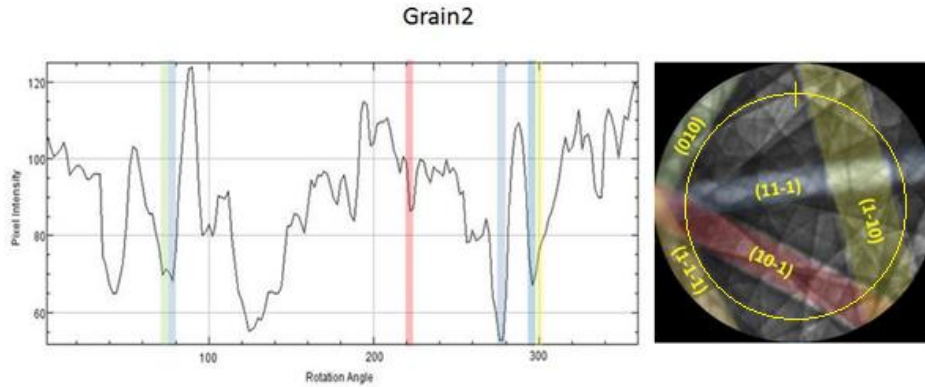


FIGURE 69: INTENSITY PROFILE OF THE GRAIN2, LINKED TO THE CORRESPONDENT ECP. DIFFRACTING PLANES OF KIKUCHI BANDS ARE INDICATED TOO.

Therefore, following angular ranges have been used for making mini-stacks:

Angular range	80.0° - 90.0°	227.0° - 247.0°	285.0° - 295.0°	310.0° - 327.0°
Concerned Kikuchi line	(010) (11-1)	(10-1)	(11-1)	(11-1) (1-10)

Such orientation behaves that TB conditions are often found in zones in which more than one Kikuchi band superimposes. That is an issue because it is really difficult to determinate which diffraction plane is concerned for a TB condition and so angular ranges can refer to more than one crystallographic planes. Moreover, a superimposed diffracting plane could cancel an eventual invisibility criterion in an angular range.

Figure70 shows how defects visibility changes in different TB conditions, involved diffracting planes are noted.

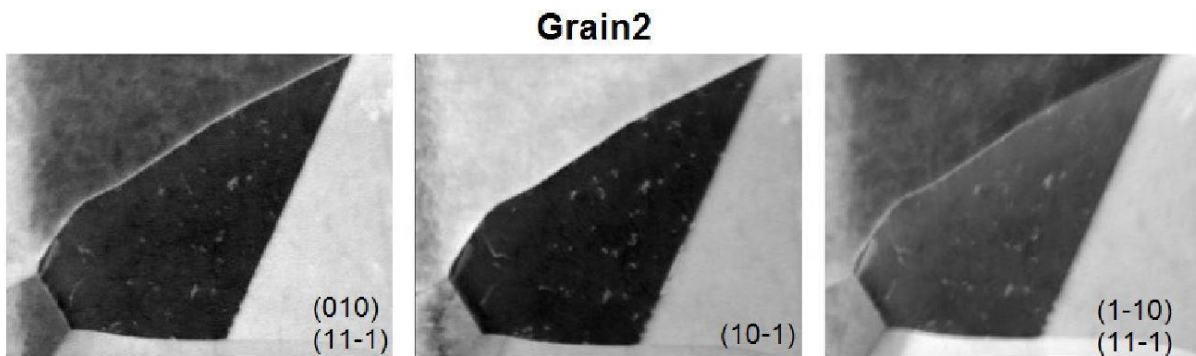


FIGURE 70: REPRESENTATION OF THE DIFFERENT TB CONDITIONS CROSSED DURING THE ROTATIONAL STACK.

Data achieved from clustering has been used in the Matlab script, using following parameters.

Pixel size	Dislocation width	thickness
5.8 nm	$5.15 \pm 1.64$ pixels	75 nm

Also in this case values of dislocation density, stocked in Figure71, have been achieved successfully. The method of intercepts has been used as a reference.

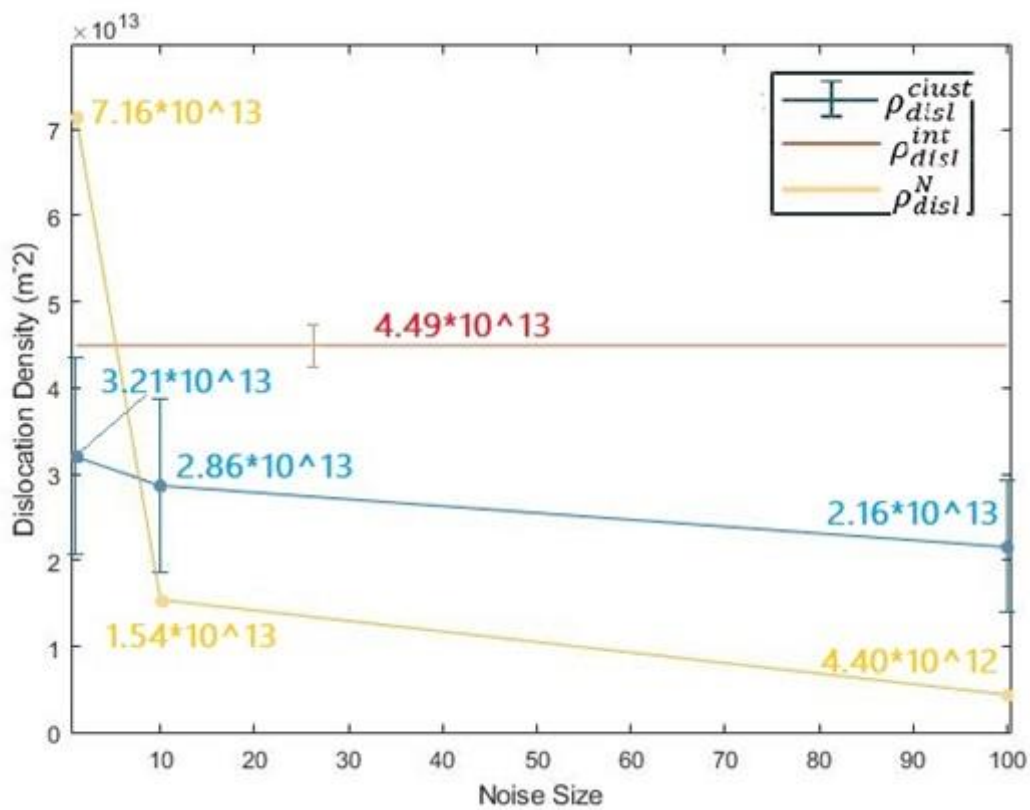


FIGURE 71: DIFFERENT VALUES OF DISLOCATION DENSITY FOR THE GRAIN2. IN RED THE VALUE ACHIEVED WITH THE TRADITIONAL METHOD OF INTERCEPT. OTHER COLORS REPRESENT VALUES OF DISLOCATION DENSITY OBTAINED VIA CLUSTERING (BLUE) AND THE N/SURFACE DISLOCATION DENSITY (IN YELLOW).

This example allows understanding the importance of the noise size value, it is in fact evident that, for this grain, the value of 1pixel is too small to be used. With this value, the number of detected features increases a lot, therefore the  $\rho_{disl}^N$  increases excessively.



## REFERENCES

---

1. **Sophie Cazottes, Michel Perez, Thierry Douillard.** *Dislocation Imaging in Scanning electron Microscopy.* Lyon : s.n., 2018.
2. *Theory and Application of Electron Channelling Contrast Imaging under Controlled Diffraction Conditions.* **Zaefferer, Stefan, et Nahid-Nora Elhami.** 2014, *Acta Materialia* 75, pp. 20-50.
3. *Theory of dynamical electron channeling contrast images.* **Y.N.Picard, M.Liu, J.Lammatao, R.Kamaladasa, M.DeGraef.** 2014, *Ultramicroscopy* 146, pp. 71-78.
4. *Crystal Orientation Mapping via Ion Channeling: An Alternative to EBSD.* **Langlois, C., T. Douillard, H. Yuan, N.P. Blanchard, A. Descamps-Mandine, B. Van de Moortèle, C. Rigotti, et T. Epicier.** 2015, *Ultramicroscopy*, Vol. 157, pp. 65-72.
5. **J.W.Morris.** *Defects in Crystals. Material Science .*
6. **CASIEZ, Lara.** Project Fin d'Etudes. *caracterisation automatique de structures de dislocation au MEB.*
7. **Bouvard, Alexis Deschamps & Didier.** *PHYSIQUE ET MECANIQUE DU COMPORTEMENT (polycopies).* 2017.
8. *Case studies on the application of high-resolution.* **Biermann, Anja Weidner & Horst.** 2015, *Philosophical Magazine*, pp. 760-793.
9. *Electron channeling patterns in the scanning electron microscope.* **David C. Joy, Dale E. Newbury, David L. Davidson.** 1982, *Journal of Applied Physics*, Vol. 53, pp. 81-122.
10. *Determination of dislocation density from hardness measurements in metals.* **S. Graça, R. Colaço, P.A. Carvalho, R. Vilar.** 2008, *Materials Letters*, Vol. 62, pp. 3812-3814.
11. *General methodology to estimate the dislocation density from.* **Ali A.H. Ameri, Nancy N. Elewa, Mahmud Ashraf, Juan P. Escobedo-Diaz.** 2017, *Materials Characterization*, Vol. 131, pp. 324-330.
12. *On the suitability of peak profile analysis models for estimating dislocation density.* **Malvika Karri, J.B. Singh, K.V. Manikrishna, B.K. Kumawat, Naveen Kumar, D. Srivastava.** 2017, *Materials Science & Engineering A*, pp. 75-81.
13. *The variation of dislocation density as a function of the stacking fault energy in shock-deformed FCC materials.* **A. Rohatgi, K.S. Vecchio.** 2002, *Materials Science and Engineering*, Vol. A328, pp. 256-266.
14. **VOLPI, Fabien.** *Microstructures e properties. Polycopies.* 2017.
15. *EVALUATION OF THE GROWTH OF DISLOCATIONS DENSITY IN FATIGUE LOADING PROCESS VIA ELECTRICAL RESISTIVITY MEASUREMENTS.* **Sevostianov, Mohammad A. Omari and Igor.** 2013, *LETTERS IN FRACTURE AND MICROMECHANIC*, pp. 229-235.

16. **Joseph I. Goldstein, Dale E. Newbury, Joseph R. Michael, Nicholas W.M. Ritchie, John Henry J. Scott, David C. Joy.** *Scanning Electron Microscopy and X-Ray Microanalysis*. s.l. : Springer.
17. **Langlois, C.** *HDR*. Lyon : s.n., 2018.
18. *Electron CHanneling ORientation Determination (eCHORD): An original approach to crystalline orientation mapping.* **C. Lafond, T. Douillard, S. Cazottes, P. Steyer, C. Langlois.** 2018, *Ultramicroscopy*, Vol. 186, pp. 146-149.
19. *Dictionary indexing of electron channeling patterns.* **M.D. Graef, S. Singh.** 2017, *Microscopy Microanalysis*, Vol. 23, pp. 1-10.
20. *Anisotropic Diffusion Partial Differential Equations for Multichannel Image Regularization: Framework and Applications.* **D. Tschumperlé, R. Deriche.** 2007, P.W. Hawkes (Ed.) *Advances in Imaging and Electron Physics*, Elsevier, pp. 149-209.
21. **Dabov K., Foi A., Katkovnik V., Egiazarian K.,** Image denoising with block-matching and 3D filtering. [En ligne] 2006. <https://doi.org/10.1117/12.643267>.
22. *Rotational-Electron Channeling Contrast Imaging analysis of dislocation.* **G. L'hôte, C. Lafond, P. Steyer, S. Deschanel, T. Douillard, C. Langlois, S. Cazottes.** 162, Lyon : Scripta Materialia, 2018.
23. **Seif, Geoge.** Towards data science. [En ligne] 5 february 2018. [Citation : 22 11 2018.] <https://towardsdatascience.com/the-5-clustering-algorithms-data-scientists-need-to-know-a36d136ef68>.
24. **C.A.Roth, T. Dreyfus.** *rapport given with the clustering program*. Lyon : s.n., 2018.
25. *The determination of dislocation densities in thin films.* **Ham, R. K.** 69, 1961, *he Philosophical Magazine: A Journal of Theoretical Experimental and Applied Physics*, Vol. 6, pp. 1183-1184.
26. *Accurate electron channeling contrast analysis of dislocations in fine grained bulk materials.* **Mansour, H., J. Guyon, M.A. Crimp, N. Gey, B. Beausir, et N. Maloufi.** 2014, *Scripta Materialia*, Vol. 84-85, pp. 11-14.
27. *Transmission Electron Microscopy : A Textbook for Materials Science.* **David B. Williams, et C. Barry Carter.** 2009, 2e éd. Springer US.
28. *Effects of Porosity on Mechanical Properties and Corrosion Resistances of PM-Fabricated Porous Ti-10Mo Alloy.* **Wei Xu, Xin Lu, Bing Zhang, Chengcheng Liu, Shaomin Lv, Shidi Yang, Xuanhui Qu.** 2018, *Metals*, Vol. 8.
29. *Coupling of Electron Channeling with EBSD: Toward the Quantitative Characterization of Deformation Structures in the SEM.* **Gutierrez-Urrutia, I., S. Zaefferer, et D. Raabe.** 9, 2013, *JOM*, Vol. 65, pp. 1229-1236.